University of Strathclyde
Electronic and Electrical Engineering Department

Maximum Power Point Tracking and Control of Grid Interfacing PV Systems

by

Isaac Owusu-Nyarko
B.Sc., M.Sc.

A thesis presented in fulfilment of the requirements for the degree of Doctor of Philosophy

October 2021

Acknowledgements

I would like to express my profound gratitude to my supervisor Dr Khaled H. Ahmed for his extensive guidance, encouragement, helpful comments, kind advice and supervision throughout my PhD period.

I also wish sincerely to thank Dr Ibrahim Abdelsalam for practical implementation help. A courteous acknowledgement is made to members of staff especially Dr Mohamed A. Elgenedy and technicians at Electronic and Electrical department in Strathclyde University who provided me with assistance during the years of research.

Finally, a heartfelt gratitude goes to my wife Naomi, and my kids Kennedy and Melvin for their sacrifices made and continuous support, encouragement and prayers throughout my PhD period.

Isaac Owusu-Nyarko

October 2021

Dedication

To my Mother, wife and children

Abstract

Grid interfacing of PV systems is very crucial for their future deployment. To address some drawbacks of model-based maximum power point tracking (MPPT) techniques, new optimum proportionality constant values based on the variation of temperature and irradiance are proposed for fractional open circuit voltage (FOCV) and fraction short circuit current (FSCC) MPPT. The two MPPT controllers return their optimum proportionality values to gain high tracking efficiency when a change occurred to temperature and/or irradiance. A modified variable step-size incremental conductance MPPT technique for PV system is proposed. In the new MPPT technique, a new autonomous scaling factor based on the PV module voltage in a restricted search range to replace the fixed scaling factor in the conventional variable step-size algorithm is proposed. Additionally, a slope angle variation algorithm is also developed. The proposed MPPT technique demonstrates faster tracking speed with minimum oscillations around MPP both at steady-state and dynamic conditions with overall efficiency of about 99.70%. The merits of the proposed MPPT technique are verified using simulation and practical experimentation. A new 0.8Voc model technique to estimate the peak global voltage under partial shading condition for medium voltage megawatt photovoltaic system integration is proposed. The proposed technique consists of two main components; namely, peak voltage and peak voltage deviation correction factor. The proposed 0.8Voc model is validated by using MATLAB simulation. The results show high tracking efficiency with minimum deviations compared to the conventional counterpart. The efficiency of the conventional $0.8V_{oc}$ model is about 93% while that of the proposed is 99.6%. Control issues confronting grid interfacing PV system is investigated. The proposed modified 0.8Voc model is utilized to optimise the active power level in the grid interfacing of multi-megawatt photovoltaic system under normal and partial shading conditions. The active power from the PV arrays is 5 MW, while the injected power into the ac is 4.73 MW, which represents 95% of the PV arrays power at normal condition. Similarly, during partial shading conditions, the active power of PV module is 2 MW and the injected power is 1.89 MW, which represents 95% of PV array power at partial shading conditions. The technique demonstrated the capability of saving high amount of grid power.

List of symbols

C	Capacitor (F)
D	Duty cycle
E_G	Bandgap of the semiconductor (eV)
f_s	Switching frequency (s)
G	Solar irradiance (W/m2)
I_{abc}	Inverter currents vector (A)
I_{ph}	Light generated current (A)
I_O	Current of diode (A)
I_{pv}	Output current of PV module (A)
I_{rr}	Reverse saturation current (A)
I_{SC}	Short circuit current of PV module (A)
k	Boltzmann's constant ($1.38\ x\ 10^{-23}$J/K)
k_v	Temperature coefficient of open circuit voltage (mV/℃)
k_i	Temperature coefficient of short circuit current (mA/℃)
K_i, K_p	Integral and proportional gain of PI controller
L	Inductance (H)
n_p	Number of Parallel connected PV cell
n_s	Series connected PV cell
P	Active output power (W)
Q	Reactive output power (AV_r)
q	Charge of electron (coulomb)
T_s	Sampling time (s)
V_{dc}	DC-link voltage (V)
V_{abc}	Inverter voltage vector (V)
V_{OC}	Open circuit voltage of PV module (V)
V_{sub}	Submodule voltage (V)

δ	Angle between PV power and voltage
ω	Fundamental frequency (rad/s)

List of abbreviations

AI	Artificial intelligent
CHP	Combine heat and power
CSI	Current source inverter
FIT	Feed-In-Tariff
FSCC	Fractional short circuit current
FOCV	Fractional open circuit voltage
GA	Genetic algorithm
GHG	Greenhouse gas
GMPP	Global maximum power point
GWO	Grey wolf optimization
IEEE	Institute of Electrical and Electronic Engineering
IEC	International Electrotechnical Commission
INC	Incremental conductance
LMPP	Local maximum power point
MPP	Maximum power point
MPPT	Maximum power point tracking technique
PI	Proportional-Integral
P&O	Perturb and observe
PSC	Partial shading condition
PSO	Particle swamp optimization
PV	Photovoltaic
STC	Standard test conditions
VSI	Voltage source inverter

Table of Contents

Chapter 1 Introduction

Chapter 2 Literature Survey on Photovoltaic System and Maximum Power Point Tracking (MPPT) Techniques

Chapter 1
Introduction

Global energy demand is on increase due to economic expansion and population growth. Approximately 85% of world's energy demand comes from burning of fossil fuels, which has exponentially increased emissions of greenhouse gas (GHG) [1.1]. Regrettably, there is inadequate fossil fuels in the word and considering the current availability and rate of energy consumption, it is important to replace energy that comes from the fossil fuels. The campaign to mitigate GHG has attracted the attention of researchers, which has improved the development of renewable power generation. Numerous works undertaken by researchers have seen significant improvement in the development of renewable energy sources such as hydroelectric, wind turbine, combined heat and power (CHP) systems and photovoltaic (PV) modules, where technical and economic feasibility of these energies have extended to utility scale level for electricity supply. Photovoltaic systems for power generation are well-thought-out as one of the most efficient, cleanliness and acceptable renewable energy because of their suitability in transportations, distributed generation, satellite systems and mobile applications [1.2].

1.1 Background and historical development of photovoltaic system

The effect of photovoltaic energy was first discovered by the French physicist (Alexandre Edmond Becquerel in 1839). This effect was seen in an electrolytic cell that was placed in electrolyte. In 1879, the first solid-state photovoltaic was invented by an American scientist called Charles Fritts. Fritts used a thin layer gold to coat semiconductor selenium to form junctions. Although, it demonstrated how a sunlight could be converted into electricity using solid material without moving parts, however, efficiency of the device was only about 1%. Right after the discovery of photovoltaic cell, researchers main aim has been to improve the PV cells efficiency. In 1888, Russian scientist Aleksandr Stoletov invented photoelectric cell using outer photoelectric effect. When people realized that fossil fuels for electricity generation will soon be depleted and there was a need for

renewable energy source, Daryl Chaplin et al., built the first hand-on photovoltaic cell, made up of semiconductor materials in 1954 at Bell Laboratories. This practical PV cell improved the previous efficiency to 6%. Later on, solar PV cell developed for earth orbiting satellites. Hoffman Electronic Company increased the efficiency to 14% and between 1950s and 1960s, solar PV system were produced for commercial purposes. Solar PV system currently provides electricity in satellite systems [1.3]. By 1980, plants for production of solar module have already built, producing above 1 MW of PV modules per year. In 2000, the production capacity reached around 100 MW of power per year. Globally, it is increasingly proving to be an alternative system to replace fossil fuel for generation of electricity. Also, since PV system technology does not produce noise pollution and harmful emission, it believes to be the best option for power generation to mitigate greenhouse emission. It plays a tremendous role in distributed generation and consumers who often uses electricity from solar PV system are likely to control their energy consumption for cleaner environment.

1.2 Growth of photovoltaic power generation

Global PV capacity shows a significant growth since 2000. The solar PV system installation capacity increased annually from 29.5 MW in 2012 to 107 MW globally in 2018, motivated by additional large utility scale leading to global reduction of PV system prices. At the end of 2018, the world's PV power installation capacity increased to 520 MW. The Global PV power capacity increased by 632.4 MW between 2018 and 2019 [1.4]. Global installation PV capacity is illustrated in figure 1.1. Unites State and China are on the top of global PV energy market with cumulative PV power capacity of 76 and 204 MW respectively in 2019. China also overtook the whole European union PV installed capacity with new PV system capacity of over 44 MW. In Europe, Germany and Italy have demonstrated through their stimulated policies, large growth of PV installation capacity even in the areas where solar energy resources are moderate. In general, the trend in PV installation capacity word-wide is increasing and expected to increase the global renewable energy capacity to fully replace conventional thermal power generation plant [1.5].

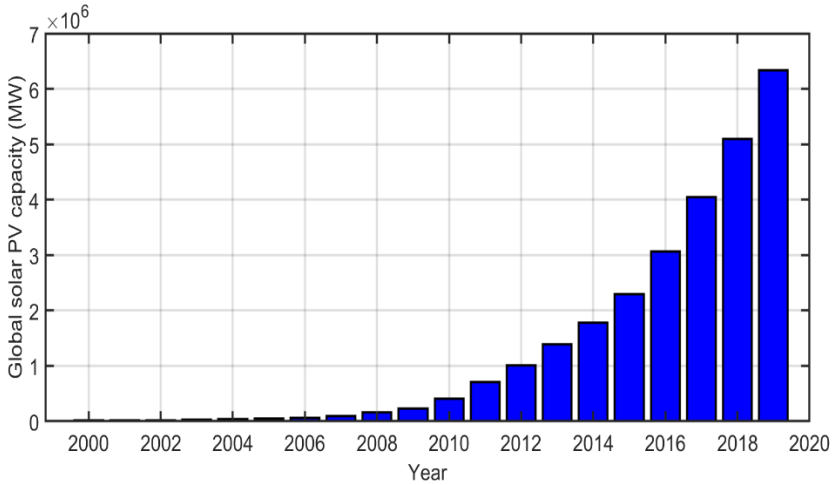

Figure 1.1. Global Cumulative installed solar PV capacity between 2000 and 2019.

1.3 Environmental impacts of photovoltaic energy system

The main source of photovoltaic energy is the sun and this does not involve emission of greenhouse gas during power generation stage. Thus, it does not contribute to ozone layer depletion. However, the production of PV module involves little emission of greenhouse gas, which is far less than greenhouse gas when fossil fuel is used to generate electricity. In comparison, the carbon emission during the manufacturing of PV module is between 14 to73 gCO_2/kWh lower than emission from natural gas which is 742 gCO_2/kWh [1.6]. The PV module can be recycled to produce raw materials at the end of its lifespan. These raw materials can then be used to produce new PV modules. The energy used to produce new PV modules is significantly reduced, compared to natural gas, contributing to about 42% reduction in carbon emission [1.7].

1.4 Cost of photovoltaic systems

The trends of solar PV market are rapidly changing and driven by a number of factors such as production of PV module and PV installation cost. In recent years, the cost of PV module production has reduced significantly and have been the main course of current development in the costs of PV system installation. Between 2007 and 2013, the production costs of the PV module have fallen below USD 1.00/W from USD 4.00/W for a rated PV system of 10 kW [1.8]. Both the costs of PV module production and installation

determine the global weighted average levelised cost of electricity (LCOE) [1.9]. Between 2010 and 2019, the global weighted average LCOE of utility scale solar PV system fell drastically from USD 0.378/kWh to USD 0.068/kWh. This reduction was because the PV module price declined by 90% between 2010 and 2019, which saw a decline by 79% of the global installed costs. In 2019, the global PV installed costs declined from USD 1000/kW to USD 995/kW, which is 18% for the first time. In 2019, India was the global lowest PV installed cost of USD 618/kW for the first time. In general, the installation costs for PV system are expensive than other renewable energy sources such as wind [1.10]. However, PV system is economically feasible and requires little maintenance compared with wind energy.

1.5 Development of photovoltaic energy in the UK

Geographical position of UK attests to the fact that solar PV system is not suitable for generation of electricity in the UK. However, due to technological advancement, the current PV module can generate electricity efficiently deprived of having irradiance of high intensity [1.11]. Due to the effective policy investment, UK PV system installation capacity has grown significantly. In 2012, the total PV system installed capacity stands at 1 MW [1.12]. The introduction of Feed-In Tariff (FIT) in 2012 boosted both installation and generation capacity of PV system. This FIT enables household in the community to generate their own electricity using PV system. In an event of extra power generation than what is needed, this additional power is sell back to the grid for payment. At the end of 2017, the UK installed PV capacity was 12.8 MW, which is 3.4% of the total electricity generation. The total installed PV capacity by 2019 was more than 13 MW [1.13]. Figure 1.2 represents UK installed PV capacity. It is important to note that FIT is no longer allow in the UK grid network as the government closed for all new application, it has replaced with smart export guarantee scheme. This scheme will only pay for your exported energy unlike FIT which pays for both generation and exported energy.

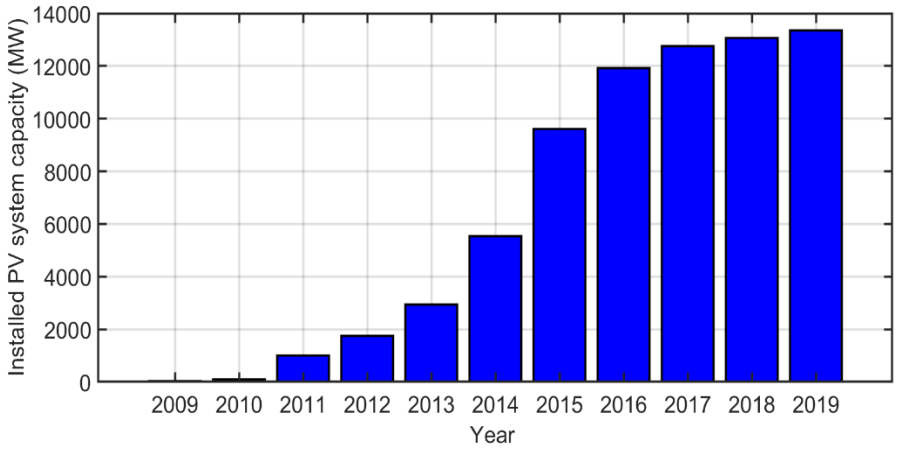

Figure 1.2. UK solar PV installed capacity.

1.6 Application of photovoltaic energy

The growth of distributed generation system with photovoltaic energy plays significant role in the near future. The advantage of this system is to increase the interfaced network capacity for reliable, efficient, and high-power quality supply [1.14]. The photovoltaic system has two main application modes: island (standalone) and grid-connected modes. With Island mode, the system operates independently deprived of interfacing to the utility grid. It is connected parallel to feed local loads. Most of Island mode system uses storage batteries to supply power to the loads during night or at low irradiance levels. This system is applicable in communities with no utility grid network or when the grid is expensive. The standalone system provides high quality output power with controlled voltage and frequency at its output. This application mode is common also in traffic signals, water pumps, Cathodic protection, communication site, satellite, and space station [1.15]. Grid connected PV systems are design to work in parallel with the utility grid. The dedicated control strategy for this PV application delivers active power to the grid. Grid connected system operates as centralized power plant or distributed generation. In centralized power plant, bulky PV power is delivered to minimizes regular use of fossil fuel for generation of electricity [1.16]. With distributed generation, consumers generate their own electricity to minimize their dependency on the grid and inject the extra power to grid.

1.7 Key challenges facing photovoltaic energy generation

Although, the photovoltaic industry outlook is positive, and is playing a crucial role in the distributed generation, the industry is facing certain challenges such as efficiency, reliability, manufacturability, subsidies, regulation, and impact of interfacing technology to the grid [1.17]. It is important to control photovoltaic system using power electronic devices either in standalone mode or grid-connected mode for interfacing and improving the efficiency of the PV module.

1.7.1 System efficiency

The efficiency of the PV system largely depends on PV module, maximum power point tracking (MPPT) controller, power converter and interfacing transformer. The solar cell materials of the previous generations reflected or absorbed most of the sunlight and only 1-2% of the sunlight could convert to electricity [1.18]. However, due to technological advancement, efficiency of the current generation of solar cell has improved significantly. Figure 1.3 shows the conversion efficiency of different solar cell technology [1.19]. The power electronic converters have impact on the efficiency of the PV system. Both single and two stage topologies of the PV system utilize power electronic converters for effective delivery of power. In a single stage topology, an inverter is used to force the PV module to generate power and interface the PV system into the grid. On the other hand, the two stage topology uses two power converters in the PV system namely, dc-dc converter and dc-ac inverter. This topology does not necessarily need a high voltage PV module as the dc-dc converter amplifies the PV voltage at one stage, however, the PV system experiences low efficiency compared with the single stage topology. The irradiance and temperature variations have significant impact on the PV characteristic curve, which is non-linear characteristic curve. This irradiance and temperature variations affect the efficiency of the PV module. To overcome such challenges, MPPT is needed to force the PV module to operate at maximum power point (MPP). In partial shading conditions [1.20], the characteristic of PV module generates multiple peaks instead of only one peak.

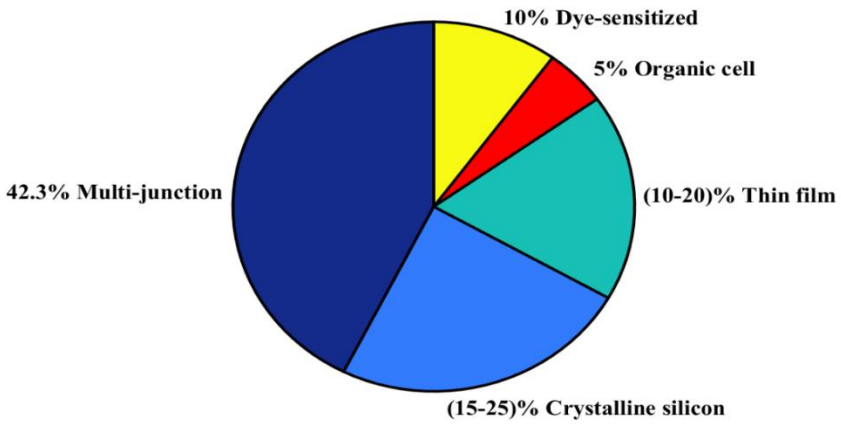

Figure 1.3. Efficiency of different solar cell materials.

1.7.2 System reliability

System reliability is the likelihood for a system including its software and hardware to be able to execute the objective of which it was designed, for a given environment and a specified time. PV system consists of PV module, power converter, MPPT controller, storage device and wire that interconnects the components. The quality of these components defines the reliability of the PV system. The most reliable component of the PV system is the PV module and requires little maintenance which has approximately 30 years of lifespan [1.21]. Standalone PV system requires good storage devices to continuously supply critical loads with power of high quality [1.22-1.24]. The most applied batteries for standalone PV system are nickel and lead acid. Reliability of the PV system can be compromised by the batteries used. The performance of the inverter and controllers have significant impact on the lifespan of the PV system [1.25]. According to the report in [1.26], at Florida solar energy center, a total of 130 grid connected PV system experienced 213 system breakdowns between 1999 to 2003 and investigation revealed that 65% of those breakdowns are due to the failure of the inverters. This means that the reliability of grid connected PV system is greatly affected by the performance of the inverter. Therefore, effective protective mechanism like anti island mode protection must be put in place to avoid system failure.

1.7.3 Grid connected PV system

Inverter in a grid connected PV system performs two main functions. One is to force the PV module to operate at maximum power point in case of single stage PV system. The second is to shape the PV current into sinusoidal form and inject it into the grid [1.27]. The evolution of inverters used in the PV system application defines the type of methods used to interface PV system to the grid. Inverter topology available in PV system are centralized inverters, string inverters, multi-string inverters and micro-inverters [1.28]. The centralized inverter grid interfacing PV system make use of a string of PV modules connected in parallel using a string diode and then interfaced to the grid through inverter. However, this grid connected PV system has disadvantages such as failure to track the actual MPP, the use of dc cable of high rated voltage and difficult to embark on large scale due to rigid design. String inverter consists of a string of PV modules and an inverter. It is a simplified version introduced to overcome limitations in centralized inverter with fewer number of PV modules configuration [1.29]. In this topology, each PV string has inverter which makes it suitable for large scale production. Each string can be operated by a separate MPPT controller and there are no string diodes losses. Thus, overall system efficiency is improved. This reduces the prices due to large-scale production. String inverter can be implemented using single stage or two stage grid connected PV system. Multi-string inverter is the modified version of string inverter where each PV string is connected to dc-dc converter, which is coupled to one inverter [1.30]. This topology has advantage over the centralized inverter since each string can be controlled separately. Expansion of multi-string inverter topology is feasible; however, the main drawback is how the inverter can amplify the very low voltage suitable for grid. In general, the choice of any evolution of inverters for grid connected has its own drawbacks which is a challenge in PV energy generation.

1.7.4 Grid code requirement

The high penetration of PV power generation has an impact on the grid stability [1.31-1.32]. Inverters interfacing PV module must be connected to the grid by obeying standards given by the regulatory body. Most of the countries have their own code of practice

enforced by government or utility companies. However, international organizations are working to ensure compliance of grid requisite standards for most countries. These organizations are International Electrotechnical Commission (IEC) and Institute of Electrical and Electronic Engineering (IEEE). Example of IEC and IEEE are IEC-61727 [1.33] and IEEE-1547 [1.34] respectively. These standards deal with challenges associated with power quality, grounding, detection of islanding operation etc. The IEEE-1547 is the modification of IEEE-519 which serves as the harmonic current limits in the two standards. In general, IEC-61727 ensures compliance of standards related to unit interface of photovoltaic system characteristics [1.35]. While IEEE-1547 ensures compliance of standards on interconnected distributed generation on electric power system [1.36]. Table 1.1 shows the summary of IEC- 161727 and IEEE-1574 standards. Inverters interfacing PV modules to the grid must fulfil strict IEC-61727 and IEEE-1574 standards codes to improve power quality. It can be seen from Table 1.1 that current harmonic injection into the grid by the inverter should not be more than 5% of the limit imposed by IEC-61727 and IEEE-1574. Pulse width modulation technique is a common method used to ensure that the injected current into the grid is controlled. This technique is common in many power electronics inverters to reduce harmonic distortion. Other technique includes reduction of switching losses [1.37]. DC injection current also has significant effect on the distribution system components. The effect of dc current is the saturation of distributed transformer, which causes distortion of waveform, power dissipation that results overheating of Components and reduction of lifetime of transformer [1.38]. Table 1.1 shows that the tolerable dc injected current should not be more than 0.5% of the rated output current for IEEE-1574 and 1.0% for IEC-61727. Many works have been done to minimize high dc current injection into the grid and this attracted lots of researchers' attention.

Table 1.1 Summary of IEC-61727 and IEEE-1547 standards for utility companies.

	IEC-61727 [1.33]	IEEE-1547 [1.34]
Nominal Power	10 kW	30 kW
Harmonic current (order-h) limits	(3-9) 4.0 % (11-15) 2.0 % (17-21) 1.5 % (23-33) 0.6 % Even harmonic in these ranges shall be less than 25% of the odd harmonic limits listed	(2-10) 4.0 % (11-16) 2.0 % (17-22) 1.5 % (23-34) 0.6 % (< 35) 0.3 %
Maximum current THD	5.0 %	
Dc current injection	Less than 1.0 % rated output current	Less than 0.5 % of rated output current
Voltage range per phase for normal operation	85 -110% (196V – 253V)	88-110% (97V – 121V)
Frequency range for normal operation	50 ± 1Hz	59.3Hz to 60

1.8 Motivation of the research

Photovoltaic (PV) module has a non-linear characteristic curve and fail to generate rated power specified by the manufacturer under normal weather condition without the use of maximum power point tracking (MPPT) in the PV system. This challenge becomes more severe under partial shading conditions as the characteristic curve generate multiple peaks. This results in significant power loss in the PV system. The literature shows different techniques for MPPT for PV module system. These techniques differ in convergence speed, number of sensors used, complexity, cost, its effectiveness, hardware implementation and other technical characteristic. In reality, so many techniques have been developed but it is difficult to effectively find which technique either newly proposed

or existing one is suitable or needs modification for effectively used in a given PV system. Given, the numerous numbers of methods for MPPTs, an effective literature survey is essential to identify loopholes of any of these techniques and develop a suitable method to improve its performance under normal and partial shading conditions. Another issue confronting PV system is how to interface multi-megawatts PV system into the grid network. Failure to achieve proper interfacing of PV system to the grid ends up losing the stability of the entire network and this could lead to a total blackout. This challenge can be addressed by controlling the power electronic converter robustly. Thus, efficient and reliable inverter design and robust control system for grid interfacing system are the main concern.

1.9 Thesis objectives

In this thesis, a comprehensive study on the grid interfacing of multi-megawatt PV system is discussed. Focusing on the following objectives:

- Review comprehensively common maximum power point tracking (MPPT) techniques.
- Develop a new efficient MPPT technique for grid connected PV systems.
- Develop a new MPPT technique for partial shading condition to track the global MPP.
- Investigate grid interfacing multi-megawatt PV system with robust and efficient control.

1.10 Structure of the thesis

The thesis is structured into seven chapters. Chapter one presents the general background of photovoltaic power generation and its main drivers in both island and grid interfacing mode perspectives. It further highlighted the impact of photovoltaic energy on environment and the challenges in both island and grid connected PV system. The motivation, and objectives of this thesis are presented in this chapter.

Chapter two presents literature review of photovoltaic systems and commonly used maximum power point tracking technique (MPPT), which includes their suitability in the PV system applications.

Chapter three discusses new optimum proportionality constants values based on the impact of temperature and irradiance for fractional open circuit voltage (FOCV) and fractional short circuit current (FSCC) MPPT. MATLAB/SIMULINK simulations are used to verify the effectiveness of the new optimum proportionality on the performance of both MPPT techniques.

Chapter four provides detailed discussion on the limitations of conventional variable step-size incremental conductance MPPT. Additionally, a new variable step-size technique is proposed to address limitations of conventional variable step-size MPPT. This chapter demonstrates the effectiveness of the proposed variable step size incremental conductance MPPT with an autonomous scaling factor over the conventional counterpart using simulation and experimentation.

Chapter five discusses the limitations of conventional 0.8Voc model for partial shading conditions. A new 0.8Voc model is proposed to estimate the peak global voltage for medium voltage megawatt photovoltaic system integration. The effectiveness of the proposed model is verified using simulation.

Chapter six investigates control issues and implementation for grid interfacing of multi-megawatt photovoltaic system. The new 0.8Voc model is utilized to optimize the active power in the grid interfacing of multi-megawatt photovoltaic system. The effectiveness of the system is verified using simulation.

Chapter seven presents the general conclusion, contributions of the author and recommendations for future work.

References

[1.1] B. Bose, "Global Warming: Energy, Environmental Pollution, and the Impact of Power Electronics," Industrial Electronics Magazine, IEEE, vol. 4, pp. 6-17, 2010.

[1.2] S. Krauter and T. Depping, "Satellite monitoring system for remote PV-systems," Conference Record of the Twenty-Ninth IEEE Photovoltaic Specialists Conference, 2002., 2002, pp. 1714-1717.

[1.3] K. K. Ng, Complete Guide to Semiconductor Devices: Wiley, 2002.

[1.4] Global cumulative installed solar PV capacity 2000-2019. [Online]. Available : https://www.statista.com/statistics/280220/glob al-cumulative-installed-solar-pv-capacity/

[1.5] International Energy Egency, Photovoltaic Power Systems Programme. [Online]. Available: https://iea-pvps.org/wp content/uploads/2020/04/IEA_PVPS_Snapshot_2020.pdf

[1.6] Muhammad Tawalbeh, Amani Al-Othman, Feras Kafiah, Emad Abdelsalam, Fares Almomani, Malek Alkasrawi, Environmental impacts of solar photovoltaic systems: A critical review of recent progress and future outlook, Science of The Total Environment, Volume 759, 2021, 143528,

[1.7] T. Tsoutsosa, N. Frantzeskakib and V. Gekasb. "Environmental impacts from the solar energy technology", Enerfgy policy, vol. 33, 289-296, 2005.

[1.8] RENEWABLE ENERGY TECHNOLOGIES: COST ANALYSIS SERIES, Solar Photovoltaics. [Online]. Available: https://www.solar-united.org/wp-content/uploads/2017/02/RE_Technologies_Cost_Analysis-SOLAR_PV.pdf

[1.9] Marcel Šúri, Thomas A. Huld, Ewan D. Dunlop, Heinz A. Ossenbrink, Potential of solar electricity generation in the European Union member states and candidate countries, Solar Energy, Volume 81, Issue 10, 2007, Pages 1295-1305.

[1.10] J. Kneifel, David Webb Eric O'Rear, " Energy and Economic Implications of Solar Photovoltaic Performance Degradation" 2016. [Online]. Available: https://nvlpubs.nist.gov/nistpubs/SpecialPublications/NIST.SP.1203.pdf

[1.11] A. Stafford and S. Irvine, UK Photovoltaic Solar Energy Road Map: Centre for Solar Energy Research. [Online]. Available:

https://connect.innovateuk.org/c/document_library/get_file?uuid=b5d43db3-260c-43ff-b3a8-8ae0bbf00cb6&groupId=154351.

[1.12] The Department of Energy and Climate Change. [Online]. Available: http://www.decc.gov.uk/.

[1.13] UK Solar Capacity: Is the Future of Solar Cloudy? [Online]. Available : https://www.greenmatch.co.uk/blog/2019/09/uk-solar-capacity

[1.14] S. R. Bull, "Renewable energy today and tomorrow," in *Proceedings of the IEEE*, vol. 89, no. 8, pp. 1216-1226, Aug. 2001, doi: 10.1109/5.940290.

[1.15] M. A. Elgendy, B. Zahawi, and D. J. Atkinson, "Assessment of Perturb and Observe MPPT Algorithm Implementation Techniques for PV Pumping Applications," Sustainable Energy, IEEE Transactions on, vol. 3, pp. 21-33, 2012.

[1.16] Sun bridge Solar. [Online]. Available: http://sunbridgesolar.com/pacificnorthwest-solar/solar-farms/.

[1.17] D. Tagare, Electricity Power Generation:The Changing Dimensions Wiley-IEEE Press 2011.

[1.18] A. Luque, "Will we exceed 50% efficiency in photovoltaics?," Journal of Applied Physis, vol. 110, pp.031301-031301-19, 2011.

[1.19] R. Venkateswari, S. Sreejith, Factors influencing the efficiency of photovoltaic system, Renewable and Sustainable Energy Reviews, Volume 101, 2019, Pages 376-394.

[1.20] G. Lijun, R. A. Dougal, L. Shengyi, and A. P. Iotova, "Parallel-Connected Solar PV System to Address Partial and Rapidly Fluctuating Shadow Conditions," Industrial Electronics, IEEE Transactions on, vol. 56, pp. 1548-1556, 2009.

[1.21] G. Petrone, G. Spagnuolo, R. Teodorescu, M. Veerachary, and M. Vitelli, "Reliability Issues in Photovoltaic Power Processing Systems," Industrial Electronics, IEEE Transactions on, vol. 55, pp. 2569-2580, 2008.

[1.22] B. N. Alajmi, K. H. Ahmed, S. J. Finney, and B. W. Williams, "Fuzzy-LogicControl Approach of a Modified Hill-Climbing Method for Maximum Power Point in Microgrid Standalone Photovoltaic System," Power Electronics, IEEE Transactions on, vol. 26, pp. 1022-1030, 2011.

[1.23] E. Serban and H. Serban, "A Control Strategy for a Distributed Power Generation Microgrid Application With Voltage- and Current-Controlled Source Converter," Power Electronics, IEEE Transactions on, vol. 25, pp. 2981-2992, 2010.

[1.24] T. F. Wu, C. H. Yang, Y. K. Chen, and Z. R. Liu, "Photovoltaic inverter systems with self-tuning fuzzy control based on an experimental planning method," in Industry Applications Conference, 1999. Thirty-Fourth IAS Annual Meeting. Conference Record of the 1999 IEEE, 1999, pp. 1887-1894 vol.3.

[1.25] J. A. Halliday, T. Markvart, and J. N. Ross, "Battery management for PV systems," Power Engineer, vol. 17, pp. 46-46, 2003.

[1.26] Florida Solar Energy Center [Online]. Available:http://www.fsec.ucf.edu/en/

[1.27] M. Calais and V. G. Agelidis, "Multilevel converters for single-phase grid connected photovoltaic systems-an overview," *IEEE International Symposium on Industrial Electronics. Proceedings. ISIE'98 (Cat. No.98TH8357)*, Pretoria, South Africa, 1998, pp. 224-229 vol.1.

[1.28] S. B. Kjaer, J. K. Pedersen, and F. Blaabjerg, "A review of single-phase gridconnected inverters for photovoltaic modules," Industry Applications, IEEE Transactions on, vol. 41, pp. 1292-1306, 2005.

[1.29] B. Verhoeven et al.. (1998) Utility Aspects of Grid Connected Photovoltaic Power Systems. International Energy Agency Photovoltaic Power Systems, IEA PVPS T5-01: 1998. [Online]. Available: www.iea-pvps.org

[1.30] M. Meinhardt and G. Cramer, “Past, present and future of grid connected photovoltaic- and hybrid-power-systems,” in Proc. IEEE-PES Summer Meeting, vol. 2, 2000, pp. 1283–1288.

[1.31] F. Blaabjerg, R. Teodorescu, M. Liserre, and A. V. Timbus, "Overview of Control and Grid Synchronization for Distributed Power Generation Systems," Industrial Electronics, IEEE Transactions on, vol. 53, pp. 1398-1409, 2006.

[1.32] B. Sahan, Arau, x, S. V. jo, No, C. ding, and P. Zacharias, "Comparative Evaluation of Three-Phase Current Source Inverters for Grid Interfacing of Distributed and Renewable Energy Systems," Power Electronics, IEEE Transactions on, vol. 26, pp. 2304-2318, 2011.

[1.33] Characteristics of the Utility Interface for Photovoltaic (PV) Systems, IEC 61727 CDV (Committee Draft for Vote), 2002.

[1.34] IEEE Standard for Interconnecting Distributed Resources with Electric Power Systems, IEEE Std. 1547, 2003.

[1.35] S. Halpin, "Comparison of IEEE and IEC harmonic standards," in Power Engineering Society General Meeting, IEEE, pp. 2214-2216, 2005.

[1.36] "IEEE Application Guide for IEEE Std 1547, IEEE Standard for Interconnecting Distributed Resources with Electric Power Systems," IEEE Std 1547.2-2008, pp. 1-207, 2009.

[1.37] C. Yaow-Ming, W. Hsu-Chin, C. Yung-Chu, L. Kung-Yen, and S. Shian-Shing, "The AC Line Current Regulation Strategy for the Grid-Connected PV System," Power Electronics, IEEE Transactions on, vol. 25, pp. 209-218, 2010.

[1.38] University of Strathclyde, A technical report on "An Investigation on DC Injection into Low-voltage AC System," Project Steering Group Work Stream 4 Project WS4-P11, Contract number DG/CG/00002/00/00, DTI/OFGEM Distributed Generation Co-ordinating Group,June 2005.

Chapter 2

Literature survey on photovoltaic system and maximum power point tracking (MPPT) Techniques

This chapter discusses the literature of photovoltaic system and commonly used maximum power tracking (MPPT) techniques. This review includes the composition of the photovoltaic system, which are photovoltaic cell, module and array. The output characteristic curve of PV module is discussed. The classification of the commonly used (MPPT) techniques including their advantages and drawbacks are discussed. A detail comparison which include their application suitability in PV system is also presented.

2.1 Composition of Photovoltaic system

Photovoltaic system is the energy system designed to use solar irradiance to generate electricity. This system consists of modules that have been connected in group of series-parallel form and has fundamental component as solar cell. Figure 2.1 shows the structure of photovoltaic system. The rated power of solar module depends on the number of solar cells used in the design.

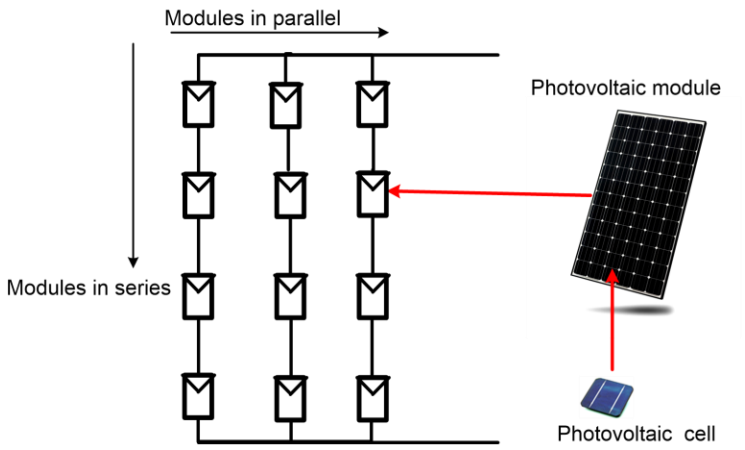

Figure 2.1. Structure of photovoltaic system.

2.1.1 Solar cell

Solar cell is an electrical device that transforms light energy into electricity. It is made up of semiconductor materials, which serves as the fundamental component of the PV module. Since solar cell is made of semiconductor materials, its electrical characteristics such as voltage, current and resistance vary when exposed to light. It behaves as conductor when exposed to light and becomes insulator at low temperature conditions. There are two layers in semiconductor: negative charge on one layer and positive on the other. Electrons are released from the negative layer when solar cell absorb photons after it has exposed to the light. Through the external circuit, these electrons flow to positive layer, which produces electric current [2.1]. Silicon is the most commonly used semiconductor material for solar cell [2.2]. There are different types of solar cells, however amorphous, monocrystalline and multicystalline are the most commonly used solar cells for commercial purposes. These solar cells have merits and demerits based on the targeted application [2.3].

2.1.2 Equivalent circuit of photovoltaic cell

The equivalent circuit of the PV cell with single diode is shown in figure 2.2. The mathematical model that defines the current-voltage characteristic equation are written as follows:

$$I_{pv\_cell} = I_{ph} - I_o - \frac{V_o}{R_p} \tag{2.1}$$

where, I_{pv_cell} is the output current of PV cell, I_{ph} and I_o are light generated current and current of diode respectively. V_o is the voltage across the diode, I_{pv_cell} is the output current of the PV cell and R_p is the parallel resistance. I_o is given by:

$$I_o = I_s \left[exp\left(\frac{V_o}{\alpha V_t}\right) - 1 \right] \tag{2.2}$$

where, α and V_t are ideality factor of the diode and thermal voltage respectively.

The thermal voltage is written as:

$$V_t = \frac{kT}{q} \tag{2.3}$$

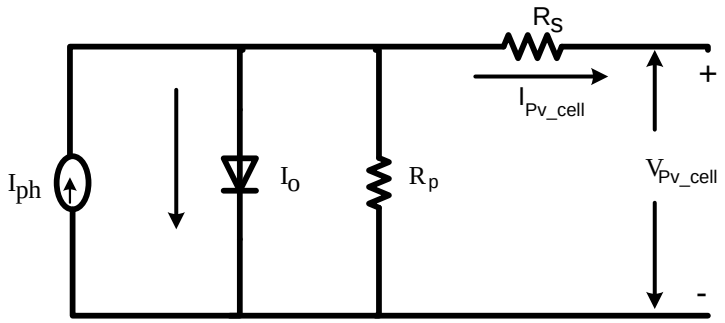

Figure 2.2. Equivalent circuit model for PV cell.

where, T and k are p-n junction temperature (in kelvins) and Boltzmann's ($1.38\,x\,10^{-23}$J/K) constant respectively, q is the charge of electron. The voltage across the diode is given by:

$$V_o = V_{pv\_cell} + I_{pv\_cell}R_s \tag{2.4}$$

where V_{pv_cell} is the output voltage of PV cell. Using equations (2.2), (2.3) and (2.4), the general current voltage characteristic of PV cell in equation (2.1) can be re-written as:

$$I_{pv\_cell} = I_{ph} - I_s\left[exp\left(\frac{V_{pv\_cell} + I_{pv\_cell}R_s}{\alpha V_t}\right) - 1\right] - \frac{V_{pv\_cell} + I_{pv\_cell}R_s}{R_p} \tag{2.5}$$

This current-voltage characteristic expression for PV cell involves five parameters namely α, I_{ph}, I_s, R_s and R_p. The values of R_s and R_p are assume constants even at variable weather conditions [2.4], where I_{ph} and I_s are given by the following expression:

$$I_{ph} = [I_{SC} + k_i(T - T_{STC})]\frac{G}{G_{STC}} \tag{2.6}$$

$$I_s = I_{rr}\left(\frac{T_{STC}^3}{T^3}\right)exp\left(\frac{qE_G}{\alpha k}\right)\left(\frac{1}{T_{STC}} - \frac{1}{T}\right) \tag{2.7}$$

where, I_{rr} and E_G are reverse saturation current and band-gap of the semiconductor material respectively. T is the reference temperature, T_{STC} is the temperature at standard

test conditions, G is the solar irradiance, G_{STC} is the solar irradiance at standard test conditions (STC) and q is the electron charge ($1.60217646\ x\ 10^{-19}C$).

2.1.3 Photovoltaic module

Photovoltaic modules consist of group of series and parallel connected PV cells seal in an environmentally protective laminate and are the basic building block of PV systems. The PV module performance is evaluated according to its output dc power under STC and this STC defined module operating temperature as 25° C with irradiance at 1000 W/m^2 under air mass 1.5 spectral distribution [2.5]. The current-voltage relationship of PV module is obtained in equation (2.8) using the equivalent circuit of identical PV cells connected in series and parallel.

$$I_{pv} = n_p I_{ph} - n_p I_s \left[exp\left(\frac{q\left(V_{pv} + R_s I_{pv}\right)}{\alpha k T n_s} \right) - 1 \right] - \frac{V_{pv} + R_s I_{pv}}{n_s R_p} \quad (2.8)$$

where, n_p and n_s are number of parallel and series connected PV cell respectively, I_{pv} and V_{pv} are PV module output current and voltage respectively. The PV output characteristic is the current-voltage (I-V) and power-voltage (P-V) curves under STC. The parameters which

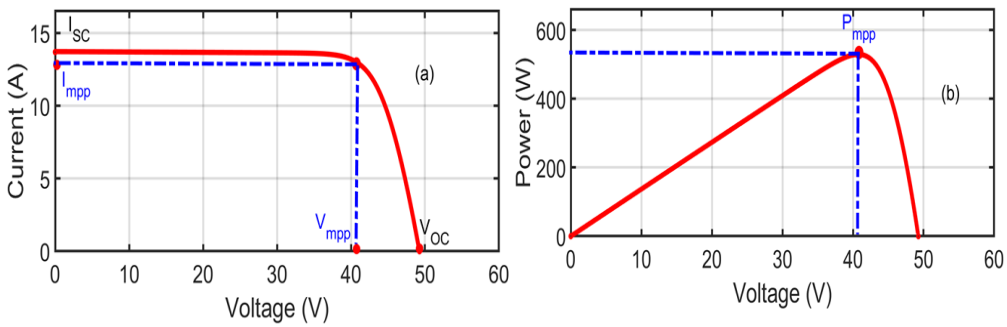

Figure 2.3. PV output characteristic showing five key parameters.

describe the PV output characteristic are short circuit current (I_{SC}), current at maximum power point (I_{mpp}), voltage at maximum power point (V_{mpp}), open circuit voltage (V_{oc})

and power at maximum power point (P_{mpp}). Figure 2.3 shows the PV module characteristic curves with these parameters. Apart from the aforementioned key parameters, temperature coefficient of short circuit current, k_i and temperature coefficient of open circuit voltage k_v also play crucial role on the performance of PV characteristic under variable weather conditions. These parameters are provided by the manufacturer datasheet. Table 2.1 shows a typical manufacturer data sheet of a PV module SX-80W.

Table 2.1. PV module parameters (SX-80W).

Parameter	**Value**
Maximum power (P_{max})	80 W
Voltage at P_{max} (V_{mp})	16.80 V
Current at P_{max} (I_{mp})	4.75 A
Short-circuit current (I_{SC})	5.17 A
Open circuit voltage (V_{OC})	21.00 V
Temperature coefficient of (I_{SC})	(0.065 ± 0.015)mA/℃
Temperature coefficient of (V_{OC})	-(80 ± 10)mV /℃

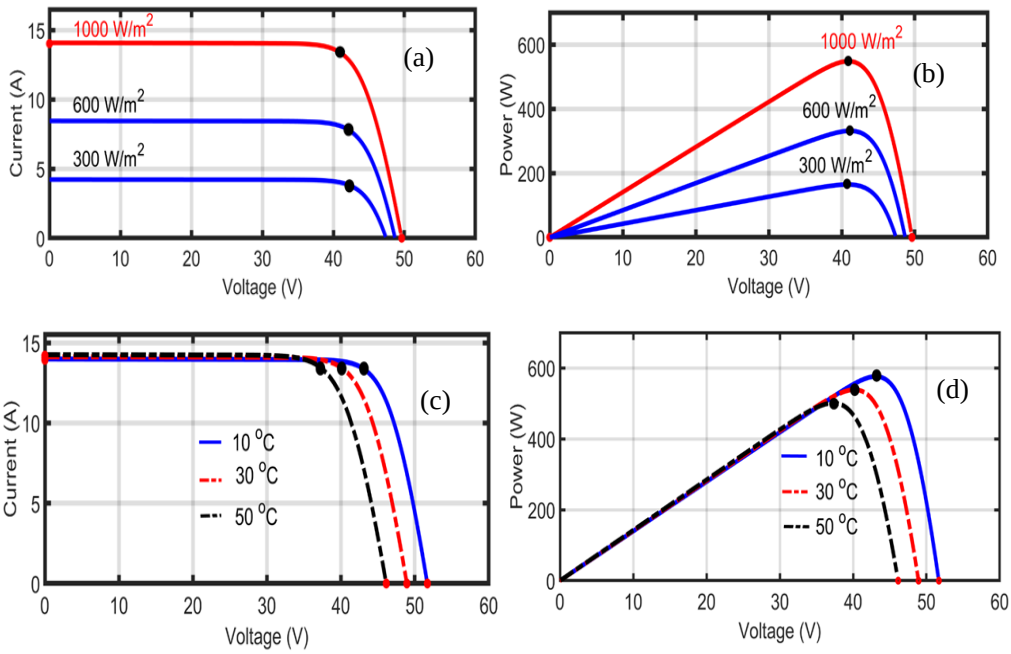

Figure 2.4. Effect on PV module. (a,b) variable irradiance, (c,d) variable temperature.

Figure 2.4 (a,b) and (c,d) show that the performance of the PV characteristic largely depends on the variation of irradiance and temperature [2.6]. It can be seen that, temperature has extensive impact on V_{oc} but little impact on I_{sc}. Also I_{sc} shows a direct significant dependence on irradiance while the V_{oc} dependency on irradiance follows logarithmic function [2.7].

2.1.4 Photovoltaic array

PV array comprises a number of series and parallel connected PV modules to achieve the needed rated output power. The rated power depends on the number of PV module assembled. The output power from the PV array is the total power generated from each PV module [2.8]. The output power of the PV array is given by:

$$P_{array} = I_{pv}N_p \times V_{pv}N_s \tag{2.9}$$

where, N_p is the number of strings connected in parallel in the PV array, N_s is the number of PV module connected in series to form a string. Each PV module in a string should

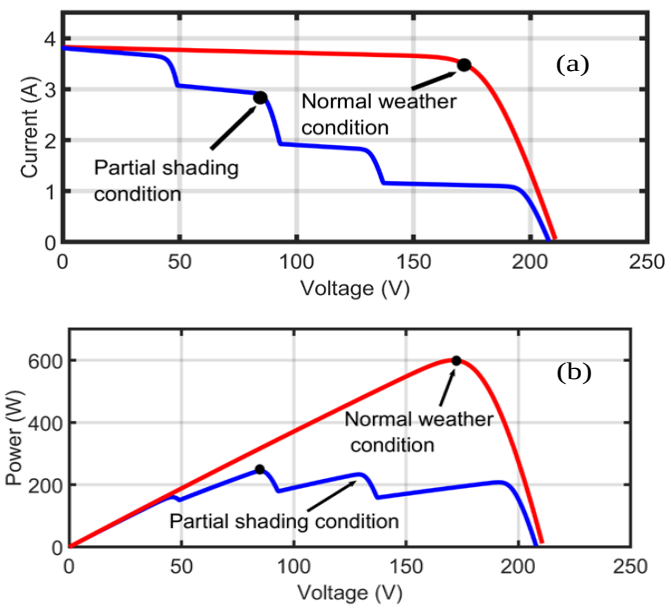

Figure 2.5. I-V and P-V characteristic curve under normal and partial shading conditions.

have the same parameter values to obtain the same parallel voltage. The graph of current versus voltage and that of power versus voltage are temperature and irradiance dependent. When PV modules in a given PV system is exposed to uniformly distributed irradiance, single peak is generated on the P-V and I-V characteristic curves [2.9]-[2.11]. However, when the PV modules are exposed to non-uniformly distributed irradiance, multiple peaks are generated on the P-V and I-V curves. Figure 2.5 demonstrates the impact of irradiance on the PV array system. The PV system is a string with 10 series connected PV modules. The simulation result shows that under uniformly distributed weather conditions, only one peak is generated by the PV characteristics, however, under partial shaded conditions where PV module received non-uniformly distributed irradiance, multiple peaks are generated with significant reduction of PV output power.

2.2 Photovoltaic system

The two modes of operation for PV system are grid connected and standalone. In each mode of operation, MPPT is essential at any weather conditions to force the PV modules to operate at maximum power point (MPP).

2.2.1 Concept of maximum power point tracking (MPPT) technique

At any given point in time, the PV module operates at a particular voltage and current. To ensure that maximum power is delivered by the PV module, it is imperative to force the PV module to operate at such operating point. This point corresponds to peak of the P-V curve or the kneel of the I-V curve. The simple way to do this is to force the voltage of the PV module to be that at the MPP or regulate the current as that of MPP using power interface. The power interface can be of any topology of dc-dc converter such as boost, buck, Cuk, SEPIC and buck-boost converters [2.12]-[2.13]. The power interface is controlled to include the MPPT algorithm. The MPPT algorithm controls the voltage of the PV module or the duty cycle of the power converter interface. Assume that boost converter is used, MPPT must generate duty cycle equivalent to the duty cycle of the boost converter given by;

$$D = 1 - \frac{V_{pv}}{V_O} \tag{2.10}$$

where, V_{pv} is the output voltage of the PV module, and V_O is the voltage of the battery (islanded operation) or the dc link (grid connected). Figure 2.6 demonstrates the three different operating points namely, A, B and C of the PV module under variable irradiance conditions. When irradiance changed from G_1, to G_3 through G_2, the operating point of the PV module also changes from point A to B and then finally to C. Depending on the position of the operating point, the MPPT generates the suitable duty cycle to control the converter to ensure that operating point of the PV module lies at the exact positions of A, B or C.

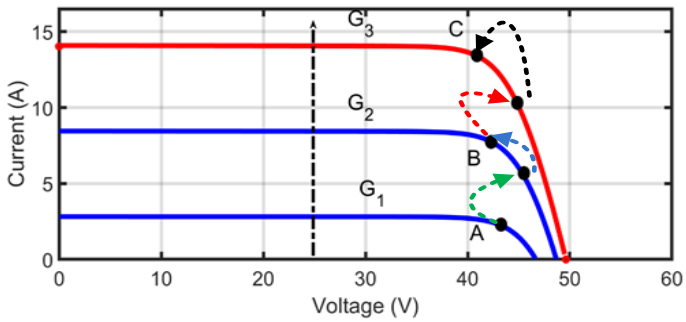

Figure 2.6. Controlling the operating point of PV module using MPPT.

2.2.2 Implementation strategies of MPPT

Implementation strategy is an important factor to consider when choosing MPPT for a given PV system application. This depends on the knowledge of the end-users on analog circuitry or digital circuitry as well as the number of sensors required to implement the MPPT. Based on these factors, MPPT technique can be categorized into four according to its implementation. Most MPPT techniques use current sensor or voltage sensor or combination of current and voltage sensors for their implementation. Figure 2.7 shows

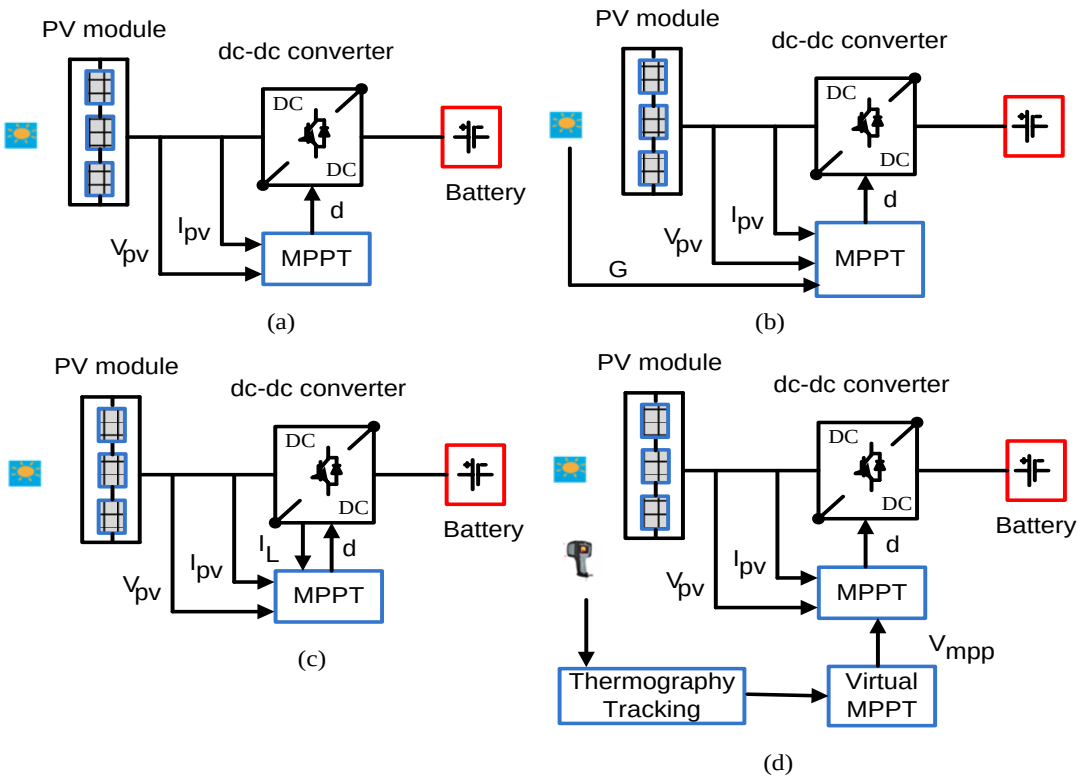

Figure 2.7. Different implementation strategies for MPPT: (a) Two sensors at PV module, (b) Additional sensor for irradiance, (c) additional sensor to measure inductance current, (d) additional sensor for thermography camera.

various methods for implementing MPPT. The implementation strategy for MPPT shown in figure 2.7(a) requires either voltage sensor or current sensor or combination of both, connected between the PV module(s) and the power converter. It is important to note that many MPPT techniques are being implemented by this strategy [2.14-2.15]. Figure 2.7(b) shows another method for implementing MPPT where additional irradiance sensor apart from the voltage and current sensors is required. Most MPPT techniques based on this implementation are expensive [2.14]. Other MPPT techniques including sliding mode (SM) control require two current sensors of high bandwidth for practical implementation [2.16]. These two sensors are for the measurement of PV module(s) current and inductor current. MPPT technique with more current sensors are expensive. Currently, thermographic camera has also been employed in the PV system application to identify

ageing cells, hotspots of PV module during partial shading and to visualize the surface temperature of the PV module(s) [2.17-2.19]. Figure 2.7 (d) shows MPPT implementation scheme based on thermography principles. This implementation scheme requires sensor for thermography camera which makes the MPPT expensive. Thus, implementation scheme without complexity, cost effective and more efficient are the best factors to consider. Among four implementation schemes discussed above, only Figure 2.7 (a) implementation scheme with two sensors connected between PV module and power converter is common for most MPPT applications. This thesis focuses on this (Figure 2.7 (a)) implementation scheme to investigate MPPT techniques under different classification groups.

2.2.3 Classification of MPPTs

Generally speaking, there are two key factors that need to be well-thought-out when assessing the performance of MPPT techniques [2.20]. These factors are steady-state and dynamic operating conditions. During the steady-state conditions, the weather condition is fixed, the operating point of the PV module is around MPP and the efficiency of MPPT at this condition is a measure of MPPT performance. During variable weather condition, the operating point of the PV module changes and the new MPP need to be tracked. This is the dynamic condition and the efficiency at this condition describes the tracking performance of MPPT. The actual efficiency is normally higher than 98% [2.21]. The literature shows many MPPT techniques proposed by many researchers [2.22]. These MPPT techniques can be classified into three groups according to their characteristics, namely, model based, heuristic and hybrid techniques [2.23]-[2.25].

- Model based technique uses the concept of the PV module mathematical model to track MPP [2.24]. This method provides faster tracking speed; however, the performance of this technique is largely affected by the accuracy of the mathematical model of the PV module constant parameters.
- Heuristic technique uses trial and error tracking technique to locate MPP [2.24]. The principle behind this model is that, the algorithm perturbs the PV output voltage. The algorithm then observes the impact due to the perturbation and a suitable feedback

correction is initiated. The advantage of this model is that it does not require parametric data for its implementation compared to the model-based method. However, the main drawback is that the technique performs several iterations before reaching MPP and its performance is poor under rapidly changing irradiance and temperature conditions.

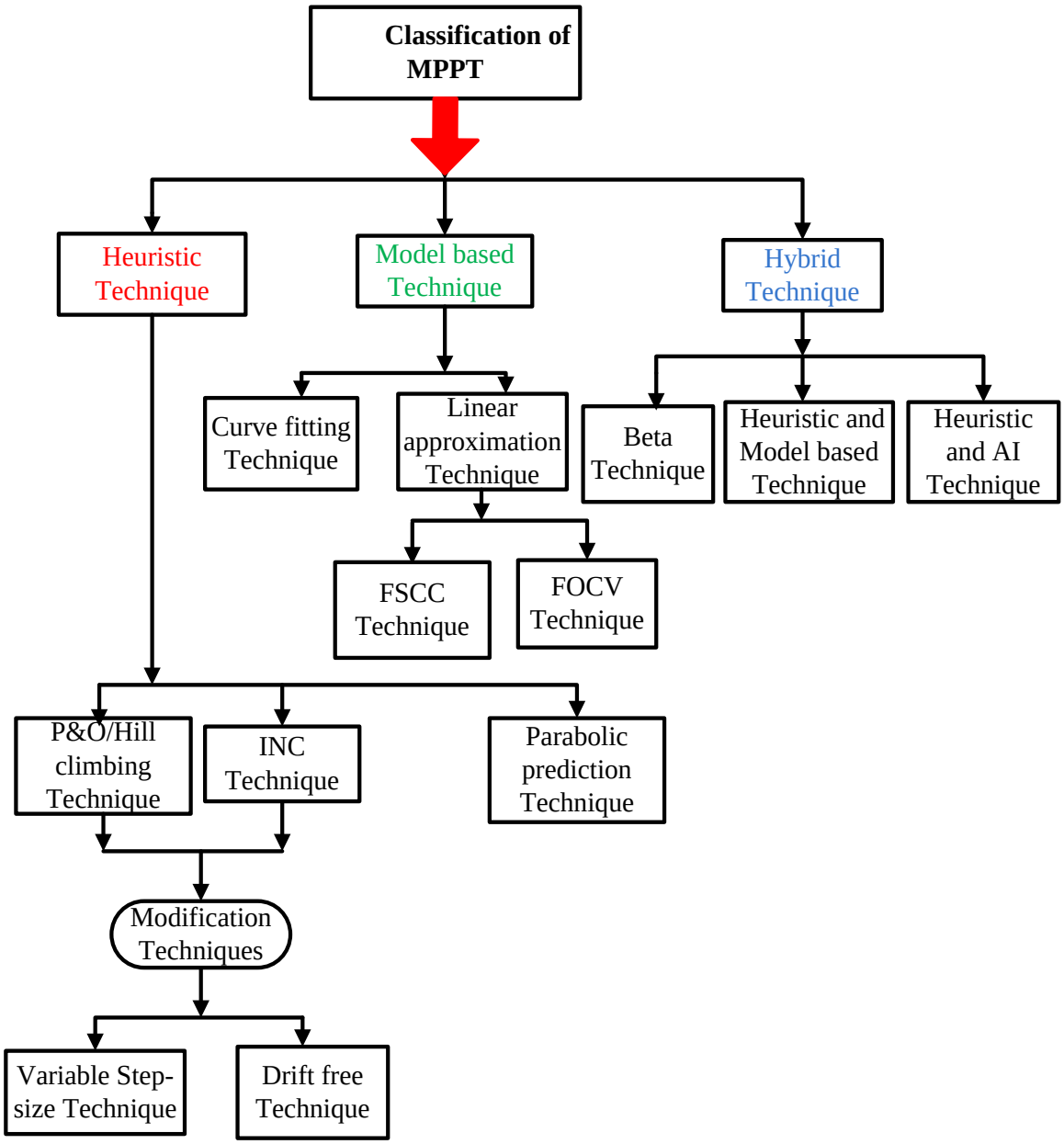

Figure 2.8. Classifications of MPPT based on implementation scheme.

- Hybrid technique is the combination of model based and heuristic methods in which the merits of these two techniques are used to outweigh their disadvantages [2.19]. There are two operating stages under this technique namely, steady state and dynamic state. During the dynamic state, the location of MPP is calculated and operating point is moved closed to it using model based technique. The heuristic technique then used to track the MPP at steady-state.

2.3 Heuristic MPPT techniques

2.3.1 Incremental conductance (INC) and perturb observe (P&O)/Hill climbing techniques

INC and P&O/hill climbing are the most common heuristic MPPT techniques in PV system application. The tracking mechanism of INC and P&O are illustrated by the following mathematical expressions deduced from the P-V characteristic curve shows in figure 2.9 (a) and (b). The PV module has an output power given as:

$$P_{pv} = V_{pv} I_{pv} \tag{2.11}$$

By differentiating equation (2.11), the slope of PV module is obtained in equation (2.12).

$$\frac{dP_{pv}}{dV_{pv}} = I_{pv} + V_{pv} \frac{dI_{pv}}{dV_{pv}} \tag{2.12}$$

Thus, INC algorithm can be expressed as in (2.13), (2.14) and (2.15).

$$\frac{dP_{pv}}{dV_{pv}} = 0, \qquad \frac{dI_{pv}}{dV_{pv}} = -\frac{I_{pv}}{V_{pv}} \quad \text{at the MPP} \tag{2.13}$$

$$\frac{dP_{pv}}{dV_{pv}} > 0, \qquad \frac{dI_{pv}}{dV_{pv}} > -\frac{I_{pv}}{V_{pv}} \quad \text{at the left of MPP} \tag{2.14}$$

$$\frac{dP_{pv}}{dV_{pv}} < 0, \qquad \frac{dI_{pv}}{dV_{pv}} < -\frac{I_{pv}}{V_{pv}} \quad \text{at the right of MPP} \tag{2.15}$$

Similarly, the mathematical expression for P&O is given by:

$$dP_{pv} = 0 \ , At\ the\ MPP \tag{2.16}$$

$$dP_{pv} > 0 \ \&\& \ dV_{pv} > 0 \ , To\ the\ \ left\ of\ MPP \tag{2.17}$$

$$dP_{pv} < 0 \ \&\& \ dV_{pv} > 0 \ , To\ the\ right\ of\ MPP \tag{2.18}$$

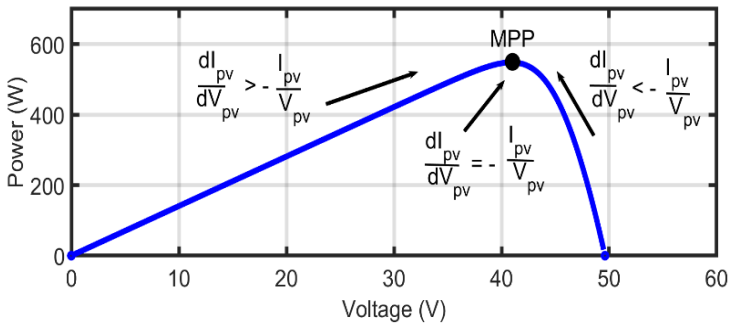

(a)

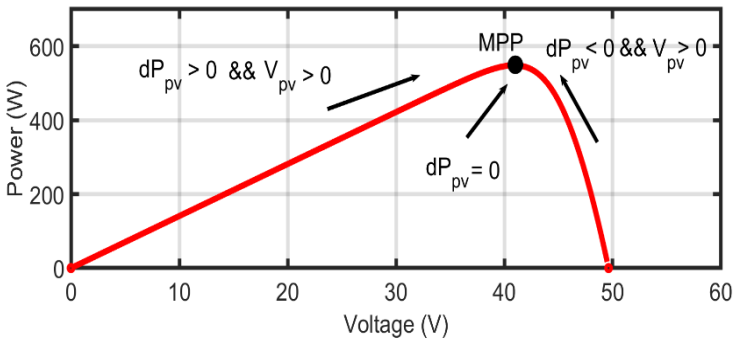

(b)

Figure 2.9. The principles of operation of (a) INC MPPT, (b) P&O MPPT.

Both these algorithms involve direct measurement of current, voltage or power in more accurate response. With INC MPPT technique, the MPP is tracked by comparing

(dI_{pv}/dV_{pv}) to (I_{pv}/V_{pv}). The operation of the PV module is kept around MPP once MPP is reached unless there is a change in the current of PV module which means both irradiance and MPP have changed. Then, the algorithm controls the PV module voltage to follow the reference to continuously track the new MPP. Also, with P&O MPPT technique, the perturbation is provided to the PV module voltage and this translates to an increase or decrease in power. If the increase in voltage leads to an increase in power, this means the operating point is to the left of the MPP and hence further voltage perturbation is required towards the right to reach MPP. Otherwise, if the increase in voltage leads to a decrease in power, this means that the current operating point is to the right of the MPP and hence a reversed voltage perturbation is required towards the left to reach the MPP. In this way the algorithm converges towards the MPP with several perturbations. It is important to note that P&O and hill climbing use the same concept for optimum operating search. Hill climbing works by perturbing the PV module voltage by changing the duty cycle of the power converter and observing its effect on the output power of the PV module until maximum power is extracted. Table 2.2 illustrates the perturbation directions of P&O MPPT. The steady state performance of both INC MPPT and P&O MPPT techniques are demonstrated using figure 2.10. Q is the point positioned on the left of MPP while S is the point positioned at the right of MPP. R is the point on MPP. Assuming perturbation is provided to the PV module and the operating point is shifted from Q to R. This means that INC MPPT and P&O MPPT are operating in the conditions of $dI_{pv}/dV_{pv} > -I_{pv}/V_{pv}$ and $dP_{pv} > 0$ && $dV_{pv} > 0$ respectively. If, further perturbation is applied and shifts the operating point from R to S the INC MPPT

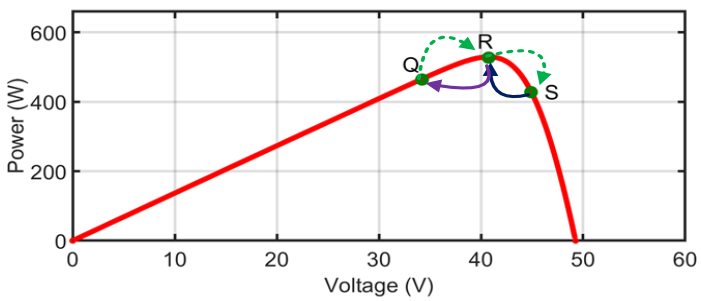

Figure 2.10. Steady state performance of INC MPPT and P&O MPPT.

and P&O MPPT satisfied the conditions of $dI_{pv}/dV_{pv} < -I_{pv}/V_{pv}$ and $dP_{pv} < 0$ && $dV_{pv} > 0$ respectively. This trajectory of movement of operating point from Q to S through R and then from S to R and finally to Q constitutes steady state oscillations around MPPT. In most circumstances, INC MPPT and P&O MPPT tracking process follow the right trajectory toward the MPP. Nevertheless, at some point under rapid increased in irradiance, the operating point drift from MPP resulting in substantial power loss [2.26].

Table 2.2. Direction of Perturbation in P&O.

Initial voltage perturbation, V_{pv}	**PV power change, dP_{pv}**	**Next perturbation**
Positive	Negative	Negative
Positive	Positive	Positive
Negative	Negative	Positive
Negative	Positive	Negative

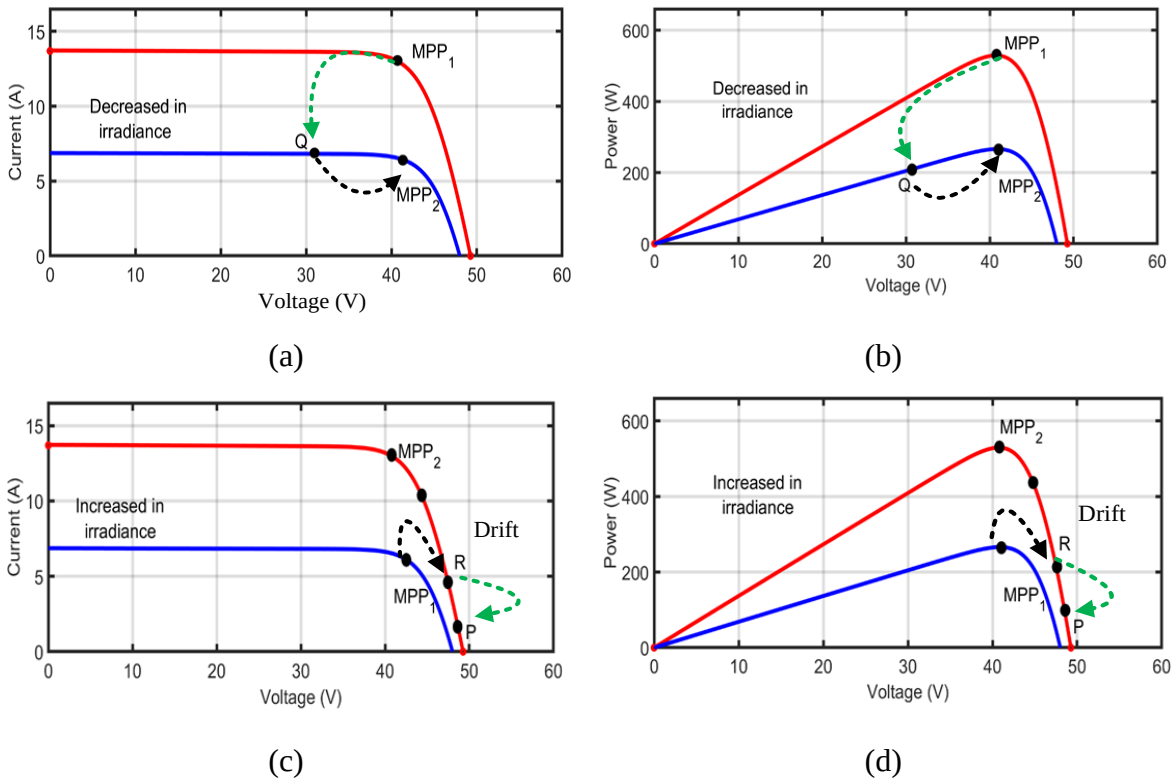

Figure 2.11. Effect of drift on INC MPPT and P&O MPPT (a,b) Current, power under sudden decrease in irradiance, (c,d) Current, power under sudden increase in irradiance.

Figure 2.11 shows the effect of drift on MPPTs operating point during rapid changes in irradiance. During rapid decrease in irradiance, the operating point move from MPP1 to Q. At this condition, change of PV module current, voltage and power decreased as shown in Figure 2.11(a,b). Both INC MPPT and P&O MPPT techniques operate in the conditions $dI_{pv}/dV_{pv} > -I_{pv}/V_{pv}$ and $dP_{pv} > 0$ && $dV_{pv} > 0$ respectively. Thus, both techniques follow the right trajectory toward MPP2 with no drift. Conversely, when the irradiance increased suddenly, the operating point shifted from MPP2 to R. The change in PV module current, voltage and power at this condition increased as shown in Figure 2.11(c,d). However, both INC MPPT and P&O MPPT techniques operate in the conditions of $dI_{pv}/dV_{pv} < -I_{pv}/V_{pv}$ and $dP_{pv} < 0$ && $dV_{pv} > 0$ respectively. Therefore, both techniques follow wrong trajectory toward P. Thus, these techniques experienced drift when approaching MPP1. The problem of drift is as a result of the failure of algorithm to distinguish the increased in PV output power due to the modulation of duty cycle from

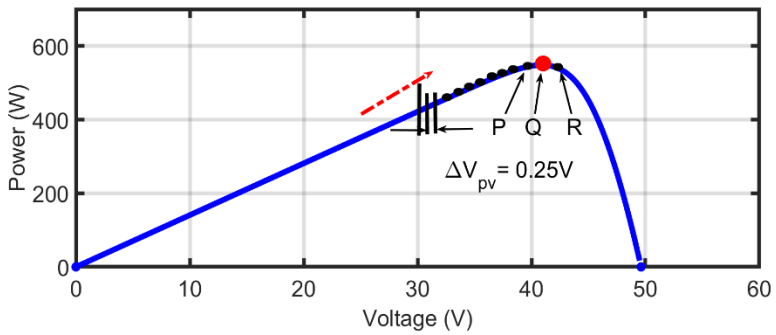

(a)

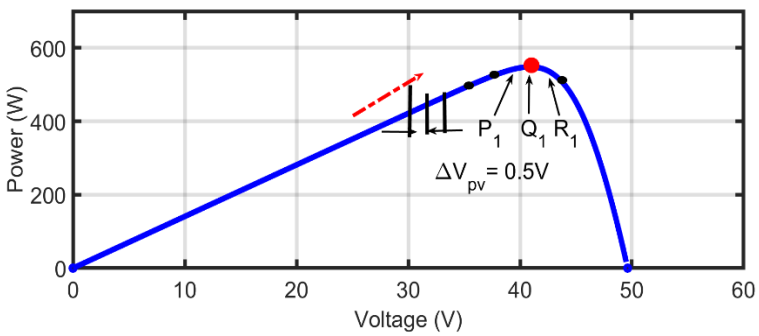

(b)

Figure 2.12. The INC and P&O techniques, (a) 0.25V step-size, (b) 0.5V step-size

variable irradiance [2.27]. The tracking performance of both INC MPPT and P&O MPPT largely depend on fixed step size [2.28]. However, it is difficult for both techniques to achieve good dynamic and steady state performance with fixed step size. The use of small step size results in lesser oscillations around MPP but the algorithms use more time to reach MPP. Conversely, the use of big step size speed-up the tracking process, however, significant oscillations are noticed at steady state. Figure 2.12 demonstrates the effect of fixed step size on both INC MPPT and P&O MPPT techniques. Two different values namely, 0.25V and 0.5V are applied in the two algorithms. It is evident that, with 0.25V step-size in Figure 2.12 (a), the algorithms require more steps to reach MPP. This means the algorithms use more time to reach MPP. Also, with 0.5V step size in Figure 2.12 (b), the algorithms require few steps to reach MPP. Smaller step size results in lower oscillations around MPP while bigger step size results in more oscillations around MPP. It is evident from the discussions that both INC MPPT and P&O MPPT techniques have two major limitations.

- Operating point drifts away from MPP during rapid increased in irradiance.
- Trade of issues due to fixed step size used for tracking MPP. The effect is slow tracking speed or significant oscillations around MPP.

Many modifications of INC MPPT and P&O MPPT have been presented in the literature to address these limitations. The following discuss some modification of these algorithm.

A) Drift free technique

Several modifications in the literature have been presented to address drift problem in MPPT techniques during changes in irradiance. A solution is proposed in [2.29], where a constraint is applied on the step-size of the perturbation. However, large change in irradiance requires large perturbation step-size and this constitutes significant steady state oscillations. A solution is proposed in [2.30] by defining the boundary condition to establish the upper and the lower limit for PV power change, (dP_{pv}). Since the threshold value of (dP_{pv}) is irradiance dependent, the solution is not optimum. Full curve evaluation algorithm is also proposed in [2.31]. In this solution, the trend of the entire P-V characteristic curve is evaluated under fast changes in irradiance. However, it is

impossible to evaluate the behavior of the P-V curve under fast changes in irradiance due to the changes in operating point under such condition. Since an increase in irradiance results in drift, it is important to introduce a change in output current of PV module, (dI_{pv})

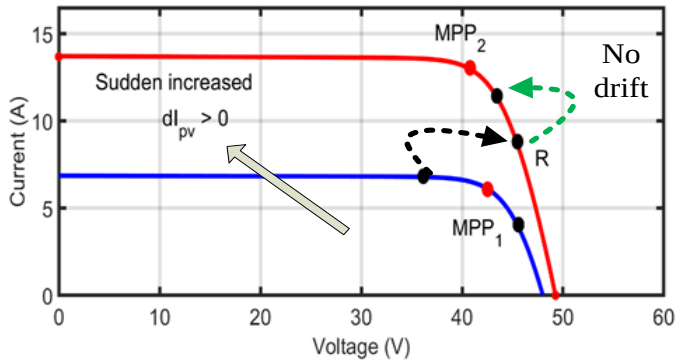

(a)

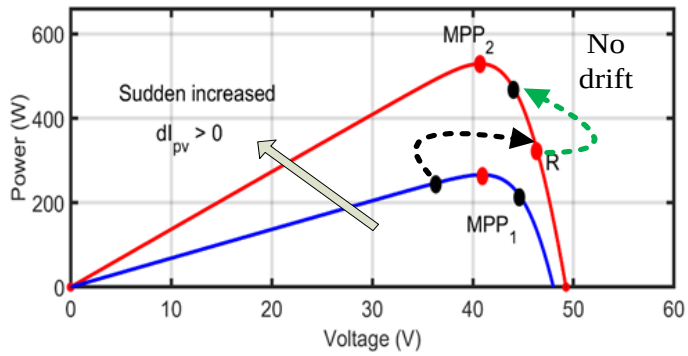

(b)

Figure 2.13. Drift free analysis of INC MPPT and P&O MPPT techniques.

in (2.14) and (2.17). This is because a change in irradiance is directly proportional to the change (dI_{pv}). Thus, the authors in [2.32-2.33] integrated the change in current (dI_{pv}) of the PV module in addition to the change in PV module power, (dP_{pv}) and voltage (dV_{pv}) in the decision process to avoid drift under rapidly changing in irradiance. Figure 2.13 demonstrates drift free of INC MPPT and P&O MPPT. Thus, P&O is modified given by the following expression.

$$dP_{pv} > 0 \;\&\&\; dV_{pv} > 0\,,\; dI_{pv} > 0,\;\; To\ the\ \ right\ of\ MPP \tag{2.19}$$

$$dP_{pv} > 0 \;\&\&\; dV_{pv} < 0,\; dI_{pv} < 0,\;\; To\ left\ of\ MPP \tag{2.20}$$

Similarly, INC MPPT technique is modified as,

$$\frac{dI_{pv}}{dV_{pv}} > -\frac{I_{pv}}{V_{pv}}, \qquad I_{pv} > 0\;\; To\ the\ right\ of\ MPP \tag{2.21}$$

$$\frac{dI_{pv}}{dV_{pv}} < -\frac{I_{pv}}{V_{pv}}, \qquad I_{pv} < 0\;\; To\ the\ left\ of\ MPP \tag{2.22}$$

b) Variable step-size modification

In general, fixed step side is being used in both INC and P&O MPPTs to draw maximum power from the PV module. The tracking speed and steady state oscillation are dependent on the size of step value. However, the method used to choose the step size value is not generic and system dependent. Bigger step size value for drawing power from the PV Module contributes to faster speed tracking, however, the algorithm experiences more oscillations at steady state. Conversely, smaller step size value minimizes oscillations at steady state, however, algorithm spends longer time to reach MPP. Thus, INC and P&O MPPTs have tradeoff issues. To address this issue, variable step size technique was developed in [2.34]. This technique is based on the gradient of the P-V characteristic curve and initially applied in only P&O and hill climbing techniques. Also, certain parameters to explain the technique further were not given. A variable step size is introduced in [2.35] and this developed a simple approach to improve tracking speed and to reduce oscillations of the algorithm. This technique was extended in INC MPPT and is based on the slope of the P-V characteristic curve [2.34] and the slope of P-D characteristic curve [2.36]. Figure 2.14 shows that the slope (dP_{pv}/dV_{pv}) of the P-V characteristic curve differs at the left and right side of the P-V characteristic curve and varies with magnitude and so a scaling factor, N is required to adjust the slope in order to balance the left and right asymmetry of

the P-V characteristic curve. The main drawback of this technique is that N is a fixed value and not be suitable for all irradiance and this asymmetry becomes more substantial when irradiance decreases as demonstrated by dotted line in Figure 2.14. A new variable step size is proposed in [2.37] which uses symmetrical method. The mathematical expressions related to this method is given by

$$\begin{cases} A = 1 - \left|\frac{I_{pv}}{V_{pv}}\right| \Big/ \left|\frac{dI_{pv}}{dV_{pv}}\right| , To\ the\ right\ of\ MPP & (2.23) \\ B = 1 - \left|\frac{dI_{pv}}{dV_{pv}}\right| \Big/ \left|\frac{I_{pv}}{V_{pv}}\right| , \ To\ the\ left\ of\ MPP & (2.24) \end{cases}$$

The functions A and B are symmetrical to the MPP and remains symmetrical even in an event of changes in irradiance conditions and becomes more adaptive than asymmetrical. Several amendments have been presented to address the drawbacks in variable step-size MPPT technique. In [2.38], two step-size values were applied to limit oscillations at steady-state. The selected values of step-size only minimise oscillations at the selected irradiance conditions. A new variable step-size fuzzy logic-based INC technique has been

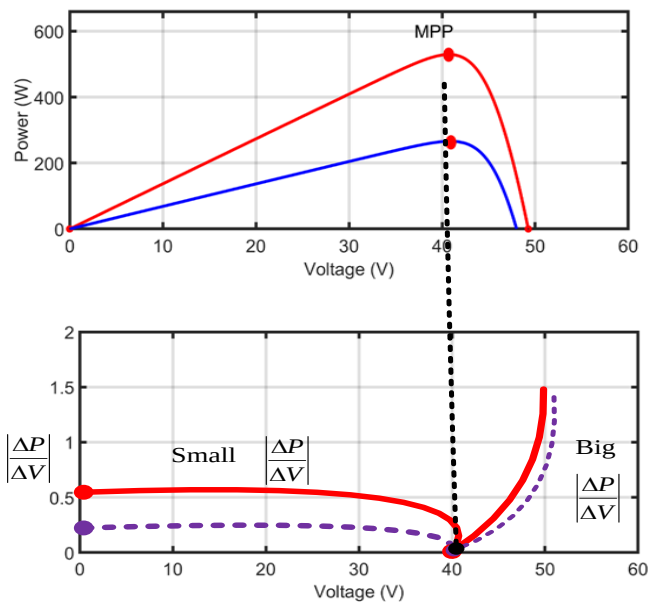

Figure 2.14. Variable step-size algorithm.

discussed in [2.39]. The fuzzy logic controller varies the fixed step-size value to reach MPP quickly. The algorithm allows fast and accurate convergence under different operating conditions. However, the process is complicated and system dependent as it is required to store MPP values in advance. In [2.40], the slope of the PV curve was compared with two arbitrary points on the I-V curve to select three different step-size values suitable for the whole operating range. Although the algorithm improves the dynamic performance, it encounters poor steady-state performance around MPP. An enhancement was introduced in [2.41] by removing all division terms to avoid the impact of small changes in the voltage values. Therefore, oscillation is reduced significantly, however, the algorithm experienced slow tracking speed at the initial operating stage of the PV system. On the other hand, modifications have been also presented to select a suitable scaling factor for the conventional variable step-size in INC technique. In [2.42], a root locus technique was derived to obtain an optimum value of the scaling factor. The algorithm achieved steady-state accuracy and dynamic response only at selected irradiance conditions. In [2.43], two different scaling factor values were introduced. Although, the MPP is tracked, selected scaling factors are not optimum under all operating

Table 2.3. INC and P&O with variable step-size.

Reference	Perturb step-size	Comments
[2.31]	$d(k) = d(k-1) + M\frac{dP_{pv}}{dV_{pv}}$	It has more computational complexity however, the scaling factor, M is automatically calculated.
[2.46]	$d(k) = d(k-1) \pm \left\lvert \frac{dP_{pv}/\Delta d}{P_{pv}/d} \right\rvert$	Due to the derivative term, the technique has high computational complexity
[2.47]	$d(k) = d(k-1) \pm \frac{M\lvert dP_{pv}\rvert}{d(k-1)}$	M is predefined and not system dependent. It can only work effectively under selected irradiance conditions.
[2.48]	$d(k) = d(k-1) + M\frac{dP_{pv}}{dV_{pv}}$	The derivative term is less non-linear; however, the M is predefined and fail to adjust the perturb step-size under variable weather conditions.

circumstances. Regarding P&O MPPT technique, several modifications have been proposed and published in the literature. In [2.44], a solution is proposed to vary the perturb value. Although, the proposed algorithm provides fast response with reduced oscillation around MPP, however, the variable perturbation size is irradiation dependent and may fail to perform effectively under partial shading condition. A parameter estimation approach measured PV current and voltage to estimate the irradiance and temperature is proposed in [2.45]. The proposed solution reduced the tracking time with reduced oscillation but the algorithm has high computational complexity and the estimated parameters do not provide true MPP. Table 2.3 further shows different variable step size expressions suggested in the literature to address drawbacks in both INC and P&O MPPT.

2.3.2 Parabolic prediction technique

Parabolic prediction method is also a family of heuristic method. It is believed that this method provides a good approximation of the variation of PV module power as a function of variation of PV module voltage [2.49-2.50]. The basic concept of the parabolic prediction is demonstrated in Figure 2.15 where parabolic function $Q(x)$ is adopted to estimate the objective function $f(x)$ given by:

$$Q(x) = \ Ax^2 + Bx \ + C \tag{2.25}$$

By locating three point (x_o , x_1 , x_2) on the objective function $f(x)$, equation (2.25) is transformed as follows:

$$Q(x) = f(x_o)\ \frac{(x - x_1)(x - x_2)}{\Delta x_{o1} * \Delta x_{02}} + f(x_1)\frac{(x - x_o)(x - x_2)}{\Delta x_{10} * \Delta x_{12}} + f(x_2)\frac{(x - x_o)(x - x_1)}{\Delta x_{20} * \Delta x_{21}} \tag{2.26}$$

where $\Delta x_{i\,j} = x_i - x_j \qquad i\,, j = 0\,, 1\,, 2$

This concept is mimicked to derive mathematical expression using P-V characteristic curve where optimum working condition can be obtained to give maximum PV output power. With the P-V characteristic curve shown in Figure 2.16, the parabolic function is written as:

$$P_{pv} = AV_{pv}^2 + BV_{pv} + C \tag{2.27}$$

where, A, B and C are constants. Three points, (V_1, P_1), (V_2, P_2) and (V_3, P_3) are assumed to be on the P-V characteristic curve. To demonstrate the iteration process for parabolic technique, (V_1, P_1), (V_2, P_2) and (V_3, P_3) are measured to calculate the constants values A, B and C. Figure 2.17 explains the iteration stages of parabolic

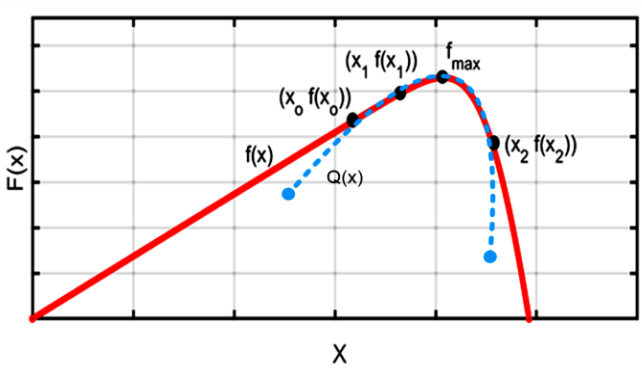

Figure 2.15. Parabolic approximation technique

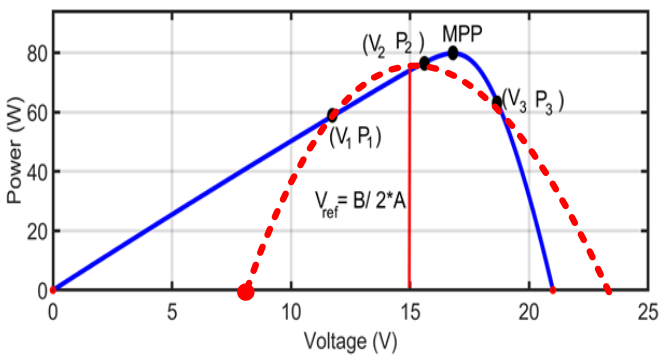

Figure 2.16. Approximating P-V characteristic curve using Parabolic technique.

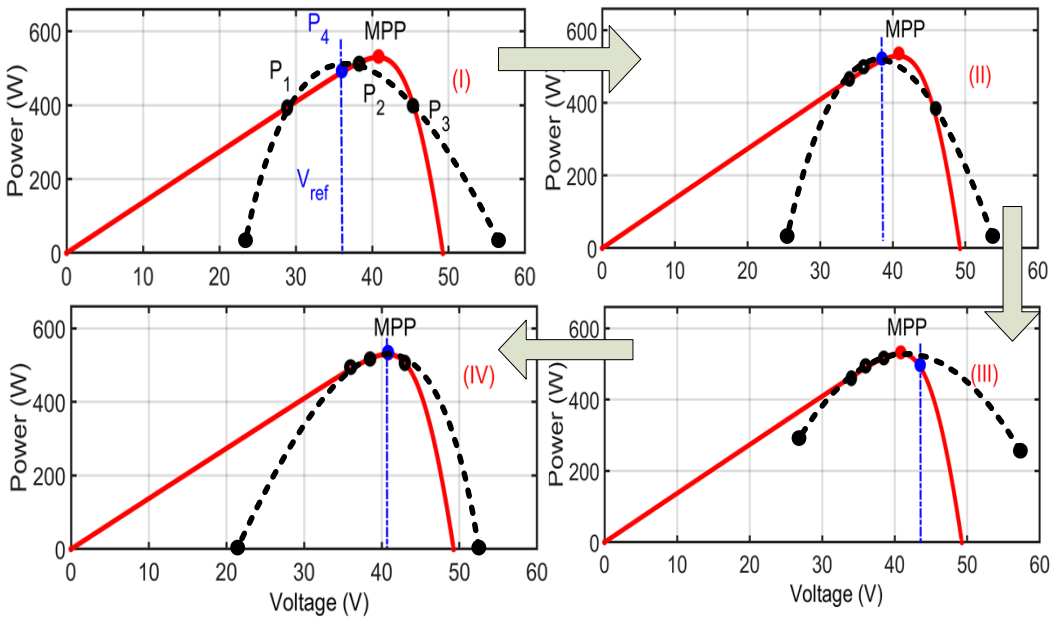

Figure 2.17. Demonstrating iteration stages for parabolic prediction MPPT.

technique to locate MPP. By moving the operating point towards the vertex of the curve which is the peak voltage given by

$$V_{peak} = -\frac{B}{2A} \tag{2.28}$$

where, $A < 0$. After locating the new position of the operating point, the corresponding value of P_4 is compared to the measured value of, P_1, P_2 and P_3. The least among these P_1, P_2, P_3 and P_4 is discarded and the next iteration is performed using the rest of the three power values. This process is repeated until MPP is tracked which almost equal to the reference power given in (2.29)

$$P_{peak} = C - \frac{B^2}{4 * A} \tag{2.29}$$

The coefficient A, B and C are calculated using the three-sampling voltage and power values based on three different duty cycle explained in [2.51 -2.53] as

$$P_1 = AV_1^2 + BV_1 + C \tag{2.30}$$

$$P_2 = AV_2^2 + BV_2 + C \tag{2.31}$$

$$P_3 = AV_3^2 + BV_3 + C \tag{2.32}$$

Thus, the peak voltage, V_{peak} and the reference power, P_{peak} can be calculated. This technique has fast convergence speed; however, the selected initial point determines the rate at which the technique converges at the MPP [2.54]. A solution based on parabolic prediction is proposed in [2.55] to draw maximum power from the PV module where, the three previous working duty step and their power data are used to establish parabolic curve. The results demonstrate good dynamic response under variable weather condition. In [2.56], a parabolic prediction is proposed where the number of current scans equal to the series connected solar modules are utilized to calculate the global maximum power point (GMPP) under partial shading condition. The results show fast tracking GMPP with efficiency around 99.6%.

2.4 Model based method

Model based MPPT techniques are those algorithms, which do not give the true MPP. They are linear approximation and curve fitting techniques.

2.4.1 Linear approximation technique

The most commonly used linear approximation techniques are the fractional open-circuit voltage (FOCV) [2.57] and fractional short-circuit current (FSCC) [2.58] techniques. Figure 2.19 shows the linear relationship that exists in FOCV and FSCC MPPT techniques. Both FSCC and FOCV MPPT techniques use near linear relationship between the current at maximum power point, I_{mpp} and short circuit current, I_{sc} and voltage at maximum power point, V_{mpp} and open circuit voltage, V_{oc} respectively to track MPP. The advantage of this technique is that it is easy to implement and also, only one sensor is required. However, the technique has some disadvantages. First, it does not give the true MPP since it only provides an estimated MPP. Second, its implementation requires momentarily shutting down the PV array and measure the open circuit voltage under a given temperature and irradiance conditions. This process leads to substantial power loss. It was also stated in [2.59] that, k_{FOCV} is not valid under partial shading conditions and the algorithm requires additional modification to update k_{FOCV}. Such modification adds

to the implementation complexity and leads to additional power loss. Also, under variable weather conditions, the current at maximum power point, I_{mpp} is nearly linearly related

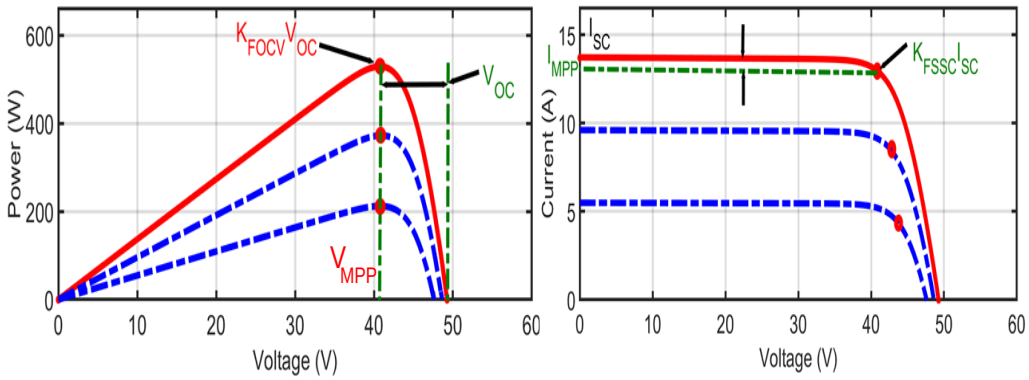

Figure 2.19. FOCV and FSCC MPPT demonstrating approximate linear relationship.

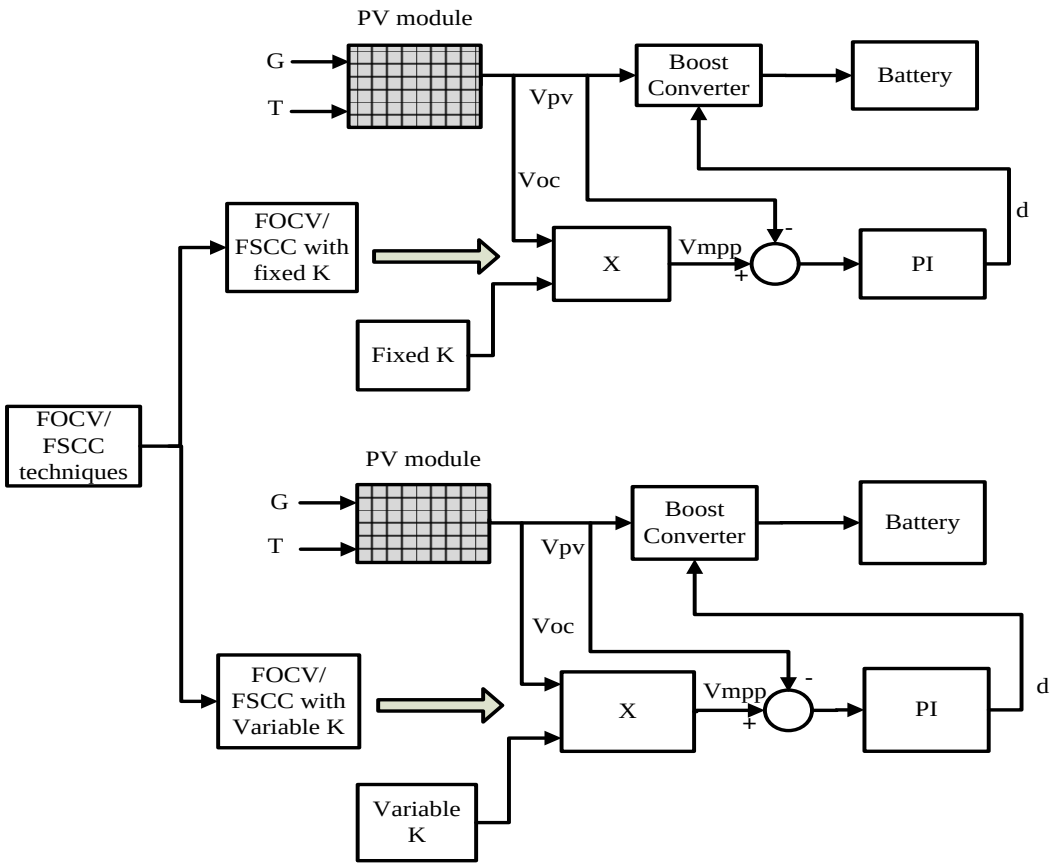

Figure 2.20. Research classification of FOCV MPPT and FSCC MPPT techniques.

to the short circuit current, I_{sc}. Also, this technique requires only one sensor however, measuring of I_{sc} during operation is the main challenge. The power converter requires modification by adding additional switch to momentarily short the converter and measure the I_{sc}. This adds to the implementation complexity and increases cost. Also, measuring of I_{sc} also constitutes power loss as it requires periodically disconnecting the power converter circuit. This technique also does not give the true MPP. In order to improve the tracking performance of this algorithm under partial shading conditions, [2.59] proposed a sweeping of PV array voltage from open circuit to short circuit in order to update k_{FSSC}. A solution is also introduced in [2.60] to estimate short circuit current without disconnecting the PV module circuit. This enables the algorithm tracks better while atmospheric conditions changes. The FOCV and the FSCC MPPT algorithms can be classified to operate with either fixed or with variable proportionality constant (k_{oc} or k_{SC}) as shown in Figure 2.20. Several FOCV and FSCC MPPT based algorithms with fixed proportionality constant have been proposed in the literature as summarized in Table 2.5. In these techniques, a fixed value of proportionality constant is utilized to establish the operating point of the PV array by comparing the measured PV voltage (V_{pv}) with reference PV voltage (V_{ref}). The MPP at fixed value of k is inaccurate at variable irradiation condition thus, FOCV MPPT and FSCC MPPT suffer tracking power loss. On the other hand, FOCV and FSCC MPPT based algorithms with variable proportionality constant are adopted in literature as summarized in Table 2.6. In these techniques, the proportionality constants are varied according to the changes in irradiation and utilized to establish the optimum operating point of the PV array by comparing the measured V_{pv} with reference voltage, V_{ref}. Such variation aims to improve the tracking efficiency of the MPPT algorithms.

Table 2.5. FOCV and FSCC with fixed proportionality constants survey.

Ref.	Measured parameter	Methodology	Comment
[2.61]	I_{PV}	This method adopted FSCC MPPT to detect changes in irradiance and further used it to move the operating point close to MPP to minimize oscillation power in the hybrid system of both FSCC MPPT and P&O MPPT.	Inaccurate tracking during rapidly changing weather conditions.
[2.62]	I_{PV}	In this method, the difference between I_{PV} and I_{sc} is used to control the measurement of I_{sc} to minimize the power loss in FSCC MPPT.	Poor tracking due to fixed value of K in case of varying irradiance condition.
[2.63]	V_{PV}	This method combined FOCV technique with controllable load with constant voltage current sink to measure the MPP in high concentration photovoltaic modules.	Effective tracking is achieved only at steady state because of the fixed value of K.
[2.64]	V_{PV}	The method detects the open circuit voltage and then calculate the upper and lower limit to obtain a range around the MPP. This range drive the operating point closer to the MPP.	It has high tracking efficiency and low system cost feature.
[2.65]	I_{PV}	This method utilizes the relationship between optimum operating current and the short circuit current to obtain maximum output power from the PV panel. This was proposed to be used in multiple PV and chopper module system.	The technique has good tracking capability but performed poorly under variable irradiance conditions.
[2.66]	V_{PV}	Semi-pilot cell is used for periodical measurement of open circuit voltage which is performed on one PV cell located at the edge of a PV panel.	This method is capable of providing high average power to the load during irradiance change. However, it is prone to poor tracking performance due to irradiance change.
[2.67]	I_{PV}	In this method, graphical approach is used to measure short circuit current, I_{sc} where curve fitting technique is used to establish the relation between I_{sc} and I_{PV}	This method makes use of data base and capable of supplying power, but does not provide true MPP because it involves many approximations.

[2.68]	V_{PV}	In this method, a functional low power management application on-chip with FOCV MPPT was designed using CMOS technology. This technique achieved high efficiency through self-synchronize diode and was capable of reducing power loss due to substrate diode negative voltage.	This method reduces the complexity of the system as it uses few components for implementation.
[2.69]	V_{PV}	This method uses intelligent fractional order open circuit voltage coupled with incremental conductance. This method gives the intelligent measurement of voltage and current.	The suggested novel controller can reduce the tracking time less compare to the conventional technique
[2.70]	V_{PV} & I_{PV}	In this method, both FOCV and FSCC techniques were integrated in PV system to harness power. These two MPPT controllers determine the required optimum operating point.	Poor tracking performance during changes in irradiance.
[2.71]	I_{PV}	A two-stage hybrid system of FSCC and INC was developed where FSCC technique was used to force the PV system to operate near MPP before INC technique is applied to track the actual power.	The system demonstrated high tracking speed.

Table 2.6. FOCV and FSCC with variable proportionality constants survey.

Ref	Measured parameter	Methodology	Comment
[2.72]	V_{PV}	Two input parameters of fuzzy logic enhanced by fractional open circuit voltage MPPT technique is introduced to track MPP.	Accurate tracking of PV output power at extreme weather condition with good efficiency.
[2.73]	I_{PV}	In this method, the FSCC MPPT is used to determine the new operating point and also further used to determine the perturbation size to control the irradiance.	Good tracking during changes in irradiance but not cost effective because it requires sensor for irradiance measurement.

[2.74]	V_{PV}	This method combined the ant colony optimization method with enhanced fuzzy agent. In this case, FOCV MPPT is made to enhance the initial starting point of the traditional fuzzy MPPT algorithm. This technique gives fast and accurate convergence to the MPP.	The controller gives good response under extreme variation of irradiation condition.
[2.75]	V_{PV}	In this method, a PV system was modeled to detect the variation of optimal voltage factor k_{OC}. An adaptive cascade MPPT controller was formulated based on the voltage factor k_{OC}.	Good tracking performance, however, the optimal factor works effectively for only selected irradiance level.

2.4.2 Curve fitting technique

Simplification of a single diode equivalent circuit of PV cell offers reasonable reduction of computational burden, however, compromises system accuracy due to assumption of some parameters [2.76]. MPP is the peak point on the P-V characteristic curve and this point can be predicted by modeling the P-V characteristic curve offline using numerical approximations [2.77]. Curve fitting MPPT technique is used to develop mathematical function that has the best fit to a series of data point of the P-V characteristic curve. In order to achieve P-V curve fitting, a third order polynomial is used [2.78] and is given by

$$P = aV^3 + bV^2 + cV + d \tag{2.33}$$

where a , b, c and d are constants and are obtained by sampling in a span of few milliseconds of PV module voltage and power. By differentiating (2.33) gives

$$\frac{dP}{dV} = 3aV^2 + 2bV + c \tag{2.34}$$

$$At\ the\ MPP,\ \frac{dP}{dV} = 0 \tag{2.35}$$

Hence, the voltage at MPP is estimated as

$$V_{mpp} = \frac{-b \pm \sqrt{b^2 - 3ac}}{3a} \tag{2.36}$$

A solution is proposed in [2.79] to model the PV array polynomial. The parameters of the model are calculated by measuring the current and voltage at three different positions around MPP to estimate V_{mpp}. The analysis of the proposed solution in [2.79] is given by

$$I = \alpha + \beta V^{\gamma} \tag{2.37}$$

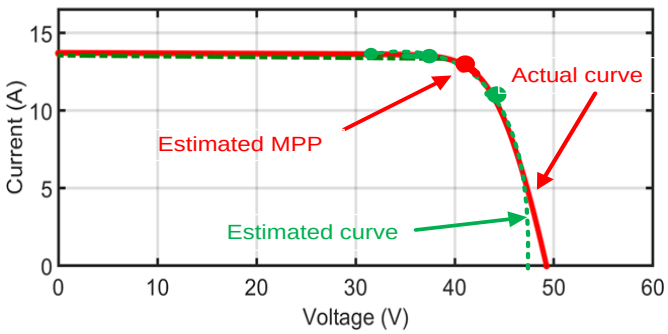

Figure 2.21. Performance of curve fitted MPPT technique.

where α, β, and γ are constants, calculated from the estimation algorithm and they represent short circuit current, open circuit voltage and fill factor of PV module respectively. These values can be estimated using three pairs of measured voltage and current values viz, (v_1, i_1) , (v_2 , i_2) and (v_3 , i_3). Differentiating (2.37) gives

$$I^I = \frac{dI}{dV} = \beta\gamma V^{(\gamma-1)} \tag{2.38}$$

Using the three coordinates of the voltage and current,

$$I_{12}^{I} = \frac{i_2 - i_1}{v_2 - v_1} \quad , \quad I_{23}^{I} = \frac{i_3 - i_2}{v_3 - v_2} \tag{2.39}$$

$$V_{12} = \frac{v_1 + v_2}{2} \quad , \quad V_{23} = \frac{v_2 + v_3}{2} \tag{2.40}$$

Thus, combining (2.37), (2,38) and (2,39) gives;

$$I_{12}^{I} = \beta V_{12}^{(\gamma-1)} \qquad I_{23}^{I} = \beta V_{23}^{(\gamma-1)} \tag{2.41}$$

where the values of α, β and γ can be calculated as follows:

$$\gamma = \frac{In\left(\frac{I_{12}^{I}}{I_{23}^{I}}\right)}{In\left(\frac{V_{12}}{V_{23}}\right)} + 1 \tag{2.42}$$

Using (2.40) and (2.41) gives,

$$\beta = \frac{I_{12}^{I}}{\gamma V_{12}^{(\gamma-1)}} \tag{2.43}$$

Hence, $$\alpha = I_1 - \beta V_1^{\gamma} \tag{2.44}$$

Figure 2.21 demonstrates the tracking process of curve fitting MPPT technique. This technique tracks faster and requires few iteration steps to reach MPP unlike heuristic technique where several iterations are required. However, curve fitting has high computational burden compared to heuristic technique. Also, the technique carefully requires selection of positions of the three coordinates for current and voltage to improve tracking performance.

2.5 Hybrid MPPT technique

Hybrid MPPT algorithm is a developing solution capable of detecting MPP effectively. This technique consists of two to three different MPPT algorithms in one MPPT technique and is specifically developed to overcome the weakness of individual MPPT algorithms. The following discusses various classifications of hybrid MPPT techniques.

2.5.1 Heuristic based MPPT hybrid with artificial intelligence (AI)

Heuristic MPPT techniques are those algorithms which track MPP without using trial and error approach [2.80]. P&O and INC MPPT algorithms are common examples and are found to be the most widely used MPPT techniques for commercial purposes because they are accurate at tracking MPP, straight forward and easy to implement. However, their tracking time and accuracy largely depend on the step size used. Thus, integration of heuristic MPPT with AI is essential to overcome such limitation both at normal and partial shading conditions where multiple peaks are generated by the P-V characteristic curve. A hybrid P&O MPPT with genetic algorithm (P&O-GA) is proposed in [2.81] to track global maximum power point (GMPP) during partial shading and intermittent conditions. Six chromosomes within the range of 10% to 90% are taken as six duty ratios. The first three chromosomes and duty cycle are applied in GA to establish the initial operating point of the hybrid P&O-GA. As the step length decreases, the step-size of the P&O decreases to track the MPP. The step size of P&O for next iteration to track GMPP is given by the following equation;

$$d_k = d_{k-1} + \Delta d_k \tag{2.45}$$

where, $\Delta d_k = \alpha \Delta d_{k-1}$ and $\alpha = 0.9$. The results show fast tracking time, less oscillation around MPP and significant reduction of number of iterations. Hybrid solution which involved P&O and particle swamp optimization (P&O-PSO) is proposed in [2.82]. In this method, conventional P&O MPPT is used to track MPP and maintains the operating point until the PV system experienced partial shading condition. Under this condition, PSO technique is then applied to search for GMPP from other local peaks until GMPP is

tracked. Hybrid INC with PSO MPPT technique is also proposed in [4.83]. This technique has two stages of operation. In the first stage, INC technique is used to track local MPP while in the second stage, PSO is employed to track GMPP under severe weather conditions. This technique tracks GMPP faster as compared to only PSO technique.

2.5.2 Heuristic based hybrid MPPT with model based MPPT technique

Fractional open circuit voltage (FOCV) and fractional short circuit current (FSCC) MPPT techniques are typical examples model based MPPT technique as they both track MPP while the PV module periodically isolates from the power converter at a point in time for the measurement of V_{OC} or I_{SC}. To improve the tracking speed and reduce the number of iterations in any of the heuristic MPPT technique such as INC and P&O MPPT techniques, a heuristic based MPPT with FSCC or FOCV is essential. This hybrid technique makes use of high tracking speed of offline MPPT and precise accuracy of online MPPT to achieve high efficiency. A hybrid is developed from P&O and FSCC MPPT techniques and presented in [2.84] where current perturbation is used instead of voltage perturbation. The results show fast tracking performance and less oscillation around MPP. A hybrid MPPT technique is proposed in [2.85] using model and model based MPPT techniques. In this technique, FSCC MPPT technique is used to bring the operating point close to the MPP while P&O is used to track the real MPP. Figure 2.22 shows a typical hybrid MPPT technique. The advantage of this technique is that it reduces the number of iteration processes to speed up the tracking, however, the algorithm performs poorly under variable irradiance and temperature conditions.

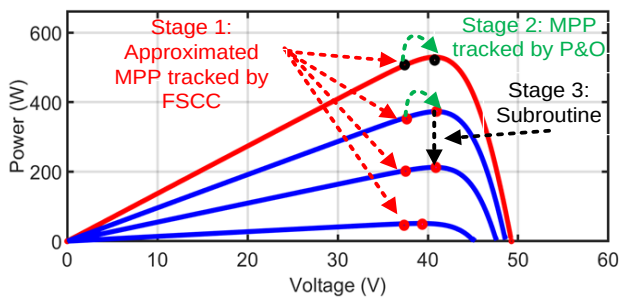

Figure 2.22. Hybrid MPPT technique.

2.5.3 Beta method

Beta method is another exceptional MPPT method in the family of hybrid MPPT method for PV system application. This technique is first proposed in [2.86] to help address issue associated with step size in conventional MPPT techniques when the operating point of the PV module is far from the MPP. The intermediate variable β_a which is calculated from V_{pv} and I_{pv} is used to establish the rules of the operation and also calculate variable step-size to track MPP. This intermediate, β is calculated mathematically by

$$\beta = In\left(\frac{I_{pv}}{V_{pv}}\right) - \mu V_{pv} \tag{2.46}$$

$$where, \quad \mu = \frac{q}{N_s \varphi k T} \tag{2.47}$$

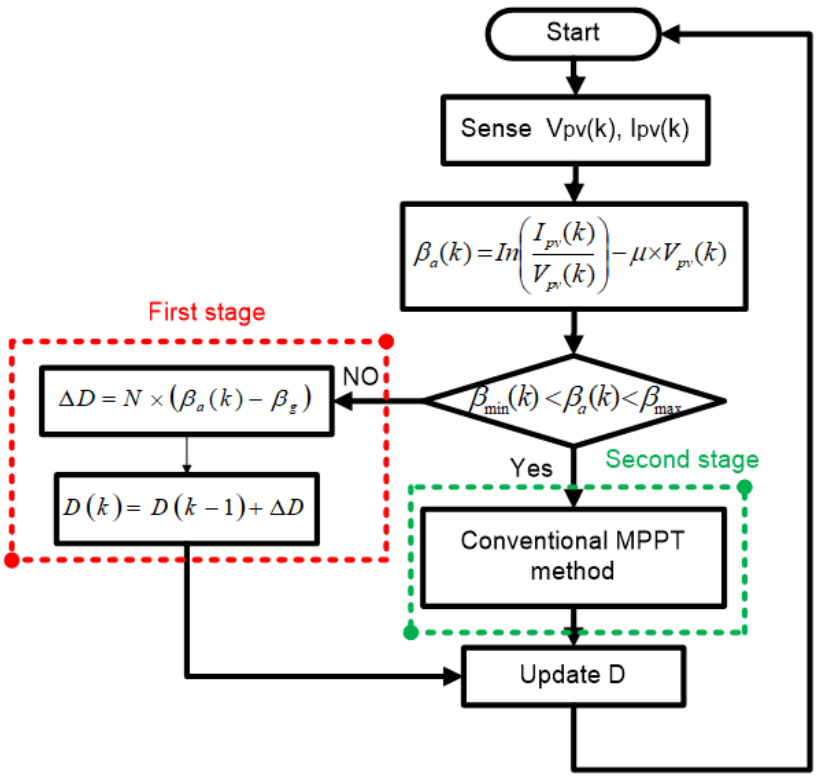

Figure 2.23. Flow chart of beta MPPT technique.

where, α is the conductance, q is the charge of an electrons, k is the Boltzmann's constant, φ is the ideality factor, T is the ambient temperature (Kelvin). The beta method is used together with one of the online MPPT technique such as P&O and INC MPPT techniques. The principle of operation is illustrated in Figure 2.23. The initial stage of this technique is the measurement of V_{pv} and I_{pv} from the PV module of which the intermediate value β_a is calculated. The range of operating for intermediate value, β_a is established based on the operating conditions of PV module such as irradiance and temperature and is given by

$$\beta_{min} < \beta_a(k) < \beta_{max} \tag{2.48}$$

Where, β_{min} and β_{max} are the minimum and maximum boundary conditions value respectively for $\beta_a(k)$. The values of β_{min} and β_{max} are calculated using variable irradiance and variable temperature. If the value of $\beta_a(k)$ is within the specified range, this means that the operating point of the PV module is close to MPP. Then the hybrid technique switches into second stage as indicated in Figure 2.23, where conventional MPPT technique is used to track MPP. If $\beta_a(k)$ fall outside the range of β_{min} and β_{max}, this means the operating point of the PV module is far from the MPP. The Beta technique then switch into first stage with variable step size value calculated as

$$\Delta D = N \times \left(\beta_a(k) - \beta_g\right) \tag{2.49}$$

where, N is the scaling factor to vary the step size, and β_g is the guiding value and it is the middle value of β_{min} and β_{max}. The Beta technique then move the operating point close to the MPP, where the process is repeated by switching first and second stages depending on the operating condition at a point in time to track MPP. Different MPPT techniques were comprehensively evaluated in [2.87-2.88] and it is evident that Beta method has fast tracking performance both at steady-state and dynamic conditions with minimum power oscillations. However, its accuracy depends on the implementation and

the calculated value of β_a. Also, tuning of N and β_g is a big challenge which affects the performance of the technique [2.89].

Table 2.7 depicts advantages, drawbacks, and application of Hybrid MPPT technique.

Table 2.7. Advantages, drawbacks and applications of hybrid MPPT techniques.

Hybrid MPPT	**Advantages**	**Drawbacks**	**Application**
GWO/P&O	This has fast convergence speed with minimum power oscillation around MPP. The process of tuning is neglected by this hybrid combination.	The main drawback is its advanced level mathematical computations burden.	Grid-connected
PSO/P&O	The modelling of the algorithm and hardware implementation are much simpler.	Significant oscillation around the MPP.	Grid-connected
FSCC/P&O	The integration of both techniques records high tracking efficiency and precise tracking accuracy around MPP.	Significant power loss under dynamic weather condition.	Grid connected.
FSCC/INC	This hybrid technique is more robust and has low power oscillation around MPP under dynamic weather condition.	The technique requires sophisticated microcontroller which is costly to implement variable step-size.	Grid connected.
FOCV/P&O	This hybrid technique is less complex and easy to implement with fast tracking capability.	The technique has higher power oscillation around MPP under dynamic weather conditions.	Grid connected.
P&O/GA	The integration of both technique records fewer iterations and low population size. The algorithm locates MPP at relatively short time.	The design of the membership function is complex to achieve accurate tracking.	Grid-connected.

2.6 Comparison of MPPT algorithm

Although, there are many MPPT techniques available for PV system operations, however, it might not be clear to the user, which one is better for a given application. The main features that need to be considered when choosing MPPT for a suitable application are discussed below:

2.6.1 System implementation

Implementing MPPT techniques requires the use of circuits and these are analog and digital circuits. If one's knowledge is on analog circuitry, then fractional open circuit or short circuit current are good option. With digital circuitry with programming and software, INC, P&O/hill climbing, fuzzy logic are suitable options.

2.6.2 Number of state variables

Control variables such as current, voltage, temperature and solar irradiance are required to implement MPPT applications. It is more cost effective and easier to implement MPP with voltage sensor than current sensor. This is because current sensor is more expensive and bulkier.

2.6.3 Cost of designing MPPT circuitry

Some applications do not consider cost as issue but requires accurate MPPT device. Such applications are large scale residential, space craft, solar vehicle, industry etc. Other applications such as water pumping for irrigation and small residential applications requires low cost MPPT. It is obvious that cost is one of the factors that need to be consider when designing MPPT circuit. Also, Table 2.8 shows the performance comparison of various parameters in commonly used MPPT.

Table 2.8. The main characteristics of MPPT technique.

MPPT method	**Tracking speed**	**Tracking accuracy**	**Analog or digital?**	**Parameter tuning?**	**Sensed parameter**	**Complexity**	**Cost**
INC	Medium	Medium	Digital	No	Voltage and current	Complex	Expensive
P&O	Slow	Medium	Both	No	Voltage and current	Moderately complex	Expensive
Parabolic prediction	Fast	Medium	Digital	No	Voltage and current	Simple	Expensive
FOCV	Fast	Low	Both	Yes	Voltage	Simple	Inexpensive
FSCC	Fast	Low	Both	Yes	Current	Simple	Inexpensive
Curve fitting	Fast	Low	both	No	Voltage and current	Simple	Inexpensive
FSCC/INC	Fast	High	Both	Yes	Voltage and current	Complex	Expensive
FSCC/P&O	Fast	High	Both	Yes	Voltage and current	Moderately complex	Expensive
FOCV/P&O	Fast	High	Both	Yes	Voltage and current	Moderately complex	Expensive
GWO/P&O	Medium	High	Digital	Yes	Voltage and current	Medium	Expensive
P&O/PSO	Fast	Medium	Digital	Yes	Voltage and current	Moderately complex	Expensive
P&O/GA	Medium	Medium	Digital	Yes	Voltage and current	Moderately complex	Expensive
INC/PSO	Fast	Medium	Digital	Yes	Voltage and current	Complex	Expensive
Beta method	Fast	Medium	Digital	Yes	Voltage and current	Moderately complex	Expensive

2.7 Summary

In this chapter, the structure of the photovoltaic system configuration, which are photovoltaic cell, module and array were discussed. A summary of MPPT techniques was studied based on the implementation scheme. These MPPT techniques were categorized into three namely, heuristic, model based and hybrid methods. The performance comparison of the aforementioned MPPT techniques was discussed with high tracking accuracy except model-based method. Curve fitting and parabolic are only MPPT techniques, which require initial set points and this needs to be carefully selected. Model based and hybrid techniques generally have high tracking accuracy however, some parameters need to be tuned accurately to ensure good performance at both steady state and dynamic conditions. Also, implementation strategy, cost, application, circuitry, control variable are useful factors to be consider when selecting MPPT for given application.

In general, the comprehensive literature review discovered important limitations in FOCV MPPT, FSCC MPPT and conventional variable step-size incremental conductance MPPT. The subsequent chapters discussed the limitations and new FOCV MPPT, FSCC MPPT and variable step-size incremental conductance MPPT are suggested to overcome their limitations.

Reference

[2.1] Introduction to Photovoltaic Systems- the infinite power of Texas. Available: http://www.infinitepower.org/pdf/FactSheet-11.pdf.

[2.2] Solar Photovoltaics for Development Applications: Sandia National Laboratories, SAND93-1642, August 1993.

[2.3] K. H. Lee, K. W. J. Barnham, J. P. Connolly, B. C. Browne, R. J. Airey, J. S. Roberts, M. Fuhrer, T. N. D. Tibbits, and N. J. Ekins-Daukes, "Demonstration of Photon Coupling in Dual Multiple-Quantum-Well Solar Cells," Photovoltaics, IEEE Journal of, vol. 2, pp. 68- 74.

[2.4] M. C. Di Piazza, M. Luna, G. Petrone and G. Spagnuolo, "Translation of the Single-Diode PV Model Parameters Identified by Using Explicit Formulas," in IEEE Journal of Photovoltaics, vol. 7, no. 4, pp. 1009-1016, July 2017.

[2.5] Florida energy center. Available: http://www.fsec.ucf.edu/en/consumer/solar_electricity/basics/cells_modules_arrays.htm

[2.6] N. Femia, G. Petrone, G. Spagnuolo, and M. Vitelli, Power electronics and control techniques for maximum energy harvesting in photovoltaic systems. CRC press, 2012.

[2.7] Haider Ibrahim, Nader Anani, Variations of PV module parameters with irradiance and temperature, Energy Procedia, Volume 134, 2017, Pages 276-285.

[2.8] Y. A. Mahmoud, W. Xiao and H. H. Zeineldin, "A Parameterization Approach for Enhancing PV Model Accuracy," in *IEEE Transactions on Industrial Electronics*, vol. 60, no. 12, pp. 5708-5716, Dec. 2013.

[2.9] M. A. G. de Brito, L. Galotto, L. P. Sampaio, G. de Azevedo e Melo, and C. A. Canesin, “Evaluation of the main MPPT techniques for photovoltaic applications,” IEEE Trans. Ind. Electron., vol. 60, no. 3, pp. 1156–1167, Mar. 2013.

[2.10] P. E. Kakosimos, A. G. Kladas, and S. N. Manias, “Fast photovoltaicsystem voltage- or current-oriented MPPT employing a predictive digital current-

controlled converter," IEEE Trans. Ind. Electron., vol. 60, no. 12, pp. 5673–5685, Dec. 2013.

[2.11] O. Lopez-Lapena, M. T. Penella, and M. Gasulla, "A closed-loop maximum power point tracker for subwatt photovoltaic panels," IEEE Trans. Ind. Electron., vol. 59, no. 3, pp. 1588–1596, Mar. 2012.

[2.12] A. B. Kancherla and D. R. Kishore, "Design of Solar-PV Operated Formal DC-DC Converter Fed PMBLDC Motor Drive For Real-time Applications," 2020 IEEE International Symposium on Sustainable Energy, Signal Processing and Cyber Security (iSSSC), Gunupur Odisha, India, 2020, pp. 1-6.

[2.13] K. Nathan, S. Ghosh, Y. Siwakoti and T. Long, "A New DC–DC Converter for Photovoltaic Systems: Coupled-Inductors Combined Cuk-SEPIC Converter," in *IEEE Transactions on Energy Conversion*, vol. 34, no. 1, pp. 191-201, March 2019.

[2.14] T. Esram and P. Chapman, "Comparison of photovoltaic array maximum power point tracking techniques," IEEE Trans. Energy Convers., vol. 22, no. 2, pp. 439– 449, Jun. 2007.

[2.15] N. Kasa, T. Iida, and L. Chen, "Flyback inverter controlled by sensorless current MPPT for photovoltaic power system," IEEE Trans. Ind. Electron., vol. 52, no. 4, pp. 1145–1152, Aug. 2005.

[2.16] E. Bianconi, J. Calvente, R. Giral, E. Mamarelis, G. Petrone, C. A. Ramos-Paja, G. Spagnuolo, and M. Vitelli, "A fast current-based mppt technique employing sliding mode control," IEEE Trans. Ind. Electron., vol. 60, no. 3, pp. 1168–1178, Mar. 2013.

[2.17] Y. Hu, W. Cao, J. Wu, B. Ji, and D. Holliday, "Thermography-based virtual mppt scheme for improving pv energy efficiency under partial shading conditions," IEEE Trans. Power Electron., vol. 29, no. 11, pp. 5667–5672, Nov. 2014.

[2.18] M. Simon and E. L. Meyer, "Detection and analysis of hot-spot formation in solar cells," Solar Energy Mater. Solar Cells, vol. 94, no. 2, pp. 106–113, 2010.

[2.19] Y. Mahmoud, M. Abdelwahed, and E. F. El-Saadany, “An enhanced mppt method combining model-based and heuristic techniques,” IEEE Trans. Sustain. Energy, vol. 7, no. 2, pp. 576–585, Apr. 2016.

[2.20] R. Teodorescu, M. Liserre, and P. Rodriguez, “Grid converters for photovoltaic and wind power systems”. John Wiley & Sons, 2011, vol. 29.

[2.21] X. Li, H. Wen, L. Jiang, W. Xiao, Y. Du, and C. Zhao, “An improved mppt method for pv system with fast-converging speed and zero oscillation,” IEEE Trans. Ind. Appl., vol. 52, no. 6, pp. 5051–5064, Nov. 2016.

[2.22] B. Subudhi and R. Pradhan, “A comparative study on maximum power point tracking techniques for photovoltaic power systems,” IEEE Trans. Sustain. Energy, vol. 4, no. 1, pp. 89–98, Jan. 2013.

[2.23] N. Karami, N. Moubayed, and R. Outbib, “General review and classification of different mppt techniques,” Renew. Sust. Energy Rev., vol. 68, pp. 1–18, 2017.

[2.24] L. V. Hartmann, M. A. Vitorino, M. B. d. R. Correa, and A. M. N. Lima, “Combining model-based and heuristic techniques for fast tracking the maximum-power point of photovoltaic systems,” IEEE Trans. Power Electron., vol. 28, no. 6, pp. 2875–2885, Jun. 2013.

[2.25] N. Femia, G. Petrone, G. Spagnuolo and M. Vitelli, "Optimization of perturb and observe maximum power point tracking method," in IEEE Transactions on Power Electronics, vol. 20, no. 4, pp. 963-973, July 2005.

[2.26] X. Li, H. Wen, L. Jiang, W. Xiao, Y. Du, and C. Zhao, “An improved mppt method for pv system with fast-converging speed and zero oscillation,” IEEE Trans. Ind. Appl., vol. 52, no. 6, pp. 5051–5064, Nov. 2016.

[2.27] M. Killi and S. Samanta, "Modified Perturb and Observe MPPT Algorithm for Drift Avoidance in Photovoltaic Systems," in IEEE Transactions on Industrial Electronics, vol. 62, no. 9, pp. 5549-5559, Sept. 2015.

[2.28] Weidong Xiao and W. G. Dunford, "A modified adaptive hill climbing MPPT method for photovoltaic power systems," *2004 IEEE 35th Annual Power Electronics Specialists Conference (IEEE Cat. No.04CH37551)*, Aachen, Germany, 2004, pp. 1957-1963 Vol.3.

[2.29] N. Femia, G. Petrone, G. Spagnuolo, and M. Vitelli, “Optimization of perturb and observe maximum power point tracking method,” IEEE Trans. Power Electron., vol. 20, no. 4, pp. 963–973, Jul. 2005.

[2.30] D. Sera, R. Teodorescu, J. Hantschel and M. Knoll, "Optimized Maximum Power Point Tracker for Fast-Changing Environmental Conditions," in *IEEE Transactions on Industrial Electronics*, vol. 55, no. 7, pp. 2629-2637, July 2008.

[2.31] A. Pandey, N. Dasgupta, and A. K. Mukerjee, “High-performance algorithms for drift avoidance and fast tracking in solar MPPT system,” IEEE Trans. Energy Convers., vol. 23, no. 2, pp. 681–689, Jun. 2008.

[2.32] D. Sera, R. Teodorescu, J. Hantschel, and M. Knoll, “Optimized maximum power point tracker for fast-changing environmental conditions,” IEEE Trans. Ind. Electron, vol. 55, no. 7, pp. 2629–2637, Jul. 2008.

[2.33] M. Killi and S. Samanta, “Modified perturb and observe mppt algorithm for drift avoidance in photovoltaic systems,” IEEE Trans. Ind. Electron, vol. 62, no. 9, pp. 5549–5559, Sep. 2015.

[2.34]] A. Pandey, N. Dasgupta, and A. K. Mukerjee, “Design issues in implementing MPPT for improved tracking and dynamic performance,” in Proc. IEEE IECON, 2006, pp. 4387–4391.

[2.35] F. Liu, S. Duan, F. Liu, B. Liu, and Y. Kang, “A variable step size inc mppt method for pv systems,” IEEE Trans. Ind. Electron, vol. 55, no. 7, pp. 2622–2628, Jul. 2008.

[2.36] W. Xiao and W. G. Dunford, “A modified adaptive hill climbing MPPT method for photovoltaic power systems,” in Proc. IEEE PESC, 2004, pp. 1957–1963.

[2.37] Y.-T. Chen, Z.-H. Lai, and R.-H. Liang, “A novel auto-scaling variable step-size mppt method for a pv system,” Sol. Energy, vol. 102, pp. 247–256, 2014.

[2.38] W. Ping, D. Hui, D. Changyu and Q. Shengbiao, "An improved MPPT algorithm based on traditional incremental conductance method," 2011 4th International Conference on Power Electronics Systems and Applications, Hong Kong, 2011, pp. 1-4.

[2.39] T. Radjai, J. P. Gaubert and L. Rahmani, "The new FLC-variable incremental conductance MPPT with direct control method using Cuk converter," *2014 IEEE 23rd International Symposium on Industrial Electronics (ISIE)*, Istanbul, 2014, pp. 2508-2513

[2.40] M. A. Abdourraziq, M. Maaroufi and M. Ouassaid, "A new variable step size INC MPPT method for PV systems," 2014 International Conference on Multimedia Computing and Systems (ICMCS), Marrakech, 2014, pp. 1563-1568.

[2.41] N. N. E. Zakzouk, M. A. Elsaharty, A. K. Abdelsalam, A. A. Helal and B. W. Williams, "Improved performance low-cost incremental conductance PV MPPT technique," *IET Renewable Power Generation*, vol. 10, no. 4, pp. 561-574, 4 2016.

[2.42] M. Ahmed and M. Shoyama, "Stability study of variable step size incremental conductance/impedance MPPT for PV systems," 8th International Conference on Power Electronics - ECCE Asia, Jeju, 2011, pp. 386-392.

[2.43] L. Yang, Z. Yunbo, L. Shengzhu and Z. Hong, "Photovoltaic array MPPT based on improved variable step-size incremental conductance algorithm," *2017 29th Chinese Control and Decision Conference (CCDC)*, Chongqing, 2017, pp. 2347-2351.

[2.44] S. K. Kollimalla and M. K. Mishra, "Variable Perturbation Size Adaptive P&O MPPT Algorithm for Sudden Changes in Irradiance," in *IEEE Transactions on Sustainable Energy*, vol. 5, no. 3, pp. 718-728, July 2014

[2.45] J. Teng, W. Huang, T. Hsu and C. Wang, "Novel and Fast Maximum Power Point Tracking for Photovoltaic Generation," in *IEEE Transactions on Industrial Electronics*, vol. 63, no. 8, pp. 4955-4966, Aug. 2016

[2.46] M.-L. Chiang, C.-C. Hua, and J.-R. Lin, “Direct power control for distributed PV power system,” in Proc. Power Convers. Conf., Osaka, Japan, 2002, pp. 311–315.

[2.47] W. Xiao and W. G. Dunford, “A modified adaptive hill climbing MPPT method for photovoltaic power systems,” in Proc. IEEE 35th Annu. Power Electron. Spec. Conf., Jun. 20–25, 2004, vol. 3, pp. 1957– 1963.

[2.48] P. J. Wolfs and L. Tang, “A single cell maximum power point tracking converter without a current sensor for high performance vehicle solar arrays,” Proc. IEEE 36th Power Electron. Spec. Conf., Jun. 16–16, 2005, pp. 165–171.

[2.49] N. Femia, D. Granozio, G. Petrone, G. Spagnuolo and M. Vitelli, "Predictive & Adaptive MPPT Perturb and Observe Method," in *IEEE Transactions on Aerospace and Electronic Systems*, vol. 43, no. 3, pp. 934-950, July 2007.

[2.50] Femia, N., Petrone, G., Spagnuolo, G., and Vitelli, M. Optimization of perturb and observe maximum power point tracking method. IEEE Transactions on Power Electronics, 20, 4 (July 2005), 963—973.

[2.51] R. Li and Z. Tan, "Study on Maximum Power Point Tracking Based on Parabolic Approximation Method for Photovoltaic Power Generation System," 2018 37th Chinese Control Conference (CCC), 2018, pp. 7570-7574

[2.52] Bepinkumar, B., Arunadevi, G., Kaushik, R., Saravana, I.G., , Chilakapati, N., and Maddikara, J. B.R. "MPPT algorithm for thermoelectric generators based on parabolic extrapolation". IET Generation, Transmission & Distribution, 13, 26 May, 2019, 821-828.

[2.53] A. Chepuru and S. R, "Comparative Analysis of Recent MPPT Algorithms for Thermoelectric Generator," 2020 IEEE India Council International Subsections Conference (INDISCON), 2020, pp. 266-271

[2.54] M. N. I. Khan et al., "Modelling and simulation of an efficient Charge Controller for Photovoltaic System with Maximum Power Point Tracking," 2014 3rd International Conference on the Developments in Renewable Energy Technology (ICDRET), 2014, pp. 1-5.

[2.55] F. Pai, R. Chao, S. H. Ko and T. Lee, "Performance Evaluation of Parabolic Prediction to Maximum Power Point Tracking for PV Array," *IEEE Transactions on Sustainable Energy*, vol. 2, no. 1, pp. 60-68, Jan. 2011.

[2.56] M. H. Mobarak and J. Bauman, "A Fast Parabolic-Assumption Algorithm for Global MPPT of Photovoltaic Systems Under Partial Shading Conditions," *IEEE Transactions on Industrial Electronics, 2021*

[2.57] M. A. Masoum, H. Dehbonei, and E. F. Fuchs, “Theoretical and experimental analyses of photovoltaic systems with voltage and current-based maximum power-point tracking,” IEEE Trans. Energy Convers., vol. 17, no. 4, pp. 514–522, Dec. 2002.

[2.58] T. Noguchi, S. Togashi, and R. Nakamoto, “Short current pulse based maximum power point tracking method for multiple photovoltaic-and-converter module system,” IEEE Trans. Ind. Electron., vol. 49, no. 1, pp. 217–223, Feb. 2002.

[2.59] B. Bekker and H. J. Beukes, “Finding an optimal PV panel maximum power point tracking method,” in Proc. 7th AFRICON Conf. Africa, 2004, pp. 1125–1129.

[2.60] N. Díaz, A. Luna and O. Duarte, "Improved MPPT short-circuit current method by a fuzzy short-circuit current estimator," *2011 IEEE Energy Conversion Congress and Exposition*, 2011, pp. 211-218.

[2.61] H.A Sher, A.F Murtaza, K.E Addoweesh and M. Chiaberge, “ A Two Stage Hybrid Maximum Power Point Tracking Technique for Photovoltaic Application”, IEEE PES General Meeting, 2014, p.1-5.

[2.62] H.A Sher, K.E Addoweesh and K. Al-Haddad, “ An Efficient and Cost-Effective Hybrid MPPT Method for a Photovoltaic Flyback Microinverter”, IEEE Transaction on Sustainable Energy, vol.9, pp 1137-1144, 2018.

[2,63] Y.P Huang, “A Rapid Maximum Power Measurement System for High-Concentration Photovoltaic Modules Using the Fractional Open-Circuit Voltage Technique and Controllable Electronic Load”, IEEE Journal of Photovoltaics, vol. 4, pp. 1610-1617, 2014.

[2.64] C.C Hua, W.T Chen and Y.H Fang, “A Hybrid MPPT with Adaptive Step-Size based on Single Sensor for Photovoltaic Systems”, IEEE Int. Conf. on Inf. Science, Electronics and Electrical, 2014, p.441-445.

[2.65] T. Noguchi, S. Togashi and R. Nakamoto, "Short-current pulse-based maximum-power-point tracking method for multiple photovoltaic-and-converter module system," in IEEE Transactions on Industrial Electronics, vol. 49, no. 1, pp. 217-223, Feb. 2002.

[2.66] D. Baimel, R. Shkoury, L. Elbaz, S. Tapuchi and N. Baimel, "Novel optimized method for maximum power point tracking in PV systems using Fractional Open Circuit Voltage technique," 2016 International Symposium on Power Electronics, Electrical Drives, Automation and Motion (SPEEDAM), Anacapri, 2016, pp. 889-894.

[2.67] K. Labeeb, S. Shankar and J. Ramprabhakar, "Hybrid MPPT controller for accurate and quick tracking," 2016 IEEE International Conference on Recent Trends in Electronics, Information & Communication Technology (RTEICT), Bangalore, 2016, pp. 1533-1537.

[2.68] D. Rodriguez, C. Bernal and G. Serrano, "On-Chip Solar Energy Harvesting System Using Substrate Diode PV Cell and Fractional Open Circuit Voltage MPPT Implementation," 2019 IEEE 10th Latin American Symposium on Circuits & Systems (LASCAS), Armenia, Colombia, 2019, pp. 181-184.

[2.70] A. Ramasamy and N. Suthanthira Vanitha, "Maximum power tracking for PV generating system using novel optimized fractional order open circuit voltage-FOINC method," 2014 International Conference on Computer Communication and Informatics, Coimbatore, 2014, pp. 1-6.

[2.71] H. Trabelsi, M. Elloumi, H. Abid and M. Kharrat, "MPPT controllers for PV array panel connected to Grid," 2017 18th International Conference on Sciences and Techniques of Automatic Control and Computer Engineering (STA), Monastir, 2017, pp. 505-510.

[2.72] M. Adly, H. El-Sherif and M. Ibrahim, "Maximum power point tracker for a PV cell using a fuzzy agent adapted by the fractional open circuit voltage technique," *2011 IEEE International Conference on Fuzzy Systems (FUZZ-IEEE 2011)*, 2011, pp. 1918-1922.

[2.73] A. F. Murtaza, H. A. Sher, M. Chiaberge, D. Boero, M. D. Giuseppe and K. E. Addoweesh, "A novel hybrid MPPT technique for solar PV applications using perturb & observe and Fractional Open Circuit Voltage techniques," Proceedings of 15th International Conference MECHATRONIKA, Prague, 2012, pp. 1-8.

[2.74] M. Adly and A. H. Besheer, "An optimized fuzzy maximum power point tracker for standalone photovoltaic systems: Ant colony approach," 2012 7th IEEE Conference on Industrial Electronics and Applications (ICIEA), Singapore, 2012, pp. 113-119.

[2.75] J. Martynaitis, "Discussion of "Theoretical and experimental analyses of photovoltaic systems with voltage and current-based maximum power point tracking"," in IEEE Transactions on Energy Conversion, vol. 19, no. 3, pp. 652-, Sept. 2004.

[2.76] Y. A. Mahmoud, W. Xiao and H. H. Zeineldin, "A Parameterization Approach for Enhancing PV Model Accuracy," in *IEEE Transactions on Industrial Electronics*, vol. 60, no. 12, pp. 5708-5716, Dec. 2013.

[2.77] A. B. G. Bahgat, N. H. Helwa, G. E. Ahmad, and E. T. E. Shenawy, “MPPT controller for PV systems using neural networks,” Renew. Energy, vol. 30, no. 8, pp. 1257–1268, 2005.

[2.78] B. Subudhi and R. Pradhan, "A Comparative Study on Maximum Power Point Tracking Techniques for Photovoltaic Power Systems," in *IEEE Transactions on Sustainable Energy*, vol. 4, no. 1, pp. 89-98, Jan. 2013.

[2.79] M. J. Z. Zadeh and S. H. Fathi, “A new approach for photovoltaic arrays modeling and maximum power point estimation in real operating conditions,” IEEE Trans. Ind. Electron., vol. 64, no. 12, pp. 9334–9343, Dec. 2017.

[2.80] V. Salas, E. Olas, A. Barrado, and A. Lzaro, “Review of the maximum power point tracking algorithms for stand-alone photovoltaic systems,” Solar Energy Mater. Solar Cells, vol. 90, no. 11, pp. 1555–1578, 2006.

[2.81] K. Sundareswaran, S. Palani, and V. Vigneshkumar, ‘‘Development of a hybrid genetic algorithm/perturb and observe algorithm for maximum power point

tracking in photovoltaic systems under non-uniform insolation,'' IET Renew. Power Gener., vol. 9, no. 7, pp. 757–765, Sep. 2015.

[2.82] C. Manickam, G. R. Raman, G. P. Raman, S. I. Ganesan, and C. Nagamani, ''A hybrid algorithm for tracking of GMPP Based on P&O and PSO with reduced power oscillation in string inverters,'' IEEE Trans. Ind. Electron., vol. 63, no. 10, pp. 6097–6106, Jul. 2016.

[2.83] M. Abdulkadir and A. H. M. Yatim, ''Hybrid maximum power point tracking technique based on PSO and incremental conductance,'' in Proc. IEEE Conf. Energy Convers. (CENCON), Oct. 2014, pp. 271–276.

[2.84] S. K. Kollimalla and M. K. Mishra, "A new adaptive P&O MPPT algorithm based on FSCC method for photovoltaic system," in Proc. Int. Conf. Circuits Power Comput. Technol. (ICCPCT), Mar. 2013, pp. 406–411.

[2.85] H. A. Sher, A. F. Murtaza, A. Noman, K. E. Addoweesh, K. Al-Haddad and M. Chiaberge, "A New Sensorless Hybrid MPPT Algorithm Based on Fractional Short-Circuit Current Measurement and P&O MPPT," in IEEE Transactions on Sustainable Energy, vol. 6, no. 4, pp. 1426-1434, Oct. 2015

[2.86] S. Jain and V. Agarwal, "A new algorithm for rapid tracking of approximate maximum power point in photovoltaic systems," IEEE Power Electron. Lett., vol. 2, no. 1, pp. 16–19, Mar. 2004.

[2.87]] M. de Brito, L. Galotto, L. Sampaio, G. de Azevedo e Melo, and C. Canesin, "Evaluation of the main mppt techniques for photovoltaic applications," IEEE Trans. Ind. Electron, vol. 60, no. 3, pp. 1156–1167, Mar. 2013.

[2.88] S. Jain and V. Agarwal, "Comparison of the performance of maximum power point tracking schemes applied to single-stage grid-connected photovoltaic systems," IET Electr. Power Appl., vol. 1, no. 5, pp. 753–762, Sep. 2007

[2.89] X. Li, H. Wen, L. Jiang, Y. Hu, and C. Zhao, "An improved beta method with autoscaling factor for photovoltaic system," IEEE Trans. Ind. Appl., vol. 52, no. 5, pp. 4281–4291, Sep. 2016.

Chapter 3

New optimum proportionality constant values for fractional open circuit voltage (FOCV) and fractional short circuit current (FSCC) MPPT techniques

In this chapter, the impact of temperature and irradiation on the performance of proportionality constants in FOCV and FSCC MPPT techniques is investigated. Based on this analysis, optimum values of proportionality constants due to variation of both temperature and irradiance are obtained. A modified FOCV and FSCC MPPT techniques based on optimum values of proportionality constants are proposed. The theoretical analysis of the new techniques is carried out while simulation is used to validate the practicability of the proposed techniques.

3.1 Background

The electrical parameters of PV module such as short circuit current (I_{SC}), open circuit voltage (V_{OC}) and maximum output power (P_{max}) change with the variation of both temperature and irradiance. The band gap of solar cell reduces when temperature increases, which affects the electrical parameters such as I_{SC}, V_{OC} and P_{max} [3.1-3.3]. Generally, when the surface temperature of PV module increases, the output power decreases which leads to a decrease in efficiency [3.4]. Temperature coefficient also plays a crucial role in the performance of PV system. Research works in [3.5-3.6] shows that, an improvement of 0.1%/℃ in the temperature coefficient increases the annual output power of the PV modules by 1%. This improvement could contribute to a huge output power for PV system especially in utility scale capacity. Temperature and irradiance variations do not only affect the efficiency of the PV module but also affect the tracking performance of the MPPT technique. It is reported in [3.7-3.10] that, rapid variations of temperature and irradiance, change the tracking process of the MPPT technique. In this case the MPPT is unable to distinguish the effect of temperature or irradiance variation with respect to voltage change. Thus, the algorithm fails to track the MPP due to changes

in operating point of the PV module. The performance of FOCV MPPT and FSCC MPPT techniques are dependent on the proportionality constant. This constant enables the MPPT locate new operating point in an event of temperature and irradiance variation. Fixed proportionality constant compromises the efficiency of both FOCV and FSCC MPPT techniques at all time. The literature in chapter two shows different methods to vary proportionality constant under variable irradiance condition. However, little attention has been given in the area of temperature variation and how it affects the performance of the proportionality constants in both FOCV and FSCC MPPT technique. Thus, this chapter proposed new optimum proportionality constant values for both FOCV MPPT and FSCC MPPT technique based on the impact of temperature and irradiance variations.

3.2 Proposed optimum proportionality constant for FOCV MPPT technique

The maximum voltage, V_{mpp} under normal environmental condition is located at a value which is a fraction of V_{oc} and is given in (1) as;

$$V_{mpp} \cong k_{oc} V_{oc} \tag{3.1}$$

where, V_{oc} is the PV module open circuit voltage. Typically, the value of k_{oc} ranges between 0.73-0.85 [3.11]. Figure 3.1a shows the current-voltage characteristic curve of the five PV modules of different level of irradiance. This figure is used to generate the relationship between PV module voltage at MPP and its open circuit voltage at different irradiance conditions as shown in Figure 3.1b. It is evident that as the irradiance level changes both voltage at MPP and open circuit voltage vary accordingly. Thus, proportionality constant must also vary accordingly to improve voltage and power at MPP. The MPP for FOCV MPPT is estimated under different irradiation levels shown in Table 3.1 and temperatures 25^{o} C and 50^{o} C. The open circuit voltage is measured periodically using the flow chart and the corresponding circuit diagram in Figure 3.2a and Figure 3.3a respectively. The proportionality constant k_{OC} is varied from 0.73 to 0.91 with an interval of 0.02 until an optimum value is obtained under variable temperature and irradiance conditions. The maximum power corresponding to the optimum proportionality constant

is estimated. The corresponding FOCV MPPT algorithm tracking efficiency is depicted in Figure 3.3. The tracking performance of the MPPT algorithm is evaluated using MPPT efficiency expression given by

$$MPPT_{effic} = \frac{E_{pv}}{E_{avai}} \tag{3.2}$$

where, E_{pv} is the total extracted PV energy and E_{avai} is the available PV energy. Figure 3.4a shows the efficiency variation with k_{OC} at 25° C while Figure 3.4b shows the tracking

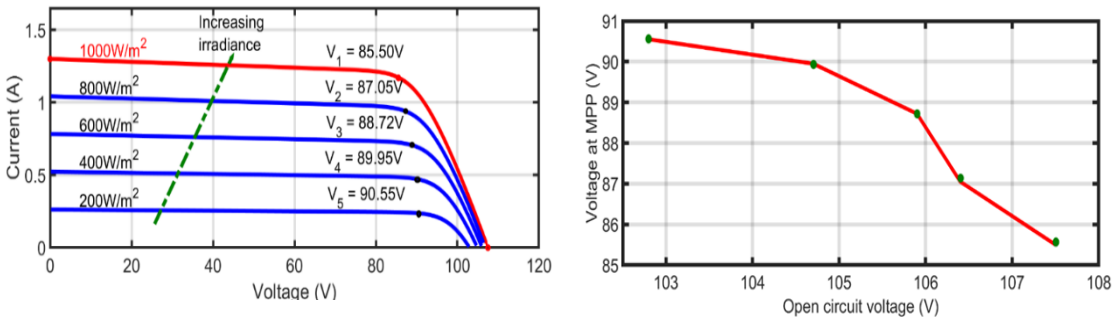

(a) (b)

Figure 3.1. (a) Current-voltage characteristic curve with different irradiance level, (b) Relationship between PV voltage and open circuit voltage.

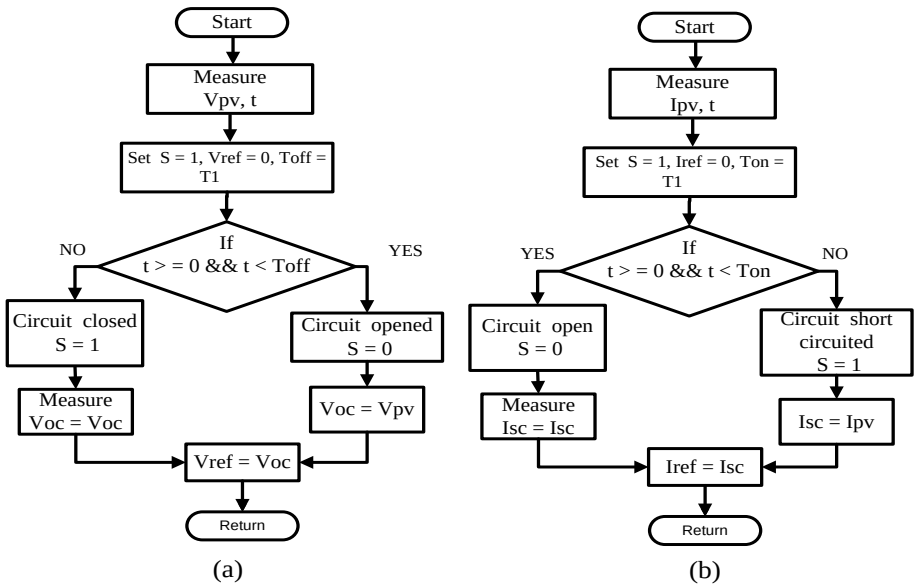

(a) (b)

Figure 3.2. Measurement of (a) open circuit Voltage, (b) short circuit current.

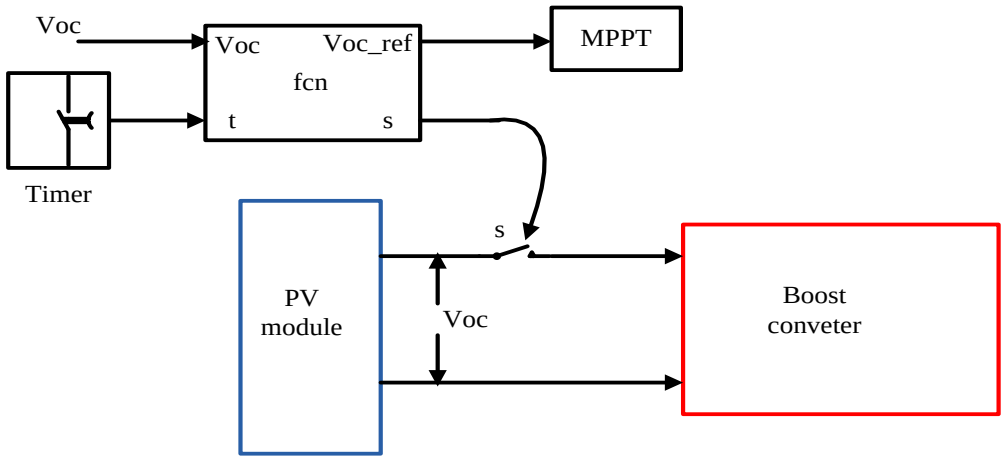

(a)

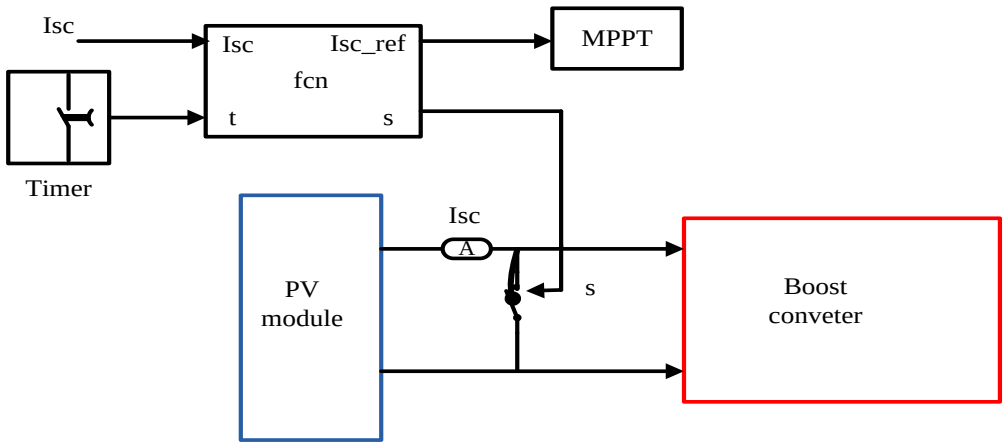

(b)

Figure 3.3. Circuit diagram for measurement (a) open circuit voltage, (b) Short circuit current

efficiency at 50° C. The values of optimum proportionality constants corresponding to the various irradiance level are plotted. It is evident that the value of k_{OC} not only depend on the irradiation level but also is temperature dependent. As a result, for a fixed irradiation the value of k_{OC} must re-tuned to gain the highest tracking efficiency. The variation of optimum k_{OC} at 25° C and 50° C for the irradiation levels in Table 3.1 is shown in Figure 3.5.

Table 3.1. Irradiance level.

Irradiance (W/m2)	500	600	700	800	900	1000	1100	1200

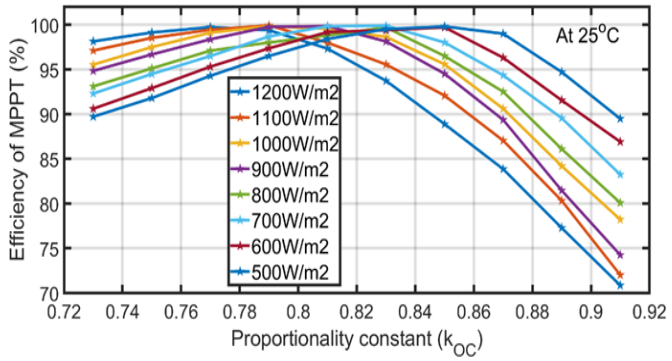

(a)

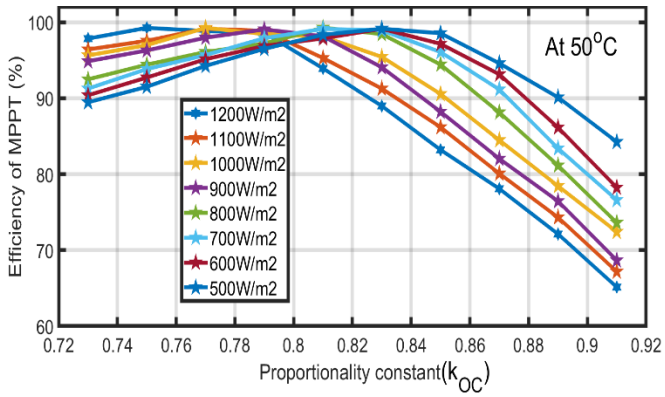

(b)

Figure 3.4. Performance of FOCV MPPT. (a) At 25℃ (b) At 50℃.

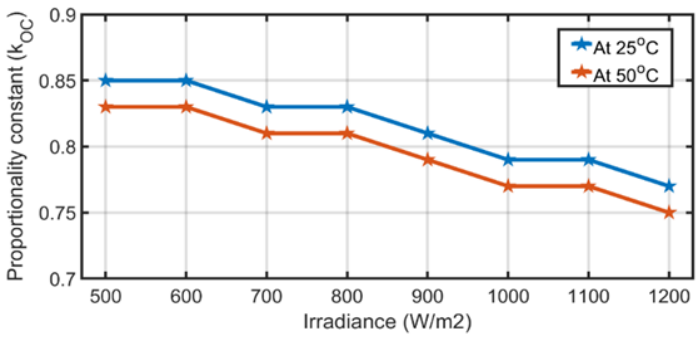

Figure 3.5. Optimum k_{OC} values for FOCV MPPT algorithm.

3.3 Proposed optimum proportionality constant for FSCC MPPT technique

The MPPT for FSCC is based on the fact that maximum current is located which is a fraction of short circuit current, I_{SC} given by

$$I_{mpp} \cong k_{SC} I_{SC} \tag{3.3}$$

where k_{SC} is the proportionality constant with typical value between 0.78-0.92 [3.12]. Figure 3.6 shows the relationship between current at MPP and short circuit current where these parameters vary under variable irradiance conditions. This means a suitable optimum proportionality constant is required at any given irradiance conditions to provide an improved PV output current and power. Similarly, the MPP using FSCC MPPT is estimated under the same irradiation levels shown in Table 3.1 and temperatures 25°C and 50°C. The proportionality constant for FSCC MPPT is varied within the range of 0.8 to 0.94 with an interval of 0.01 until an optimum value is obtained. The short circuit currents are measured periodically using the flow chart and circuit diagram in Figure 3.2b and Figure 3.3b respectively. The maximum current and power corresponding to the optimum proportionality are calculated. The corresponding FSCC MPPT algorithm tracking efficiency is depicted in Figure 3.7. Figure 3.7a shows the efficiency variation of FSCC MPPT with k_{SC} at 25°C while Figure 3.7b shows the tracking efficiency at 50°C. Therefore, for a fixed irradiation the value of k_{SC} must re-tuned to gain the highest tracking efficiency. The variation of the optimum k_{SC} at 25°C and 50°C corresponding to various irradiation levels in Table 3.1 is given in Figure 3.8.

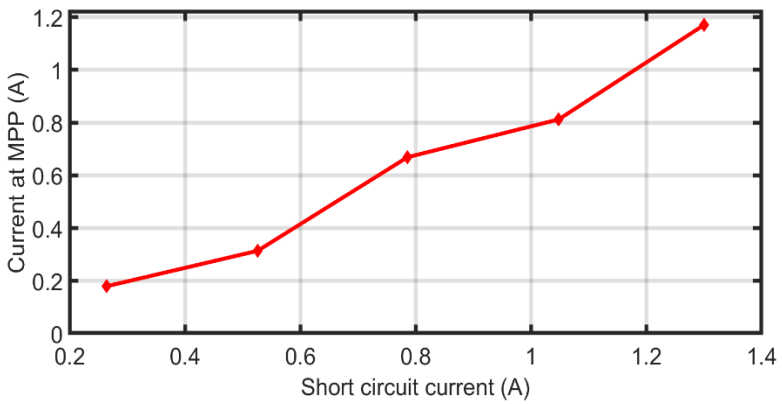

Figure 3.6. Relationship between current at MPP and short circuit current.

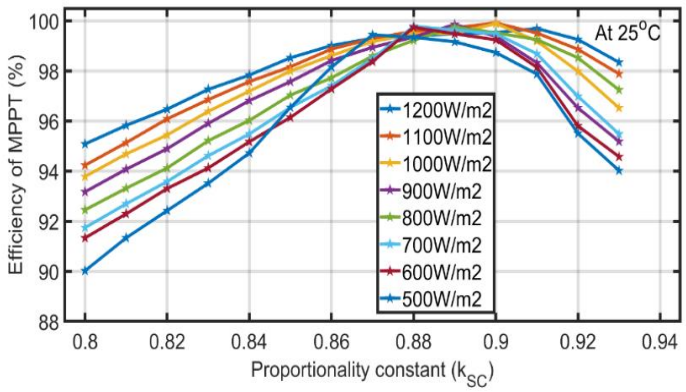

(a)

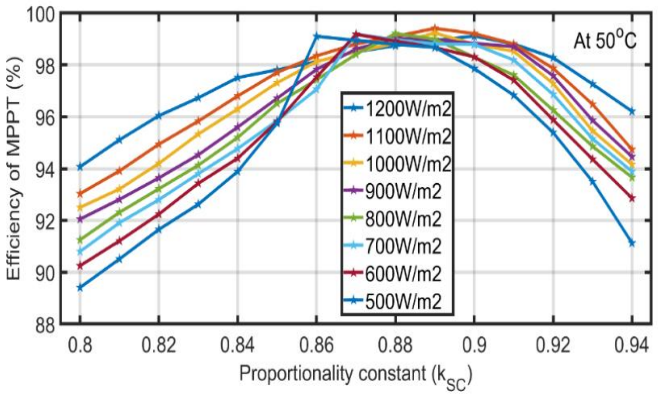

(b)

Figure 3.7. Performance of FSCC MPPT. (a) At 25^{O}C (b) At 50^{O}C.

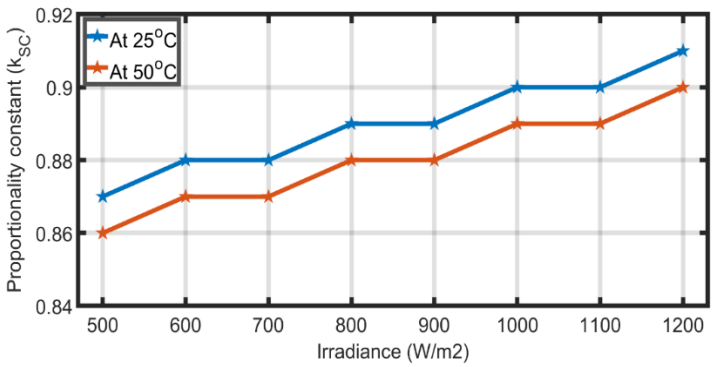

Figure 3.8. Optimum k_{SC} values for FSCC MPPT algorithm.

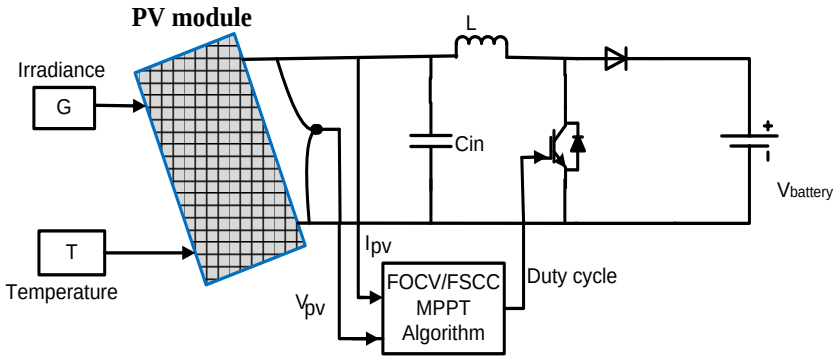

Figure 3.9. Photovoltaic system under investigation.

3.4 Impact of the proposed optimum proportionality constant value on the performance of FOCV and FSCC MPPT techniques

The effectiveness of the proportionality constants in FOCV and FSCC MPPT techniques were validated using a grid connected PV system described in Figure 3.9. The system is simulated using MATLAB/SIMULINK software. The PV array is formed by connecting 5 USL-K020 modules in series to provide overall power of 100W. The specifications of each PV module at standard test condition are given in Table 3.2. The switching frequency of the boost converter is 10kHz and the two MPPT algorithms are subjected to the same conditions of temperature and irradiance. The proposed proportionality constant values were used to improve the tracking efficiency of both FOCV and FSCC MPPT techniques. The optimum proportionality constants are implemented using look up table. Figure 3.10 shows the block diagram representation of the proposed controllers for photovoltaic system application. Opening and shorting the circuit of the boost converter becomes necessary when implementing both FOCV MPPT and FSCC MPPT techniques. Since these measurements of V_{OC} and I_{SC} involve power loss, the measurement is being done in milliseconds. Figure 3.11a shows the flow chart of FOCV MPPT while Figure 3.11b shows the flow chart of FSCC MPPT. The effectiveness of the proposed FOCV MPPT and FSCC MPPT algorithms are validated through simulation and compared with conventional FOCV MPPT and FSCC MPPT with their fixed values k_{OC} and k_{SC} respectively. A scenario is considered to implement the PV system. In this scenario, a fixed irradiation of 500W/m^2 is applied with a step temperature change of 25°C, 40°C and

Table 3.2. USL-KL020 module specifications.

Parameter	Value
Maximum output power (P_{max})	20W
Maximum power Voltage (V_{MPP})	17.1V
Maximum power current (I_{MPP})	1.17A
Nominal open circuit voltage (V_{oc})	21.5V
Nominal short circuit current (I_{sc})	1.30A
Standard Test Conditions	25°C & 1Kw/m2

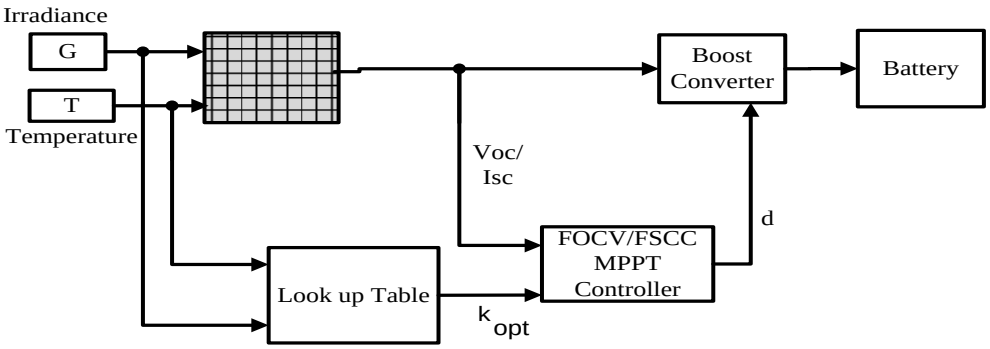

Figure 3.10. Block diagram representation of the proposed MPPT techniques.

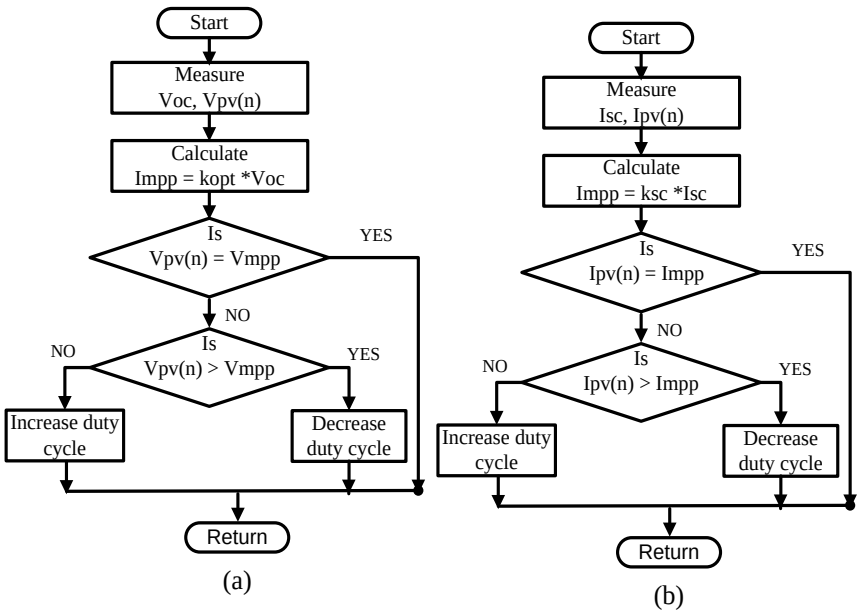

Figure 3.11. (a) Flow chart of FOCV MPPT, (b) Flow chart of FSCC MPPT.

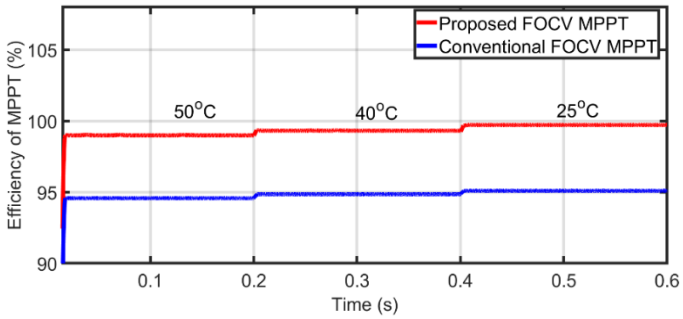

(a)

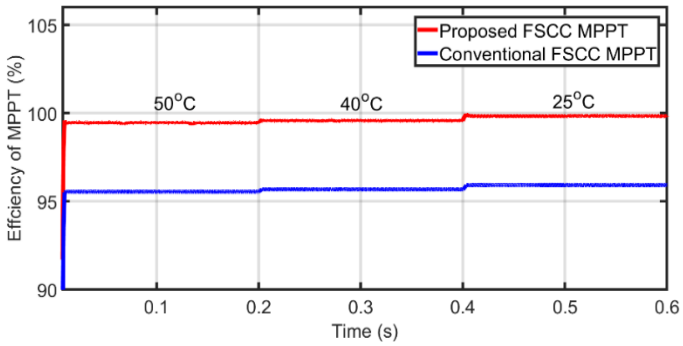

(b)

Figure 3.12. Proposed and conventional at fixed irradiance and variable temperatures(a) FOCV MPPT (b) FSCC MPPT.

50°C at 0.2s for FOCV and FSCC MPPT. The performance of the suggested methodology is observed by comparing the results obtained with traditional FOCV MPPT and FSCC MPPT. Fig. 3.12a shows the tracking efficiency of proposed FOCV MPPT controller compared with conventional FOCV MPPT. While Fig. 3.12b shows the tracking efficiency of the proposed FSCC MPPT compared with conventional FSCC MPPT. Variable irradiance is also applied with a step temperature change of 25°C, 40°C and 50°C at 0.2s for both FOCV MPPT and FSCC MPPT. Fig. 3.13a shows the tracking efficiency of FOCV MPPT and Fig. 3.13b shows the tracking efficiency of FSCC MPPT both compared with their conventional MPPT. It is evident that the two proposed MPPT controllers retuned their k values to gain high tracking efficiency when a change occurred to temperature and or irradiation where the conventional controllers lack such feature. In order to establish the impact of periodical measurement of open circuit voltage and short

circuit current on the performance of the proposed FOCV MPPT and FSCC MPPT, a step change of irradiance level (1000 900 800 700) W/m2 at 50°C is implemented. Figure 3.14 shows the performance of the two proposed MPPTs. It observed that as the number of step change increases, the more periodical measurement for open circuit voltage and short circuit current are required. This increases the losses due intermittent operation of power converter switches. Thus, the tracking power decreases substantially as the step change increases. This is the limitation of the proposed algorithms; however, the algorithms retuned their proportionality constant values to gain high tracking efficiency. In general, the impact of temperature on the performance of FOCV MPPT and FSCC MPPT become significant if their proportionality constants remain fixed under variable irradiance. However, with variable proportionality constants under variable irradiance condition, and

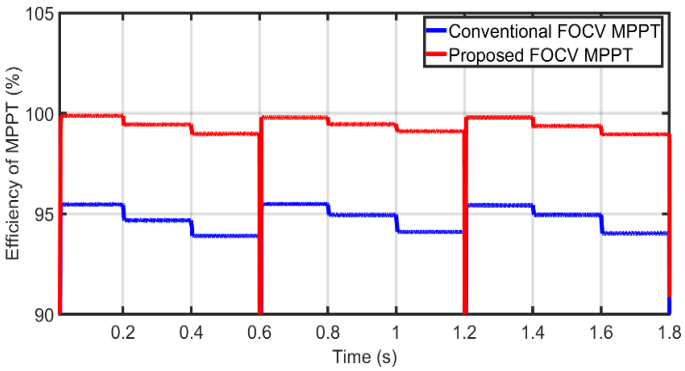

(a)

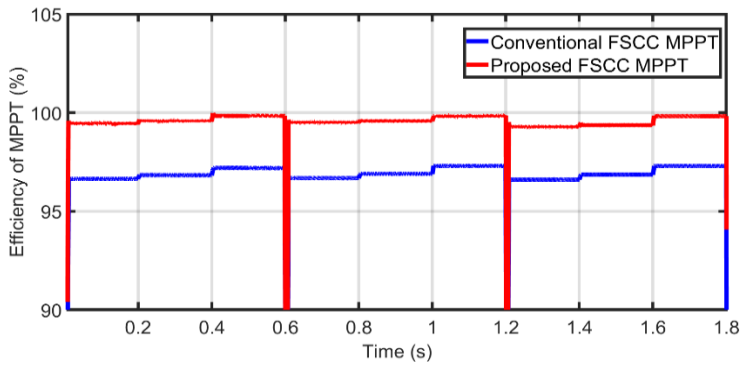

(b)

Figure 3.13. Proposed and conventional at variable irradiance and variable temperature (a) FOCV MPPT (b) FSCC MPPT.

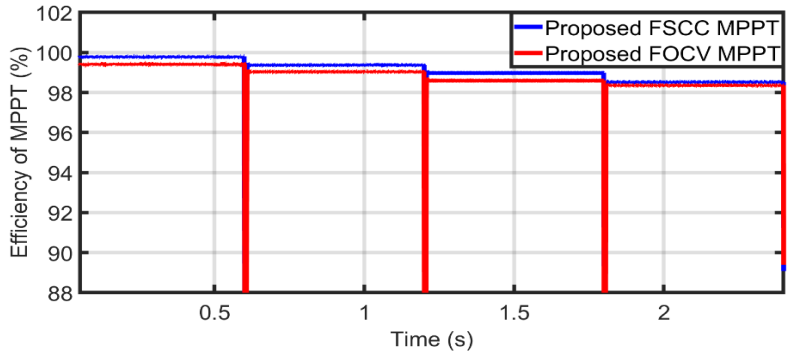

Figure 3.14. Proposed FSCC and FOCV MPPTs under step changing irradiance.

Table 3.3. Performance of proposed and conventional FOCV MPPT and FSCCMPPT under two step changes in irradiance at 50^{o}C temperature.

Temperature	**Condition**	**MPPT method**	**MPPT efficiency (%)**
50^{o}C	from 500W/m2 to 700W/m2	Conventional FOCV MPPT	96.24
		Proposed FOCV MPPT	99.07
	from 700W/m2 to 1000W/m2	Conventional FOCV MPPT	96.35
		Proposed FOCV MPPT	99.18
	from 500 W/m2 to 700W/m2	Conventional FSCC MPPT	96.72
		Proposed FSCC MPPT	99.83
	from 700 W/m2 to 1000 W/m2	Conventional FSCC MPPT	96.78
		Proposed FSCC MPPT	99.60

With temperature as high as 50^{o}C, has little impact on the performance on both FOCV MPPT and FSCC MPPT. This is because both algorithms re-tuned their optimum proportionality constants to gain high tracking efficiency. Table 3.3 and Figure 3.14 compare the performance of the proposed FOCV MPPT and FSCC MPPT. Based on their tracking efficiencies, it is evident that, FSCC MPPT exhibits good performance than FOCV MPPT even under high temperature operation condition.

3.6. Summary

In this chapter, optimum proportionality constant values due to temperature and irradiance variations for both FOCV MPPT and FSCC MPPT techniques have been explored. The

steady-state performance of each algorithm has been investigated for different levels of irradiations. Moreover, the two algorithms were tested for two different temperatures namely: 25ºC and 50ºC. At each and every specific irradiation and temperature the optimum proportionality constant is obtained. The proposed MPPT controllers have been validated to verify the design using new optimum values of k_{oc} and k_{sc} which have good performance over conventional FOCV MPPT and FSCC MPPT.

References

[3.1] D.M. Tobnaghi, R. Madatov, and D. Naderi, “The effect of temperature on electrical parameters of solar cells,” International Journal of Advanced Research in Electrical, Electronics and Instrument Engineering, vol. 2, pp. 6404-6407, 2013.

[3.2] P. Singh, S.N Singh, M. Lal, and M. Husain, “Temperature dependence of I-V characteristics and performance parameters of silicon solar cell,” Solar Energy Materials and Solar Cells 92.12, pp. 1611-1616, 2008.

[3.3] K. Nishioka, T. Hatayama, Y. Uraoka, T. Fuyuki, R. Hagihara, and M.Watanabe, “Field-test analysis of PV system output characteristics focusing on module temperature,” Solar energy materials and solar cells 75, vol.3 pp. 665-671, 2003.

[3.4] E. Skoplaki, and J.A. Palyvos, “On the temperature dependence of photovoltaic module electrical performance,” A review of efficiency/power correlations, Solar energy 83.5, pp. 614-624, 2009.

[3.5] K. Nishioka, T. Hatayama, Y. Uraoka, T. Fuyuki, R. Hagihara, and M.Watanabe, “Field-test analysis of PV system output characteristics focusing on module temperature,” Solar energy materials and solar cells 75, vol.3 pp. 665-671, 2003.

[3.6] N. H. Zaini, M. Z. Ab Kadir, M. Izadi, N. I. Ahmad, M. A. M. Radzi and N. Azis, "The effect of temperature on a mono-crystalline solar PV panel," *2015 IEEE Conference on Energy Conversion (CENCON)*, 2015, pp. 249-253.

[3.7] M. Miyatake, T. Inada, I. Hiratsuka, H. Zhao, H. Otsuka, and M. Nakano, “Control characteristics of a Fibonacci-search-based maximum power point tracker when a photovoltaic array is partially shaded,” in Proc. 4th Int. Power Electron. Motion Control Conf., Aug. 2004, vol. 2, pp. 816–821.

[3.8] D. Sera, L. Mathe, T. Kerekes, S. Viorel, and R. Teodorescu, “On the perturb-and-observe and incremental conductance MPPT methods for PV Systems,” IEEE J. Photovolt., vol. 3, no. 3, pp. 1070–1078, Jul. 2013.

[3.9] K. Ishaque, Z. Salamb, and G. Laussc, “The performance of perturb and observe and incremental conductance maximum power point tracking method under dynamic weather conditions,” Elsevier Trans. Appl. Energy, vol. 119, pp. 228–236, Apr. 2014.

[3.10] G. Escobar, S. Pettersson, C. N. M. Ho and R. Rico-Camacho, "Multisampling Maximum Power Point Tracker (MS-MPPT) to Compensate Irradiance and Temperature Changes," in *IEEE Transactions on Sustainable Energy*, vol. 8, no. 3, pp. 1096-1105, July 2017.

[3.11] F. Zhang, K. Thanapalan, A. Procter S. Carr and J. Maddy, “Adaptive Hybrid Maximum Power Point Tracking Method for a Photovoltaic System”, IEEE Transactions on Energy Conversion, vol. 28 pp. 353-360, 2013.

[3.12] S. K. Kollimalla and M. K. Mishra, "A new adaptive P&O MPPT algorithm based on FSCC method for photovoltaic system," *2013 International Conference on Circuits, Power and Computing Technologies (ICCPCT)*, Nagercoil, 2013, pp. 406-411.

Chapter 4

Modified Variable Step-Size Incremental Conductance MPPT Technique for Photovoltaic Systems

In this chapter, the limitations and structure of conventional variable step size incremental conductance (INC) technique are investigated. A new variable step size incremental conductance maximum power point tracking (MPPT) technique for photovoltaic system is proposed. The new MPPT technique utilizes the slope angle between PV module voltage and power to improve the performance of the conventional variable step size INC technique. Additionally, an autonomous scaling factor is proposed to replace the constant preset scaling used in conventional variable step-size to minimize the limitations. Simulation and experimental results are presented to validate the feasibility of the proposed variable step size incremental conductance.

4.1 Limitations of conventional variable step-size INC technique

As discussed in chapter two, the conventional variable step-size INC works differently to conventional INC algorithm with preset step-size as shown in Figure 4.1. The generated PV module output power with a large step size contributes to excessive power oscillations at steady-state, but faster dynamics response resulting in a comparatively low tracking efficiency. An opposite scenario occurs when smaller step-size is applied in the MPPT. Thus, without a suitable optimum step-size value, both steady-state accuracy and fast dynamics cannot achieve simultaneously. A variable step-size discussed in [2.35] addressed this challenge as the step-size gets smaller when the algorithm approaches MPP. The variable step-size which replaces the fixed step-size in conventional INC MPPT in [2.35] is given by:

$$D(k) = D(k-1) \pm N \left|\frac{dP_{pv}}{dV_{pv}}\right| \tag{4.1}$$

where,

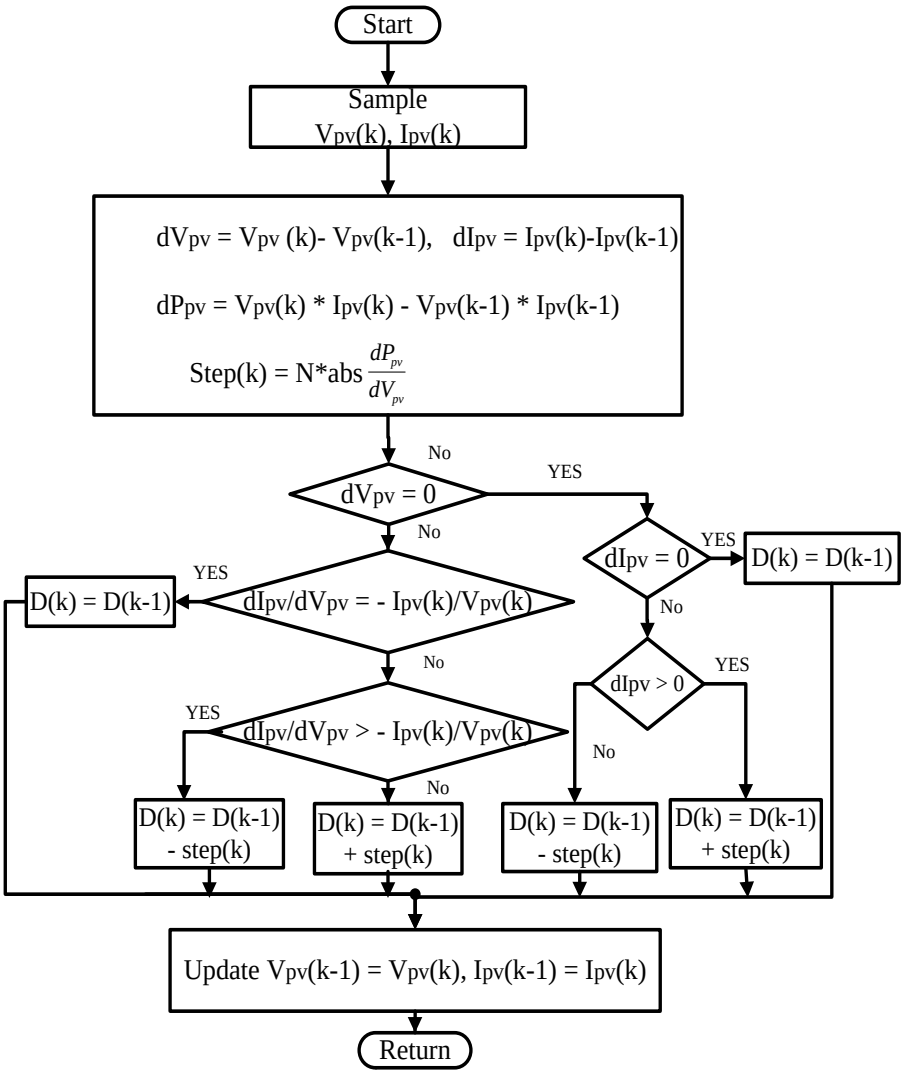

Figure 4.1. Flow chart of conventional variable step-size INC MPPT algorithm.

$$dP_{pv} = P_{pv}(k) - P_{pv}\,(k-1) \tag{4.2}$$

$$dV_{pv} = V_{pv}(k) - V_{pv}\,(k-1) \tag{4.3}$$

Where, $D(k)$ and $D(k-1)$ are the present and previous duty cycle at k and $k-1$ samples respectively, $P_{pv}(k)$ and $P_{pv}(k-1)$ are the present and previous PV module power at k and $k-1$ samples respectively, $V_{pv}(k)$ and $V_{pv}(k-1)$ are the voltage at k and $k-1$

samples. N presents the preset scaling factor necessarily used to fine-tune the step-size at the design stage to compromise between dynamic response and steady state precision.

Figure 4.2a shows the behavior of the conventional variable step-size INC in a typical PV system under different irradiance levels. The PV module output power oscillates around the MPP when PV module operates around its optimum point. It is obvious as shown in Figure 4.2a, that the PV module output power moves slowly to the new MPP when irradiance changes. The duty cycle in Figure 4.1b verifies the converter response under variable irradiance conditions. Significant duty cycle oscillations around optimum value is experienced at steady state. These oscillations are due to the high step-size value during small PV voltage change. It is importance to note form Figure 4.1b that the algorithm drifted when irradiance increased from 400 W/m2 to 1000W/m2. Figure. 4.3 verifies the impact of the scaling factor on the PV output power. It can be seen that the large scaling factor in conventional variable step-size compared to the optimum one can provide a faster dynamic response but excessive oscillations at steady state. Although, the technique in [2.35] replaces the step-size in conventional INC MPPT, it also has the following limitations:

- The scaling factor, N in conventional variable step-size INC MPPT is not optimum and only works effectively at the selected irradiance conditions.
- The variable step-size is a dependent on the slope (dP_{pv}/dV_{pv}) of P-V characteristic curve. A small change in PV module voltage increases the magnitude of the step-size. This leads to a significant power oscillation around MPP.
- The technique has slow tracking performance under variable irradiance conditions.

It is also important to mitigate the impact of the condition $dV_{pv} = 0$ by capping the step-size value. However, the algorithm will only work effectively at a selected irradiance since the step-size is not generic and system dependent. The algorithm will experience significant oscillation at different irradiance level. Based on the above limitations, a new variable step-size INC MPPT is proposed to address the limitations.

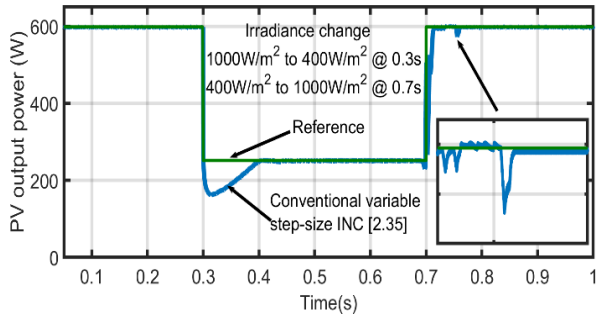

(a)

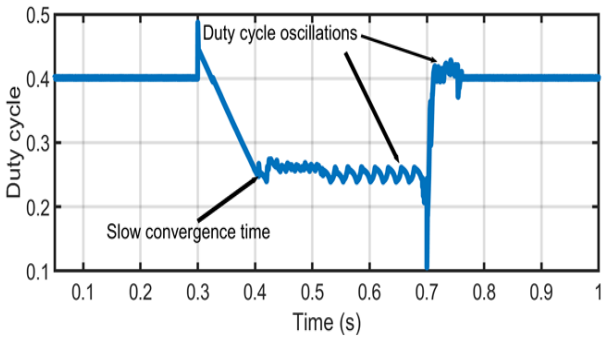

(b)

Figure. 4.2. Drawbacks of conventional variable step-size INC MPPT with optimum scaling factor: (a) PV modules output power, and (b) Duty cycle.

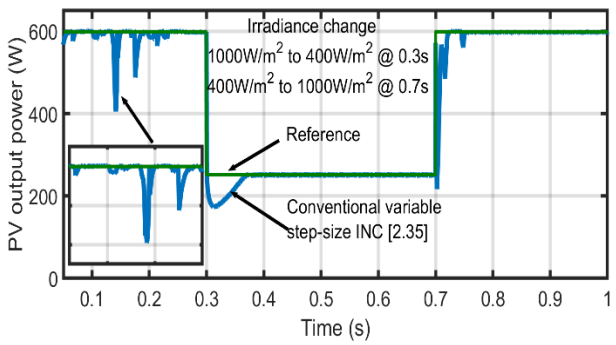

Fig. 4.3. PV module output power characteristic with bigger scaling factor compared to optimum value.

4.2 Proposed variable step-size INC algorithm

The PV module operating voltage ranges between $0-V_{oc}$, however unnecessary sampling within large range slows down the tracking speed. Limiting the search range restricts the

viable operating range, thus reduces the tracking time for the MPPT algorithm. Therefore, an initial sampling value of 76% of open-circuit voltage is embedded in the proposed algorithm to restrict search range [4.1]. This is to enable the proposed MPPT to record fewer perturbation directions before converging at MPP. Hence, the structure of proposed MPPT technique for PV system is defined by dividing the search range of the P-V characteristic curve shown in Figure 4.4 into three regions, namely A, B and C. For satisfactory speed response, the operating range for the proposed MPPT technique is given in inequality (4.4).

$$0.76V_{oc} \leq V_{pv}(k) \leq V_{oc} \tag{4.4}$$

The proposed MPPT algorithm is divided into three parts. The following subsections explained them:

4.2.1 Proposed Autonomous Scaling Factor

Conventional variable step-size technique includes a preset scaling factor, which cannot achieve both fast dynamic response and steady-state precision. Therefore, the scaling factor should be varied to reduce the power loss at steady state. Figure 4.4 shows the characteristic curve of the PV module and the study of it demonstrates an important observation near the MPP. The output voltage variation of PV module is mimicked to vary the scaling factor to enhance the tracking performance during transient and steady-state

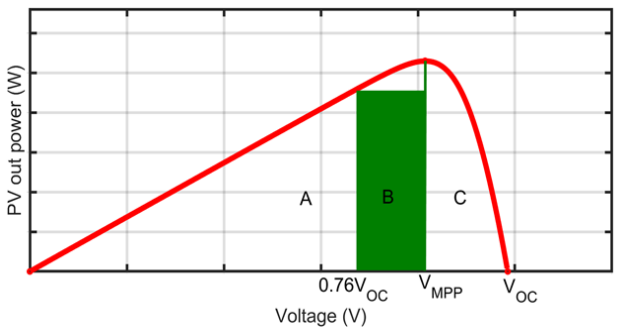

Figure 4.4. P-V Characteristic curve describing the search range.

situations. The range of voltage change for region B and C, are respectively given in equations (4.5) and (4.6).

$$\Delta V_B = V_{pv}(k) - 0.76V_{oc} \quad (4.5)$$

$$\Delta V_C = V_{oc} - V_{pv}(k) \quad (4.6)$$

To ensure an adjustable scaling factor towards the MPP, a new autonomous scaling factor is proposed, which can be illustrated in terms of ΔV_B and ΔV_C given in (4.7).

$$N_D = \frac{\Delta V_B}{\Delta V_C} = \left| \frac{V_{pv}(k) - 0.76V_{oc}}{V_{oc} - V_{pv}(k)} \right| \quad (4.7)$$

4.2.2 Estimation of V_{oc}

For accurate operation plus avoid adding any extra hardware components, the proposed variable MPPT technique estimates the V_{oc} value. This voltage is required in calculating the proposed autonomous scaling factor. Most of MPPT algorithms use either temperature or irradiance sensors or both to estimate V_{oc}. Therefore, the value can be estimated given in equation (4.8) as in [4.2- 4.4].

$$V_{oc} = V_{oc\_STC} + \alpha V_t In \left(\frac{G}{G_{STC}}\right) + k_v(T - T_{STC}) \quad (4.8)$$

Where, G_{STC}, V_{oc_STC}, and T_{STC} are the solar irradiance, open circuit voltage and temperature at standard test conditions respectively. G, V_t, T and k_v are the operating solar irradiance, thermal voltage, operating temperature, and temperature coefficient of V_{oc} respectively. [4.5]. The output current of the PV module and its short circuit current, I_{SC_STC} has a linear relationship [4.6-4.9] as in (4.9).

$$I_{PV} = \left(I_{SC\_STC} + k_i (T - T_{STC})\right) \frac{G}{G_{STC}} \quad (4.9)$$

By keeping the temperature constant ($T = T_{STC}$), the estimation of V_{oc} for the PV module given in (4.8) is updated using equation (4.9) as follows:

$$V_{oc} = V_{oc\_STC} + \alpha V_t In\left(\frac{I_{pv}}{I_{SC\_STC}}\right) \quad (4.10)$$

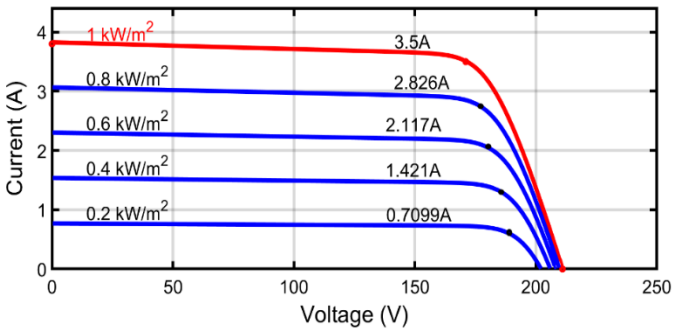

Figure 4.5. Voltage - current Characteristic curve for PV modules.

Table 4.1. Estimation of the module open circuit voltage.

Irradiance (W/m^2)	**1000**	**800**	**600**	**400**	**200**
Ambient current (A)	3.5.00	2.826	2.11	1.421	0.7099
Actual V_{oc_array}	211.00	209.60	207.70	205.30	201.70
Estimated V_{oc_array}	210.21	208.18	205.38	201.56	195.89
Deviation	0.37%	0.68%	1.11%	1.82%	2.88%

The estimated value of the open-circuit voltage for different irradiance levels is summarized in Table 4.I. The estimated values are close to the actual values. Although, under lower irradiance levels as in Figure 4.5, the expression in (4.10) shows deviations from the actual value, but the deviation is below, 3%, which is substantially low and satisfactory for a typical PV module system.

4.2.3 Slope Angle Variation Algorithm

The conventional variable step-size presented in (4.1), is dependent on the slope of the P-V characteristic curve; hence, exhibits dynamic performance deterioration under varying irradiance conditions. There is notably change of power (changing in MPP) when irradiance level changes from G_1 to G_2 as shown in Fig. 4.6a, while there is a relatively

small change in PV voltage. This results in a significant large step-size value, which may push the MPPT algorithm to take more time to reach the new MPP. To address this issue, the slope angle between PV power change and related voltage change is utilized. This can control the change in power, which eventually controls the step-size value irrespective of the variation of PV voltage. When the angle is small, the PV power change also becomes small to limit the large increase in step size. The slope angle variation can be derived from PV output power as using Figure 4.6b as follows:

$$\frac{dP_{pv}}{dV_{pv}} = \frac{\sin\delta}{\cos\delta} \tag{4.11}$$

Then,

$$\left|\frac{\sin\delta}{\cos\delta}\right| = \left|I_{pv} + V_{pv}\frac{dI_{pv}}{dV_{pv}}\right| \tag{4.12}$$

Where, δ is the angle between the PV module output power variations to the voltage variation.

$$\sin\delta = \left(I_{pv} + V_{pv}\frac{dI_{pv}}{dV_{pv}}\right)\cos\delta \tag{4.13}$$

$$\sin\delta = \left(I_{pv} + V_{pv}\frac{dI_{pv}}{dV_{pv}}\right)\frac{dV_{pv}}{\sqrt{dP_{pv}^2 + dV_{pv}^2}} \tag{4.14}$$

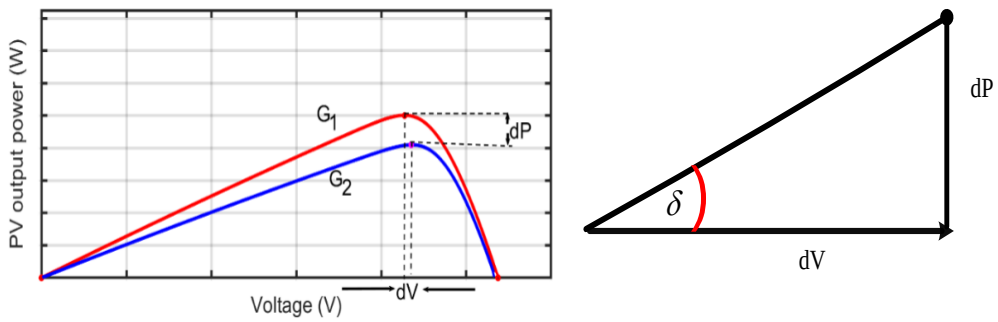

(a) (b)

Fig. 4.6. (a) Effect of irradiance on MPP, (b) Slope angle variation

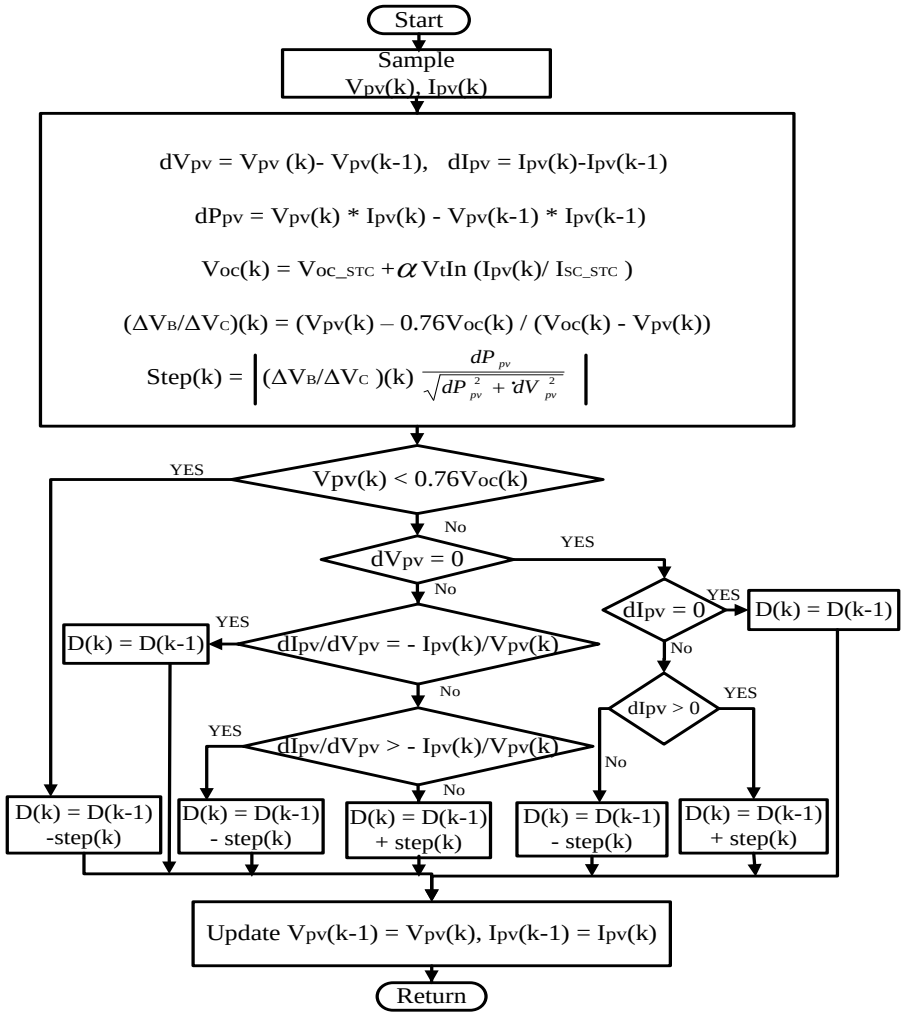

Figure 4.7. Flow chart of the proposed variable step-size INC MPPT.

$$= \frac{I_{pv} dV_{pv}}{\sqrt{dP_{pv}^2 + dV_{pv}^2}} + \frac{V_{pv} dI_{pv}}{\sqrt{dP_{pv}^2 + dV_{pv}^2}} \tag{4.15}$$

$$\sin\delta = \frac{dP_{pv}}{\sqrt{dP_{pv}^2 + dV_{pv}^2}} \tag{4.16}$$

For a small value of δ,

$$\sin\delta = \tan\delta = \frac{\sin\delta}{\cos\delta} = \frac{dP_{pv}}{dV_{pv}} \tag{4.17}$$

Using equations (4.7) and (4.16), the proposed duty cycle using the new slope angle variation algorithm can be calculated as:

$$D\ (k) = D(k-1)\ \pm \left(\frac{\Delta V_B}{\Delta V_C}\right) \frac{dP_{pv}}{\sqrt{dP_{pv}^2\ +\ dV_{pv}^2}} \tag{4.18}$$

Hence, the new proposed variable step-size is given by:

$$\Delta D_{mod} = \left| \left(\frac{\Delta V_B}{\Delta V_C}\right) \frac{dP_{pv}}{\sqrt{dP_{pv}^2 + dV_{pv}^2}} \right| \tag{4.19}$$

The operation of the proposed MPPT algorithm is represented in the flow chart shown in figure 4.7. Unlike the conventional variable step-size INC MPPT where the PV system performs several perturbations before reaching MPP, a minimum sampling value which is 0.76 of open circuit voltage is used to decide the algorithm rule. If any of sampling is below the minimum value, both the slope and variable scaling factor are determined and the duty cycle of the converter is increased; otherwise, a variable step-size with new scaling factor determined at that sampling value is applied. In this case, the algorithm ensures that the MPP is reached with fewer perturbations to improve the tracking time of the proposed MPPT. It is important to note that the proposed algorithm is restricted to operate on the condition that $V_{pv}(k)$ is less than $0.76V_{oc}$ or greater than $0.76V_{oc}$ as shown in Figure 4.7 and so the condition that $V_{pv}(k) = 0.76V_{oc}$ will not be recognised by the proposed algorithm. Thus, the algorithm will not operate at $0.76V_{oc}$.

4.3 Simulation results and discussion

The PV system under test consists of ten series-connected PV modules (the whole rated power is 600 W), a dc battery, and a dc-dc boost converter. The tested PV system is shown in Figure 4.8 and it is grid connected PV system, where the battery represents the grid and interfacing inverter. Table 4.2 shows the PV module specifications. The simulation is

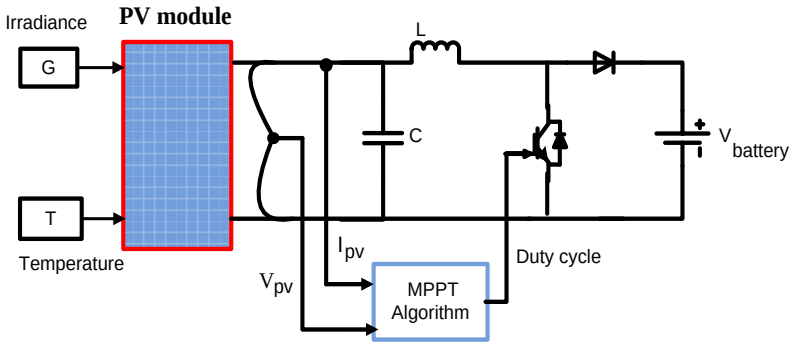

Figure 4.8**.** PV system under investigation.

Table 4.2. The PV module parameters (MSX60) [4.5].

Parameters	**Value**
PV module Short-circuit current (I_{sc})	3.8A
PV module open-circuit voltage (V_{oc})	21.1V
Maximum PV module current (I_{mpp})	3.5A
Maximum PV module Voltage (V_{mpp})	17.1V
Maximum PV module power (P_{max})	60W
temperature coefficient of V_{oc} (K_v)	-0.08$V/$℃
Temperature coefficient of I_{sc} (K_i)	0.005$A/$℃

carried out under different irradiance levels. The initial irradiance is 1000 W/m^2 and is changed to 400 W/m^2 at 0.3 s. The irradiance level then changed back to 1000 W/m^2 at 0.7 s. The proposed MPPT technique, the conventional variable step-size INC [2.35] and two existing modified techniques in [2.41] and [2.43] are simulated and compared at same conditions of irradiance and temperature. Figure 4.9a is the output power of the PV modules under variable irradiance conditions for the proposed and conventional variable step-size INC MPPT techniques. It proves that the proposed technique is more effective than conventional MPPT technique. The proposed algorithm tracks the MPP faster with minimum oscillations around MPP compared with the conventional counterpart. Figures 4.9b and 4.10a represent the converter duty cycle of proposed and conventional variable step-size INC MPPT, respectively. The duty cycle of proposed variable step-size INC MPPT reaches its optimum value with small oscillations within a satisfactory time.

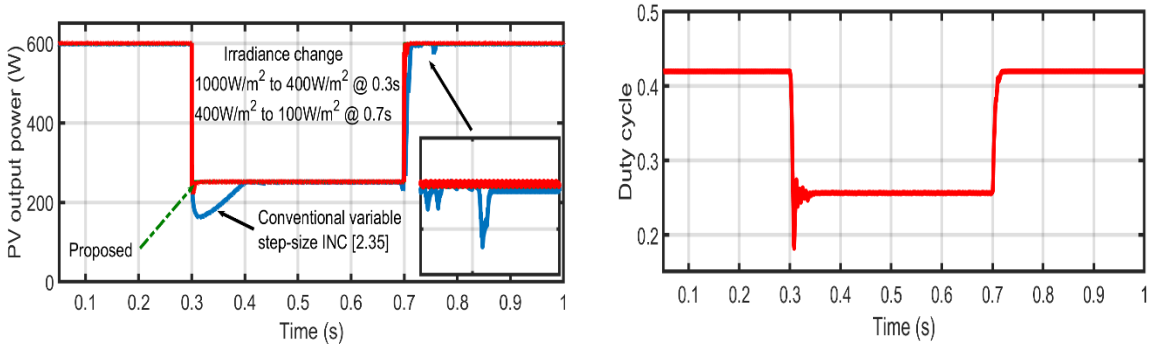

(a) (b)

Figure 4.9. Simulation of PV system for conventional and proposed MPPT technique under varying irradiance: (a) PV modules output power, (b) duty cycle for the proposed technique.

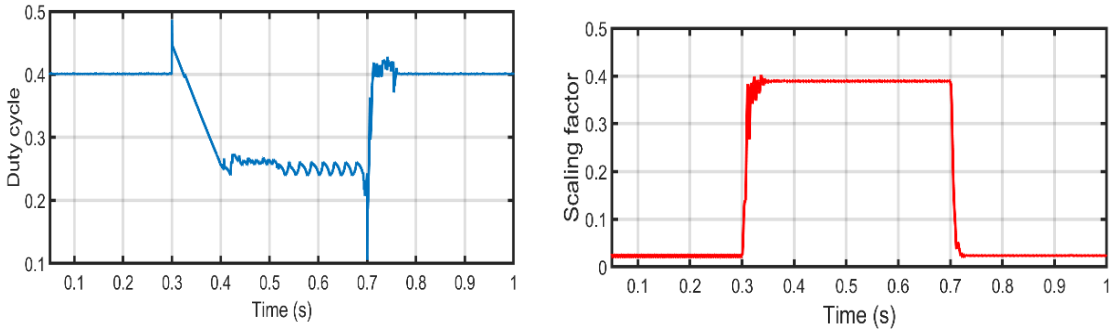

(a) (b)

Figure 4.10. Simulation results: (a) Duty cycle for conventional variable step-size INC technique; (b) proposed autonomous scaling factor during changes in irradiance.

Furthermore, during the changes in irradiance, the duty cycle of the proposed technique moves toward the optimum value faster without drift. On the contrary, the converter duty cycle of conventional MPPT technique shown in Figure 4.10a exhibits significant oscillations around its optimum value with drift when the irradiance increased from 400W/m2 to 1000W/m2. The performance of the new autonomous scaling factor is shown in Figure 4.10b. The scaling factor is adjusted irrespective to irradiance change to further improve the dynamic response. Thus, with an embedded autonomous scaling factor, the proposed MPPT tracking time is faster in start-up and for a large change in irradiance

compared to conventional variable step-size INC technique with a fixed scaling factor. It is importance to note from Table 4.1 that at low irradiance level, autonomous scaling factor value is high compared to high irradiance level. This is because at low irradiance level, the deviation of estimated value of V_{oc} is greater than that at high irradiance level. Since the denominator of the autonomous scaling factor expression is a function of V_{oc}, hence bigger scaling factor value is required as compared to higher irradiance level. The proposed algorithm shows a tremendous reduction of power oscillations at both dynamic and steady-state, and MPP is directly reached under changes in irradiance conditions. To further test the robustness of the proposed algorithm, Figure 4.11 compares the proposed technique and two other existing modified variable step-size INC MPPTs. All algorithms track optimum power point, however, the proposed MPPT technique is faster than other two techniques in [2.41] and [2.43]. The variable step-size INC technique in [2.41] tracks better than [2.43] under step change in irradiance. However, due to the elimination of the division terms (change in PV module voltage), which eventually decreases the step-size, the algorithm experiences slow tracking at start up compared with the proposed MPPT technique. Additionally, scaling factors in [2.41,2.43] are not optimum under all operating conditions. This means that under fast changing weather conditions, both techniques could fail to track MPP. Tables 4.3–4.5 present a performance comparison between the proposed MPPT technique, the conventional variable step-size INC [2.35] and two existing modified techniques in [2.41,2.43]. These tables demonstrate the tracking time, power of oscillations at MPP and tracking efficiency. Further tests were also carried out to ascertain the robustness of the proposed MPPT technique and the three MPPT techniques under

Table 4.3. Performance indicators of the proposed, conventional and two existing modified variable step-size INC MPPT under variable irradiance.

Conditions	**Variable step-size methods**	**Energy used (mJ)**	**Dynamic performance**	**Tracking accuracy**
1000W/m^2 to	[2.35]	1522	Low	Low
	[2.41]	186	Low	High
400W/m^2	[2.43]	192	Low	Low
	Proposed	163	High	High

Table 4.4. Performance analysis of the proposed, conventional and the two existing modified variable step-size INC MPPT under variable irradiance.

Conditions	Variable step-size INC Methods	Tracking time (ms)	Efficiency (%)
1000W/m2 to 400W/m2	[2.35]	120.3	98.20
	[2.41]	18.4	99.38
	[2.43]	27.3	98.01
	Proposed	12.6	99.70

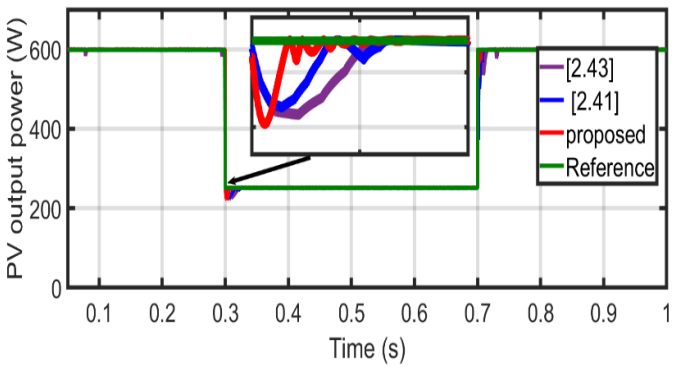

Figure 4.11. The proposed and the other two modified MPPT techniques.

Table 4.5. Tracking comparison of the proposed, conventional and the two-existing modified variable step-size INC MPPT under variable irradiance.

Variable Step-Size Methods	Average Power at 1000 W/m^2	Settling Time (s)	Oscillation at MPP, W	Efficiency (%)
[2.35]	595.2	32.88	3.3	99.45
[2.41]	596.4	13.17	2.1	99.65
[2.43]	595.7	16.50	2.8	99.53
Proposed	596.9	10.09	1.6	99.73

investigation using different irradiance levels. The irradiance levels under this scenario are from 800 W/m^2 to 400 W/m^2 at 0.3 s and then changed back to 400 W/m^2 at 0.7 s. Figure 4.12 shows the output power of the proposed, conventional [2.35] and existing modified variable step-size MPPT [2.43] techniques, while Figure 4.13 depicts the output power of the proposed technique and another existing modified variable step-size MPPT

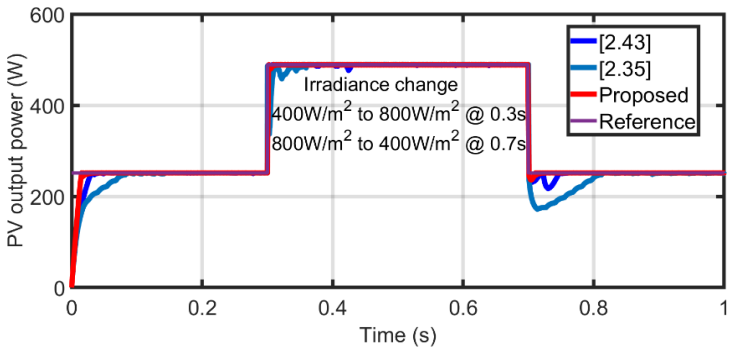

Figure 4.12. Simulation results of the proposed and conventional variable step-size MPPT under variable irradiance conditions.

Table 4.6. Tracking time with step irradiance change of the proposed, conventional and two existing modified variable step-size INC MPPT techniques.

Conditions	**Variable Step-Size INC Methods**	**Tracking Time (ms)**
800 W/m^2 to 400 W/m^2	[2.35]	88.8
	[2.41]	17.6
	[2.43]	31.2
	Proposed	10.2

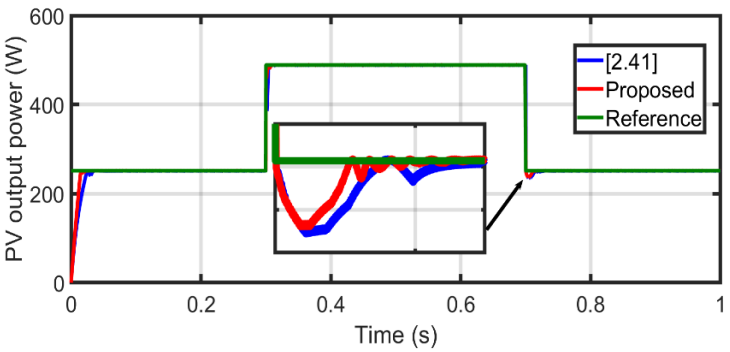

Figure 4.13. Simulation results of the proposed and the two existing modified variable step-size MPPT algorithms under variable irradiance conditions.

[2.41] techniques under study. It is evident that the proposed MPPT technique tracks faster as compared to the conventional and the two modified techniques under this condition. Table 4. 6 shows the tracking time of each algorithm under dynamic weather conditions.

In general, the proposed algorithm has high dynamic performance, high accuracy, low overshoot, and low energy for tracking. Additionally, it is obvious that the proposed MPPT technique provides higher tracking accuracy and does not require a pre-set scaling factor.

4.4 Partial Shading Analysis of the Proposed MPPT

Partial shading in the PV system is expected in the PV array where certain portions of the PV modules are exposed to unequally distributed radiation intensity. Under this condition, multiple peaks which consist of local and global maximum power points are generated in the PV characteristic curve. Conventional MPPT fails to track global maximum power point due to lack of resistance of the conventional MPPT to the local maximum power point. The effect is significant power loss in the PV system and waste of energy in the PV system under partial shading condition. The performance of the proposed MPPT technique is tested using scanning technique. Ten PV modules (MSX60) are connected in series with a bypass diode connected in parallel with each PV module. Initially, five PV modules were made to operate at 1000 W/m^2 while the remaining are partially shaded and operating at 500 W/m2. Figure 4.14 shows the arrangement of the PV modules. The output power of the PV array is shown in Figure 4.15. Clearly, it evident that the proposed MPPT has a resistance to local maxima, as this local maximum power point does not prevent the proposed MPPT from reaching the global maximum power point. To further test the robustness of the proposed MPPT, the shading pattern is changed where three of the PV modules received irradiance of 1000 W/m^2, four PV modules received 500 W/m^2 and three of the PV modules received 300 W/m^2. Figure 4.16 shows the arrangement of the PV modules with different shading conditions. Figure 4.17 shows the PV output power, which demonstrates the capability of the proposed MPPT to distinguish global maximum power from the local maximum power. To further clarify and analyse the behaviour of the proposed MPPT, the same partial shading condition of Figure 4.16 is repeated with different irradiance on unshaded PV modules. The irradiance levels were made to vary from 200 W/m^2 to 1000 W/m^2 at 0.5 s and then changed from 1000 W/m^2 to 200 W/m^2 at 1s. Figure 4.18 shows that the proposed MPPT tracks the global maximum point with

short time under variable irradiance conditions. This is due to the limited search space of the proposed algorithm to reach the global maximum power in relatively short time. The wider search space constitutes significant power loss. The ability of the proposed MPPT to track the global maximum power point without preventing from the local maximum power point demonstrates that there is a potential of real energy gain under partial shading conditions. The global maximum power tracked by the proposed MPPT is about 99.87% with minimum power oscillation.

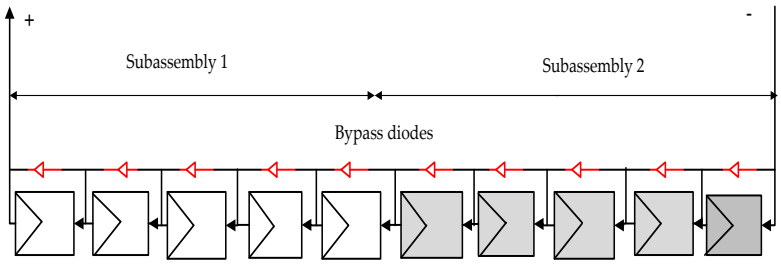

Figure 4.14. PV array under partial shading condition.

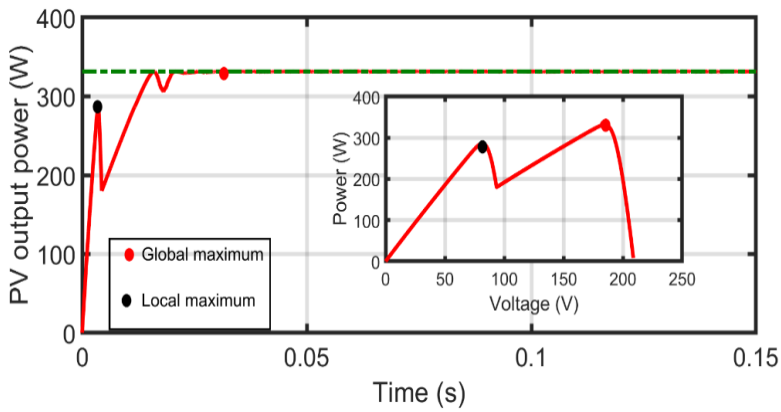

Figure 4.15. Global and local maxima under scanning.

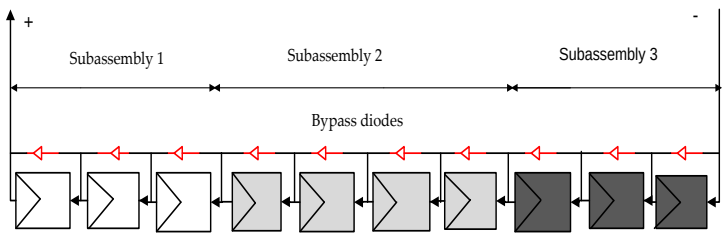

Figure 4.16**.** PV modules under partial shading condition 2.

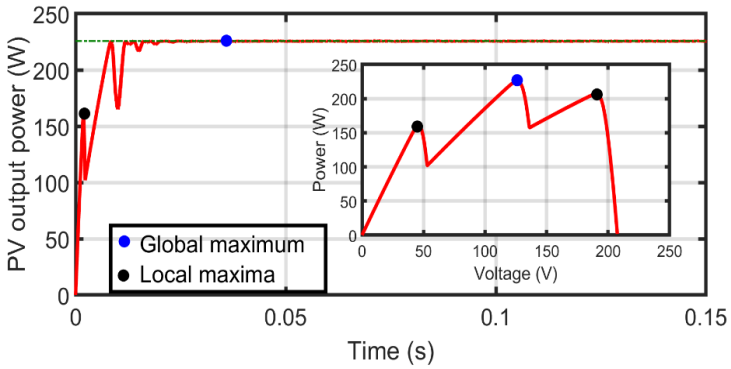

Figure 4.17. PV output power for partially shade PV system.

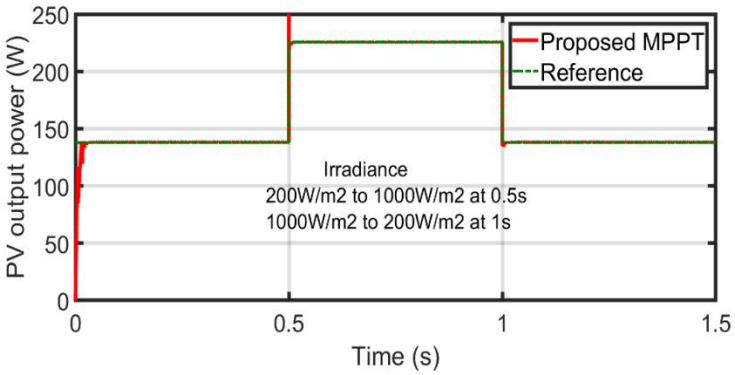

Figure 4.18. Output power for PV arrays under partial shaded condition with two irradiance levels.

4.5 Experimental results

The proposed MPPT technique and conventional variable step-size INC technique in [2.35] are experimentally evaluated in this section. Figure 4.19 shows the experimental prototype of the grid connected PV system. The experimental prototype comprises of boost converter connected to 110 V DC bus (representing the grid and interfacing inverter) and a PV emulator. The experimental setup parameters are listed in Table 4.7. The PV emulator is based on PV module parameters listed in Table 4.8, where the maximum output power and the maximum output current are set to the programmable power supply (EA-PS-83600-10 with analogue interface). The microcontroller (CY8C5888LTI-LP097) is used to set the reference output voltage based on the built-in PV model, irradiance, and the output current. For clarity, Figure 4.20 shows the flow chart of the microcontroller programme for PV emulator. To compare the dynamic performance of the two MPPT

algorithms, the irradiance level step change from 1000 W/m2 (PV output power is 300 W, PV voltage is 54.7 V) to 500 W/m2 (PV output power is 150 W, PV voltage is 51.43 V). The experimental results of the two MPPT techniques are shown in Figure 4.21. The results show a detail view of the dynamic performance of both the conventional and proposed viable step-size INC techniques during step irradiance change. It can be concluded from the results that the proposed viable step-size INC technique succeeded to track the maximum power in 60 ms, which is faster than the conventional algorithm that needs around 140 ms to track the MPP. Additionally, it can be observed from Figure 4.21 parts c and d that the dc-bus delivered output power and is more stable with minimum oscillations at steady state, however, the dc-bus output power is less than the PV rated power at maximum point; due to the boost converter switching and conduction losses and boost converter inductor wire resistance.

Table 4.7. Experimental setup parameters.

Parameters	**Value**
Boost converter Switching frequency	10 kHz
Boost converter inductance	1.5 mH
Boost converter capacitance	2200 µf
DC-bus voltage	110 V

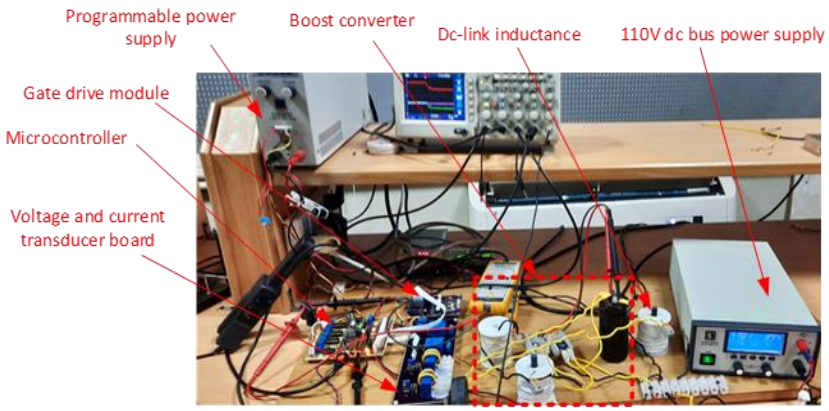

Fig. 4.19. Experimental set up.

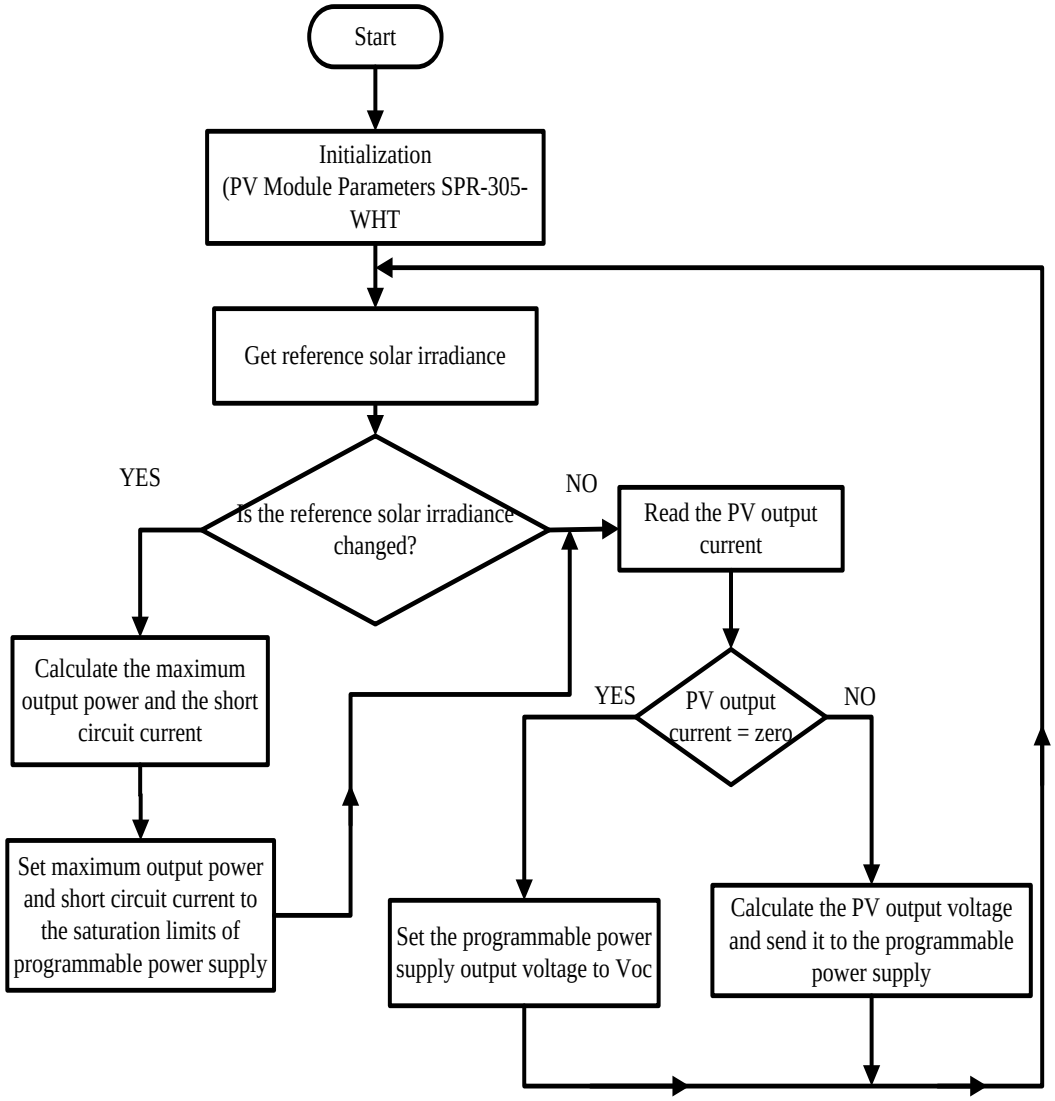

Figure 4.20. Flow chart of the microcontroller programme for PV emulator.

Table 4.8. The PV module parameters (MODEL SUNPOWER SPR-305-WHT).

Parameter	**Value**
Maximum power	305 W at STC
Number of Cells	96
Current at MPP	5.58 A
Voltage at MPP	54.7 A
Open Circuit Voltage	64.2 V
Short Circuit Current	5.96 A

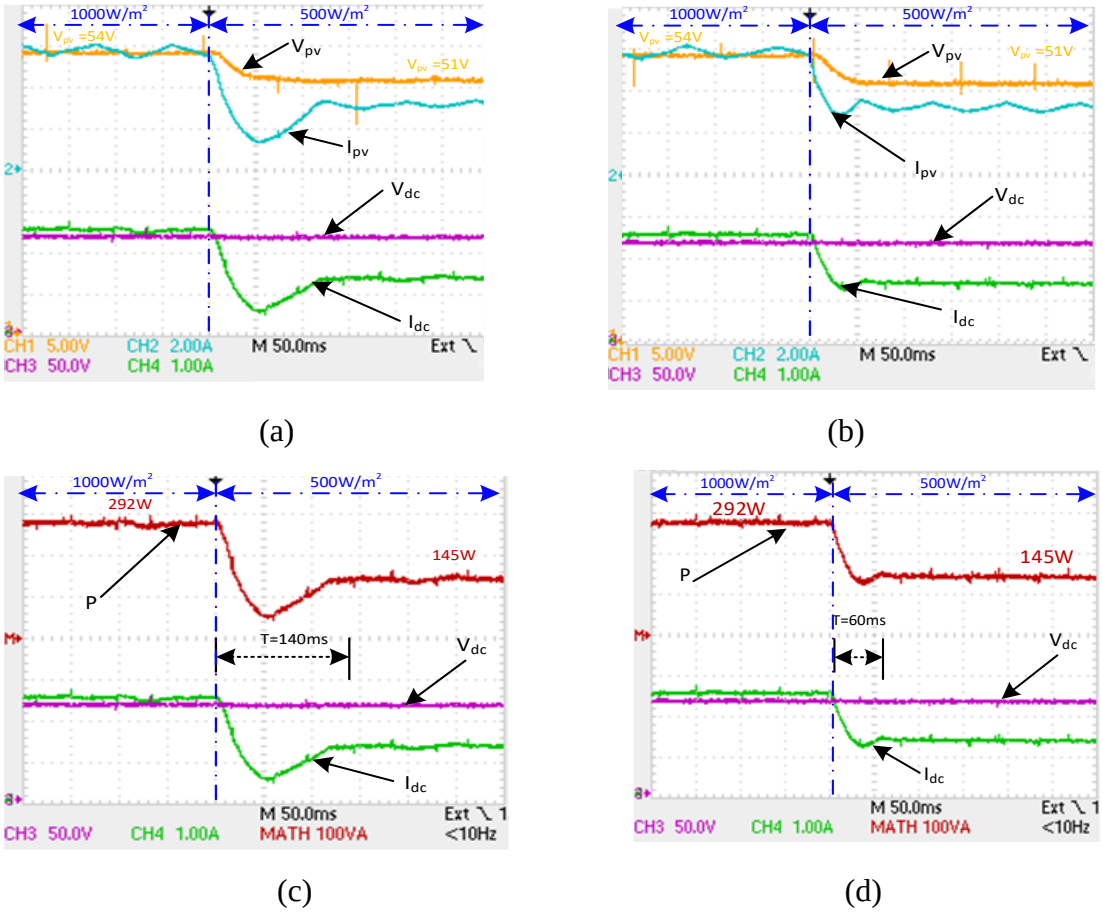

Figure 4.21. Experimental results: (a,b) The PV output voltage (VPV), PV output current (IPV), dc-bus voltage (Vdc), and dc-bus delivered current (Idc); with conventional variable step-size, and proposed MPPT respectively, (c,d) dc-bus delivered power (P), dc-bus voltage (Vdc), and dc-bus delivered current (Idc) with conventional variable step-size and proposed one respectively.

4.6 Summary

In this chapter, a modified variable step-size INC MPPT technique has been proposed. The drawbacks of conventional variable step-size in INC MPP technique has been discussed in order to tackle them via the new proposed variable step-size INC technique. A new autonomous scaling factor has been proposed. The proposed technique is capable to enhance both the steady-state and dynamic performance response. The proposed technique is more practical in operating due to autonomous response nature under sudden

changes in irradiance. Conventional, two modified and proposed variable step-size INC MPPTs have been simulated under different operating conditions using MATLAB/SIMULINK software. The feasibility and effectiveness of the proposed technique have been confirmed. The proposed MPPT technique demonstrates faster tracking speed with minimum oscillations around MPP both at steady-state and dynamic conditions. The experimental results validate the practicability and effectiveness of the new MPPT technique as well.

References

[4.1] H. R. Enslin, M. S. Wolf, D. B. Snyman and W. Swiegers, "Integrated photovoltaic maximum power point tracking converter," IEEE Transactions on Industrial Electronics, vol. 44, no. 6, pp. 769-773, Dec.1997.

[4.2] V. J. Chin, Z. Salam and K. Ishaque, "An improved method to estimate the parameters of the single diode model of photovoltaic module using differential evolution," 2015 4th International Conference on Electric Power and Energy Conversion Systems (EPECS), Sharjah, 2015, pp. 1-6

[4.3] J. Ahmed and Z. Salam, "An Accurate Method for MPPT to Detect the Partial Shading Occurrence in a PV System," in IEEE Transactions on Industrial Informatics, vol. 13, no. 5, pp. 2151-2161, Oct. 2017.

[4.4] Ahmed, J.; Salam, Z. An Improved Method to Predict the Position of Maximum Power Point During Partial Shading for PV Arrays. IEEE Trans. Ind. Informat. 2015, 11, 1378–1387.

[4.5] I. Owusu-Nyarko, K. H. Ahmed, F. Alsokhiry and Y. Al-Turki, "A New 0.8Voc Model Technique to Estimate the Peak Global Voltage for Medium Voltage Megawatt Photovoltaic System Integration," 2020 9th International Conference on Renewable Energy Research and Application (ICRERA), Glasgow, United Kingdom, 2020, pp. 439-444.

[4.6] N. Díaz, A. Luna and O. Duarte, "Improved MPPT short-circuit current method by a fuzzy short-circuit current estimator," 2011 IEEE Energy Conversion Congress and Exposition, 2011, pp. 211-218.

[4.7] B. Li, A. Migan-Dubois, C. Delpha and D. Diallo, "Irradiance Dependence of the Short-Circuit Current Temperature Coefficient of sc-Si PV Module," 2020 47th IEEE Photovoltaic Specialists Conference (PVSC), 2020, pp. 0564-0568.

[4.8] M. M. Shebani, T. Iqbal and J. E. Quaicoe, "Comparing bisection numerical algorithm with fractional short circuit current and open circuit voltage methods for MPPT photovoltaic systems," 2016 IEEE Electrical Power and Energy Conference (EPEC), 2016, pp. 1-5,

[4.9] H. Liu et al., "The Impact of Haze on Performance Ratio and Short-Circuit Current of PV Systems in Singapore," in IEEE Journal of Photovoltaics, vol. 4, no. 6, pp. 1585-1592, Nov. 2014.

[4.10] W. Bingbing, Y. Zhongdong, and X. Xiangning, “Design of simulation model of PV cells based on VSR PWM rectifier circuit,” in Proc. Int. Conf. Energy Environ. Technol., 2009, vol. 2, pp.127–130.

Chapter 5

A New 0.8Voc Model Technique to Estimate the Peak Global Voltage for Medium Voltage Megawatt Photovoltaic System Integration

This chapter reviews different techniques being used to address challenges in global maximum power point during partial shading conditions. It further analyses limitations of conventional 0.8Voc model. A new 0.8Voc model technique to estimate the peak global voltage for medium voltage megawatt photovoltaic (PV) system integration is proposed. The proposed model technique is capable of exploiting the advantages of conventional 0.8Voc, while improving its performance in the energy yield during partial shading conditions. The principles of design and theoretical analysis of the proposed algorithm are presented and feasibility also validated by simulation for medium voltage megawatt photovoltaic (PV) system integration.

5.1 Background

For PV system interconnections, standards such as IEEE 1547 2003 [5.1] and local utility interconnection regulations define the grid interface response to system disturbances. Although, PV power generation has received significant attention, the system suffers from a major limitation which is the non-linear characteristic of a PV module particularly under partial shaded conditions [5.2]. In practice, the output power from PV string is the summation of individual PV module connected in series. As demonstrated in Figure 5.1, when the PV string is exposed to uniform irradiance condition, only one peak is generated on I-V and P-V characteristic curves. The aforementioned MPPT techniques discussed in chapter two and the proposed variable step size in chapter four can successfully locate the MPP. Since conventional MPPT techniques are specifically designed to track MPP under uniform weather conditions, they may not locate GMPP unless modified under partial shading condition (PSC). The generated output power from the PV array changes with different shadow degrees of PV string and different partial shading pattern is form leading

to significant power lost. PSC in PV systems is a condition in which only a certain portion of the PV module is shaded, while other parts remain uniformly irradiated. It is typically caused by clouds formation, shadow from buildings, trees, poles, overhead cables, etc. When the PV modules is exposed to partial shading, significant amount of energy is lost because the shaded module is short circuited by its respective bypass diode. As a result, multiple P-V curves, with several local and global peaks are generated. Considering the high initial cost of installation of a PV system and low energy conversion efficiency, it is important to deploy a suitable MPPT technique to extract maximum power from the PV modules since conventional MPPT fail to distinguish global MPP from local MPP.

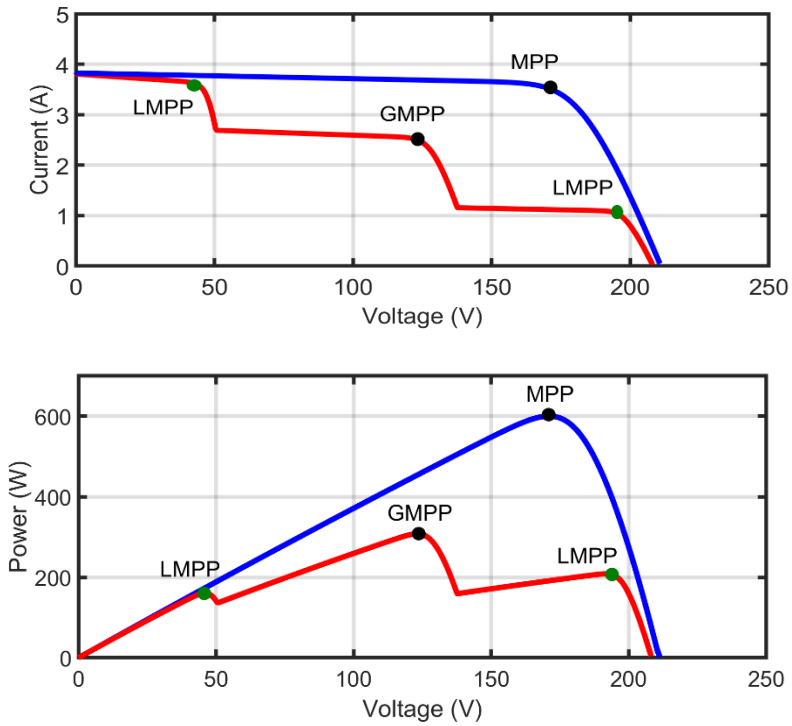

Figure 5.1. PV string under normal and partial shading conditions.

5.2 Literature survey of global maximum power point tracking (GMPPT) technique

In order to solve problems associated with PSC, different solutions have been introduced in the literature [5.3]. These solutions for PSC have been classified into group based on the features of GMPPT methods and these are;

- Extension of conventional MPPT method.
- Method based on observation of P-V and I-V characteristic curve.
- General GMPPT techniques.

5.2.1 Extension of conventional MPPT method

This technique was borne out from modification of conventional MPPT technique to have resistance against local MPP [5.4]. The methods under this group are periodic reset and curve scanning technique, widen search range technique and two-stage technique. A solution is proposed in [5.5] which involves a three points incremental P&O method. This technique improved the tracking performance of P&O under PSC, however, at some point, the algorithm trapped by local MPP. A periodic search is introduced in [5.6] to enable P&O build resistance to local MPP in order to reach global MPP. A periodic scanning on the P-V characteristic curve is proposed in [5.7] in order to track GMPP. A solution is also proposed in [5.8] where a full scanning technique was performed on the P-V characteristic curve. Although, this method is simple, the tracking speed is slow and the scanning may overlook the GMPP for long PV string. Widen search range is another simple technique of extension of conventional MPPT method for GMPP [5.9-5.11]. In [5.12], a widen search range technique is proposed by defining the regions where local optimization strategy is used to track GMPP. Although, the technique tracked GMPP, however, the widened search range slow down the tracking process. In [5.13], widen search technique is proposed to search GMPP from both left and right of the P-V characteristic curve under PSC. Although, GMPP is located but the technique is slow due to many perturbations performed within the wider search space. A great number of two-stage methods to track GMPP under PSC have been proposed in the literature [5.14-5.15]. In this technique, one stage is used to move the operating point closed to the GMPP and then tracked the actual GMPP using conventional MPPT in the other stage. A solution is proposed in [5.16] using switch impedance circuit to locate GMPP and then conventional MPPT is applied to track the actual MPPT during the second stage. This technique is simple but it requires additional circuit for implementation

5.2.2 Method based on observation of P-V and I-V characteristic curve

A comprehensive study on P-V and I-V characteristic curve have been undertaken by many authors under PSC and this study has been extended to govern GMPP technique [5.17-5.18]. Observation in [5.17] indicates that the peaks of a partial shaded P-V curve are located at the integral multiples $0.8V_{OC}$. This method is easy and straightforward to implement. Also, the tracking performance is effective since the global search method requires only the vicinities of $0.8V_{OC}$ instead of searching the whole P-V characteristic curve. The drawback of this technique is that the global peaks will overlook by this technique with long PV string.

5.2.3 General GMPPT methods

These are technique specifically designed to address GMPP issues. A great number of works has been undertaken under this category. They can be classified under segmental search method and soft computing method [5.19-5.20].

(a) Segmental search method

Several segmental search methods have been proposed in the literature to deal with PSCs including DERECT [5.19] and Fibonacci search [5.21] methods. Segmental search methods work by gradually restricting and shifting the optimum searching range within which GMPP can be located. With the use of Lipschitz function, DIRECT method can be utilised to progressively reduce the searching interval based on the sample values and the conditions. Figure 5.2 demonstrates the tracking process of the DIRECT method. Regarding the Fibonacci search method, the Fibonacci sequence is used to establish the length of the considered interval. For successful executing this technique, it is important to define a condition to detect PSC. The advantage of this method is that it is straight-forward to implement, however, the main drawbacks are that the algorithm may miss the actual GMPP. Also, the selection of the initial value is very challenging as this may lead to tracking local MPP instead of GMPP.

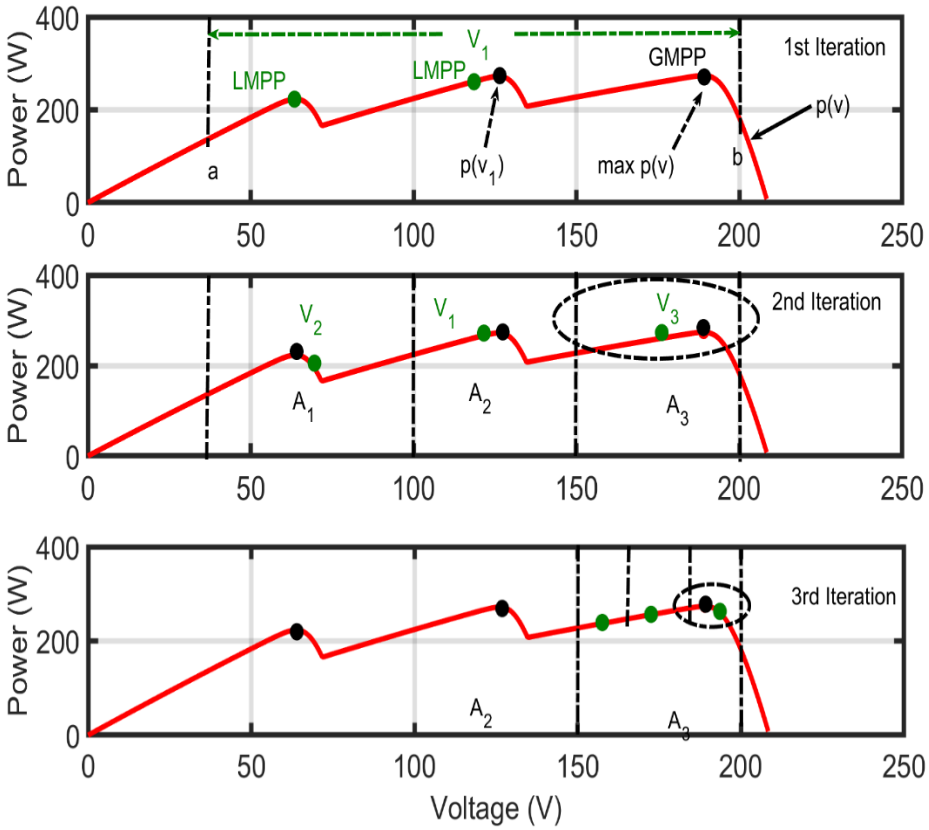

Figure 5.2. Demonstrating Iteration process of DIRECT technique under PSC.

Table 5.1. Specifications of the PV module (MSX60).

Parameters	Value
Short-circuit current (I_{sc})	3.8A
Open-circuit voltage (V_{oc})	21.1V
Current at maximum power point (I_{mpp})	3.5A
Voltage at maximum power point (V_{mpp})	17.1V
Maximum output power (P_{max})	59.85W
V_{oc} coef. of temperature (K_v)	-0.08V/℃
I_{sc} coef. of temperature (K_i)	0.003A/℃

(b) Soft computing method

Soft computing method is another GMPPT method which include anti-colony optimization [5.22], grey wolf optimization (GWO) [5.23], simulated annealing technique [5.24], particle swarm optimization technique and others [5.25-5.28] and others. All of the aforementioned techniques have been demonstrated in the literature and shown to have

good tracking performance under partial shading condition. Among these techniques, particle swarm optimization has been proven to the most useful searching technique and is based on fish schooling and bird flocking pattern [5.29]. With PSO different duty cycles for different number of particles is used. These duty cycles are called particle position and is given by;

$$d_i\ (k+1) = d(k) + V_i(k+1), \qquad i = 1, 2, \ldots . N \tag{5.1}$$

where, N is the total number of particles, V_i is the velocity of particles, i, is the number of iterations and k is the sample value. PSO has accurate tracking performance under different patterns of partial shading conditions [5.30]. Also, the algorithm has almost no oscillation around GMPP since the velocity is zero. However, the drawback is that it takes long time for searching the GMPP and has several perturbation steps before converging to GMPP. The literature review discovered some limitations in the method based on observation of P-V and I-V characteristic curve (conventional 0.8Voc model) .This chapter discussed the limitations and a new 0.8Voc model is suggested to overcome the limitations.

5.3 Voltage and current relationship of PV modules under partial shading condition

The PV module operating under partial shading condition acts as a load instead of power source as this module is forced to operate at a reverse biased region. This leads to highly localized power dissipation [5.31] in the form of heat, which results unrepairable damage to the shaded PV module. Hence, it is necessary to employ bypass diodes in the entire PV array system as shown in Figure 5.3 to prevent localized power dissipation under partial shading conditions. These bypass diodes are added to the PV configuration system to protect the modules during partial shading condition from self-heating. During normal weather conditions, the bypass diodes have no impact on the PV configuration system and become reverse biased. However, when the PV modules are exposed under partial shading conditions, the bypass diodes become forward biased and the current flows through the diodes instead of the PV module. Thus, multiple peaks appear on the P-V characteristic

curve. It is important to establish the relationship between current and voltage in order to appreciate the behavior of PV modules operating under partial shading condition. For this purpose, a single string of *N* number of PV modules in Figure 5.3a is used. The PV modules are subjected to three different irradiance level. The irradiance levels are G_1, G_2, and G_3, where $G_1 > G_2 > G_3$ and the number of PV modules under these irradiance levels are N_1, N_2, and N_3 respectively. Due to three different level of irradiance, three different steps are generated by the I-V curve shown in Figure 5.3b. The curve is divided into three regions where the first region has current due to irradiance level G_1 and the other remaining PV module are shaded in subassembly and bypassed due to lower irradiance level. The voltage expression is given as follow:

$$V = N_1V_1 - N_2V_d - N_3V_d \tag{5.2}$$

$$V = V_{sub1} - N_2V_d - N_3V_d \tag{5.3}$$

Where, V_{sub1} is the voltage of one module in subassembly 1. V_d is the voltage across the diode, however, the voltage across the diode is negligible.

Thus, equation (5.3) is modified as:

$$V = V_{sub1} \tag{5.4}$$

The expression for, V_{sub1} is written as [5.32]

$$V_{sub1} = N_1\left[V_{oc} + \frac{1}{A}\,In\,\left(1 - \frac{G_2}{G_1}\right)\right] \tag{5.5}$$

The expression for current due to G_1 is given by:

$$I_{r1} = \frac{G_1}{G_n}\left(I_{SC,\ n} + K_1\Delta T\right) - \frac{I_{SC,n} + K_1\Delta T}{\exp\left(A\left(V_{SC,n} + K_v\Delta T\right)\right) - 1}\left[exp\,(AV) - 1\right] \tag{5.6}$$

In the subassembly 2, the irradiance level G_2 generated current in step 2. The $(N_1 + N_2)$ generated power while G_3 modules are bypassed. Thus, expression for voltage and current is given by:

$$V = V_{sub1} + N_2 V_2 \tag{5.7}$$

$$I_{r2} = \frac{G_2}{G_n}\left(I_{SC,\ n} + K_1\Delta T\right) - \frac{I_{SC,n} + K_1\Delta T}{\exp\left(A\left(V_{SC,n} + K_v\Delta T\right)\right) - 1}\left[exp\ (AV) - 1\right] \tag{5.8}$$

In the subassembly 3, the expression for voltage of the generated power for all modules are given by:

$$V = V_{sub2} + N_3 V_3 \tag{5.10}$$

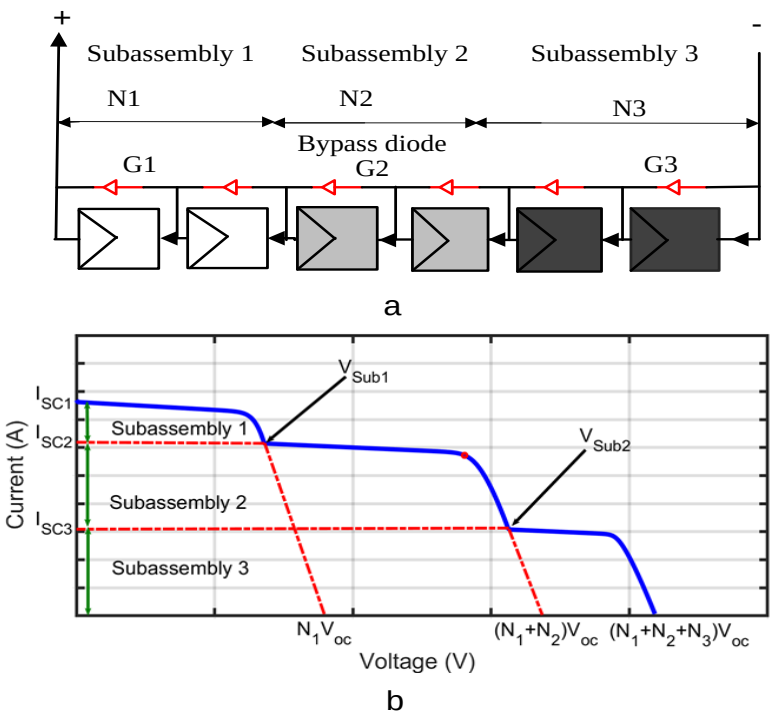

Figure 5.3. PV modules under (a) partial shading conditions. (b) I-V characteristic curve.

$$V = V_{sub1} + N_2\left[V_{oc} + \frac{1}{A}\,In\left(1 - \frac{G_3}{G_2}\right)\right] + N_3 V_3 \tag{5.11}$$

Also, the current expression due to G_3 in the region 3 is given by

$$I_{r3} = \frac{G_3}{G_n}\left(I_{SC,\ n} + K_1\Delta T\right) - \frac{I_{SC,n} + K_1\Delta T}{\exp\left(A\left(V_{SC,n} + K_v\Delta T\right)\right) - 1}\left[exp\,(AV) - 1\right] \qquad (5.12)$$

Therefore, the general expression for voltage of PV string under partial shading condition is given by:

$$V_S = \sum_{k=1}^{n} V_{sub,k-1} + N_k V_k\ ;\ [V_{sub} = 0\ \ if\ n = 1] \qquad (5.13)$$

where, n represents the total number of subassembly and k for the number of subassemblies. Also, the general expression for string current is given by:

$$I_S = \sum_{k=1}^{n} \frac{G_k}{G_n}\left(I_{SC,n} + K_1\Delta T\right) - \frac{\left(I_{SC,n} + K_1\Delta T\right)}{exp\left(\frac{V_{oc,n} + K_v\Delta T}{\alpha V_t}\right) - 1}\left[exp\left(\frac{V}{\alpha V_t} - 1\right)\right] \qquad (5.14)$$

In order to validate the expression of (5.11), ten PV modules with specifications shown in Table 5.1 were connected in series as a case study. The modules were allowed to exposed to the following irradiance level: (1000, 1000, 800, 800, 800, 700, 700, 400, 400, 400) W/m2. Figure 5.4 shows the simulation result of the voltage of subassembly module under partial shading condition. Using the expression of (5.11), the calculated value of the voltage at subassembly 1, V_{sub1} is 33.10V compared with the simulation value of 31.60V. Furthermore, the calculated value of voltages of subassemblies V_{sub2} and V_{sub3} are 90.60V and 132.03V respectively while the simulation value of V_{sub2} and V_{sub3} are 89.10V and134.71V respectively. The calculated values agree with the simulated values. Although, there are some deviations, however these are normal for a PV system operation.

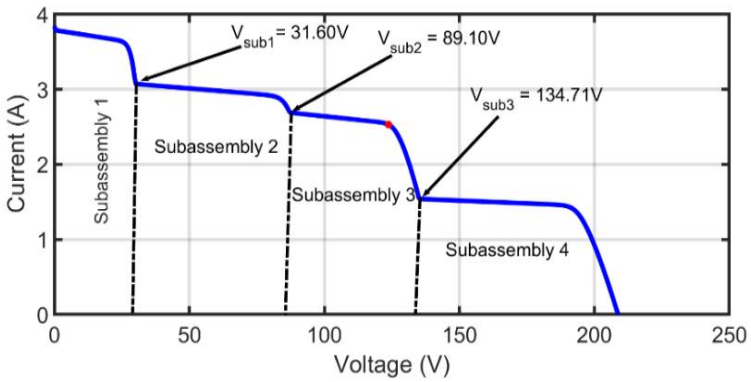

Figure 5.4. Position of voltage of subassembly module under partial shading condition.

5.4 Limitations of $0.8V_{OC}$ model technique

Under uniform weather conditions, the peak voltage at MPP is estimated by equation (5.15) as:

$$V_{GMPP} = 0.8 \times N \times V_{oc,M} \tag{5.15}$$

where, N is the number of PV modules in the string, $V_{oc\mathrm{M}}$ is the open-circuit voltage of the module.

Taking the same line of argument further, it is suggested in [5.17] that the local peaks (thus MPP) of a partial shading curve are located around the multiples of $0.8V_{oc}$. This idea is developed from the following critical observations made by the author in [5.17] after conducting a study on the P-V characteristic curve:

(1) The global peak may be situated at the left of P-V characteristic curve.
(2) The displacement between any two successive peaks is approximately 0.8 of Voc.
(3) When the P-V characteristic curve moved back and forth or sideways, the magnitude of peaks increases until global peak is reached and after that, the magnitude of the subsequent peaks decreases continuously.

From the critical observation stated above, it could be deduced that the global MPP may not be situated only at the left of the P-V characteristic curve as claimed in [5.17] but rather could be situated at the left or the right or at the middle of the P-V characteristic curve as justified by Figure 5.5(a), (b) and (c). Additionally, when the P-V characteristic curve is traversed or moved sideways, the magnitude of the peaks may increase at the point in time and then decreased until global peak is reached which is contrary to the claim made by

[5.9] in critical observation (3). This assertion is justified in Figure 5.5(d). In Figure 5.5(d), the PV power increases from P_1 to P_2 but suddenly decreases at P_3 before increased to reach global MPP at P_4. Also, depending on the nature of the PV system with specific number of modules, the model is bound to experience a significant deviation. Additionally, the performance of the model depends largely on the complexity of shading pattern. For a PV system with different PV modules, with different irradiance level, peak value estimated by $0.8V_{oc}$ model is significantly deviated. Therefore, the assertion that the displacement between any two successive peaks is approximately 0.8Voc is incorrect. For clarity, the following example explains the limitations in $0.8V_{oc}$ model. Consider ten modules, which are exposed to the following irradiance patterns: [1000 1000 1000 700 700 700 700 300 300 300] W/m2. As seen in Figure 5.5 the first subassembly comprises 3 PV modules (N=3). The first subassembly comprises 3 PV modules (N=3). Therefore, the estimated peak voltage is 50.64V, while the actual peak is 45.78V. Similarly, when irradiance changed to 700 W/m2, the number of PV module in the second subassembly is 7. Hence, the estimated peak voltage is 118.16V while the actual peak is 123.10V. Finally, when the irradiance changed to 300W/m2, the estimated peak is 168.80 while the actual is 192.2V. Figure 5.7 depicts the actual peaks value as against the estimated values. Clearly, the estimated values deviate from the actual value. The $0.8V_{oc}$ model experiences higher deviation from the actual value at lower irradiance level, which is contrary to the theory that the local peaks are located around the multiples of $0.8V_{oc}$. As the number of shading level increases, the deviation of local peaks from the actual value become more obvious. Figure 5.8 shows the flow chart of the algorithm that validate the concept of 0.8Voc under partial shading conditions. The operation of the algorithm always begins with 85% of Voc which is reference voltage as indicated in the “Main Program” in Figure 5.8. P&O is used to track the MPP. Until partial shading occurs, it maintains the operation at this MPP by continuously use conventional P&O MPPT. When any disturbance like partial shading occur, the “Main Program” notice the change and then calls the “GP track subroutine”. The

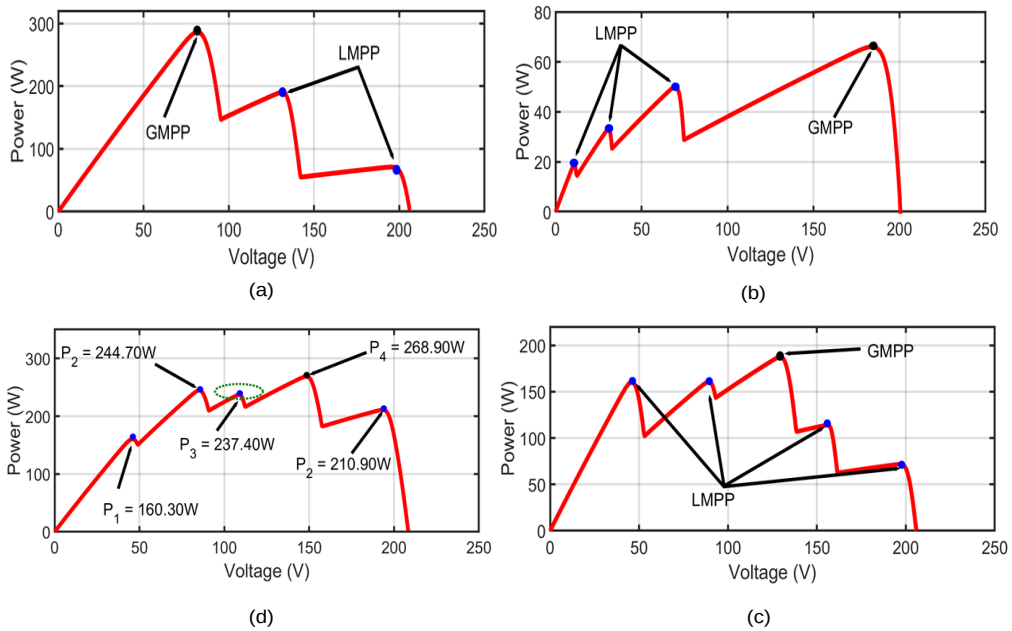

Figure 5.5. P-V characteristic curve for different irradiance level under partial shading conditions.

"GP track subroutine tracks the new first peak using P&O technique and then, pass on the control to the "Main program", which maintains the operation at this new peak. A large voltage perturbation which is around 60% to 70% of V_{OC_module} is applied to move the algorithm to next peak and P&O again used to track the new peak. This process is repeated until GMPP is reached. Some critical observations made from the P-V and I-V curves contrary to the principles of $0.8V_{oc}$ model are as follows.

(1) The peak voltages of PV modules that receive different irradiance level are different.

(2) The peak voltage may be situated at the left or right or at the middle of the P-V characteristic curve.

(3) The number of peaks is equal to the number of different irradiance level and any peak point may be a potential global MPP.

(4) The peak voltage of PV modules that receive low irradiance level has higher deviation than PV modules with high irradiance level.

(5) The number of peaks is equal to the number of different irradiance level and any peak point may be a potential global MPP.

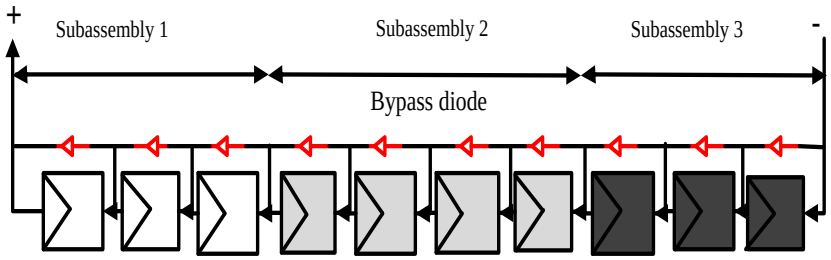

Figure 5.6. PV modules under partial shading conditions.

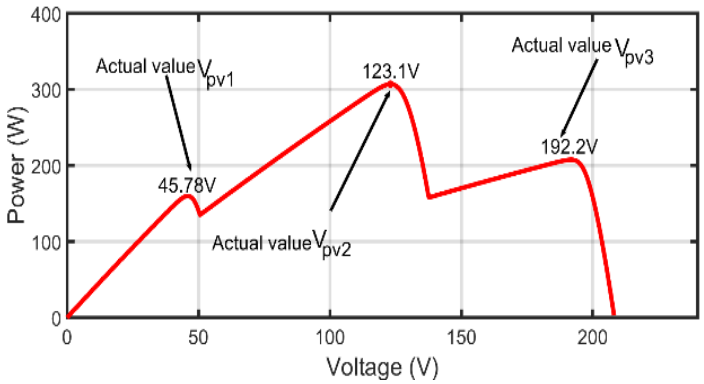

Figure 5.7. P-V characteristic curve under normal and partial shading conditions.

The limitation of 0.8Voc model becomes more obvious especially for a long PV string with complex shading patterns. Therefore, an alternative logical step was taken in [5.33] where a general relationship between the location of the peaks and Voc was established so that their positions can be predicted more accurately. A generalized expression to predict the position of the peak voltage under partial shading conditions is formulated. The proposed equation in [5.33] is given as:

$$V_{LP,k} = (\alpha \times N_{k-1} + 0.8 \times N_k)V_{oc} \quad (5.16)$$

where, k is the subassembly number, N_k is the number PV modules in the new subassembly, N_{k-1} is the number of PV modules in the previous subassembly and α is a variable parameter.

The accuracy of this model depends on subassembly voltage (V_{sub}) which is given by $\alpha N_{k-1}V_{oc}$ and is dependent on irradiance. As can be seen from Figure 5.4, the V_{sub} changes

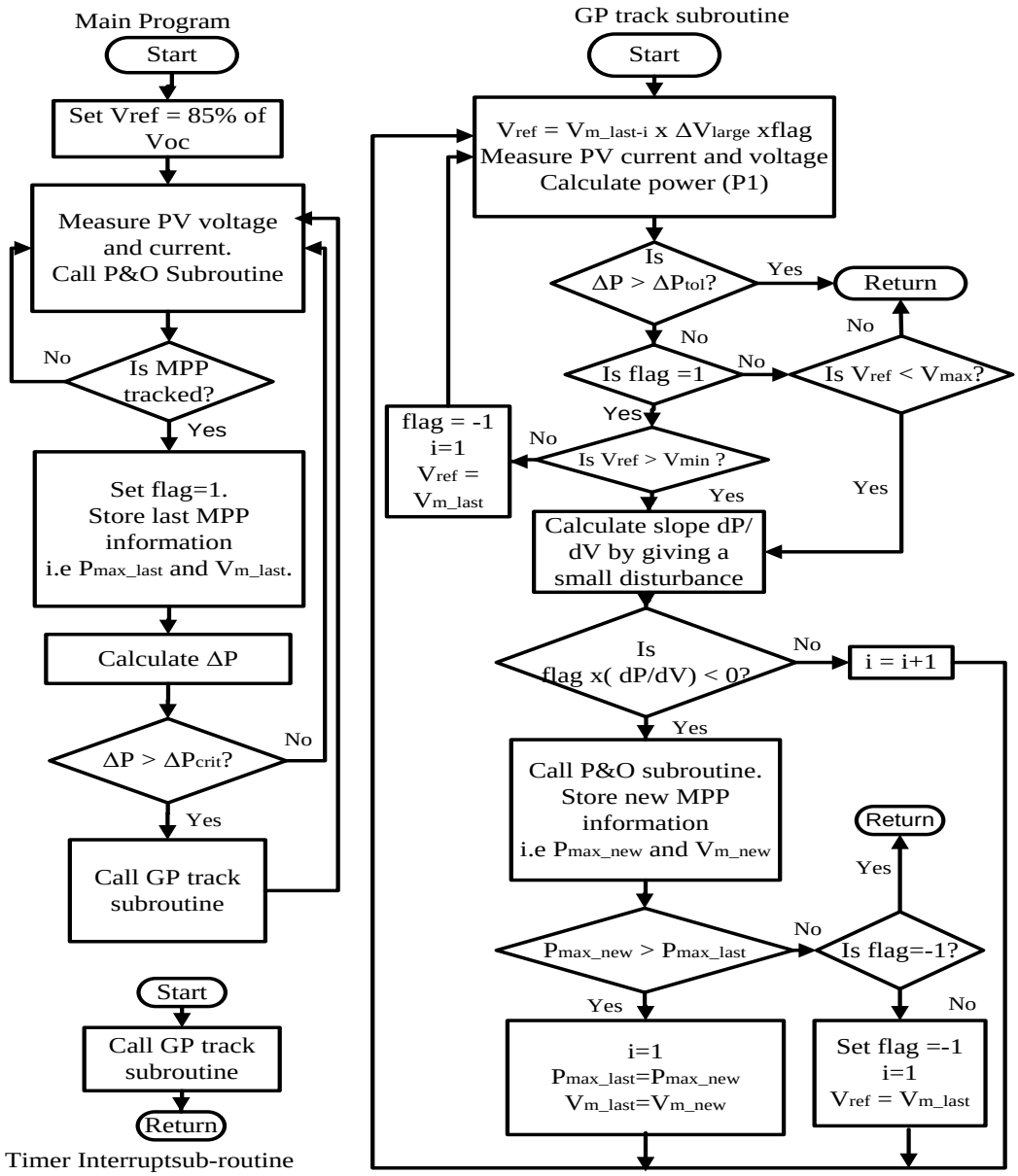

Figure 5.8. Flowchart for conventional 0.8Voc model technique.

when irradiance level fall from one level to another. Although, this model improved the performance of the conventional 0.8Voc model, the V_{sub} which is a function of α cannot provide true correction to the deviations in the conventional model. This is because α is an approximate parameter with value varying from 0.8 to 0.97. Hence, some modifications are made in this chapter to predict accurate position of peaks during partial shading conditions.

5.5 Proposed 0.8Voc model to estimate the peak voltage at global MPP

The accuracy of $0.8V_{oc}$ model depends largely on the nature of shading on the PV modules. For lower irradiance level, the local peaks experience significant deviation from the actual value. Additionally, for long PV string with several levels of shading, the voltages at MPPs deviate from the actual position. Consequently, the position of the MPP also deviates from the reference point. Therefore, it is important to address this abnormality in conventional $0.8V_{oc}$ model for performance improvement. To achieve this, the peak voltage and peak voltage deviation correction is developed from irradiance patterns.

5.5.1 Peak voltage under partial shading conditions

The open circuit voltage of PV under uniform irradiance condition can be analysed as follows:

$$V_{oc} = V_{oc\_STC} + \mu V_t In\left(\frac{G}{G_{STC}}\right) + K_v(T - T_{STC}) \quad (5.17)$$

where, G is solar irradiance, G_{STC} is the reference irradiance at standard test condition (1000W/m^2),T_{STC} is the temperature at standard test condition (25^{o}C), μ is the ideality factor, and K_v is the temperature coefficient of the open circuit voltage, V_{oc_STC} is the open circuit voltage at standard test condition and V_t is the thermal voltage. It is noted that the linear relationship between PV current and I_{SC_STC} is given as [5.34];

$$I_{PV} = \left(I_{SC\_STC} + K_I\,(T - T_{STC})\right)\frac{G}{G_{STC}} \quad (5.18)$$

The calculation of V_{oc} is done by using the measured current hence, equation (5.17) can be updated to:

$$V_{oc} = V_{oc\_STC} + \mu V_t In\left(\frac{I_{pv}}{I_{SC\_STC}}\right) \quad (5.19$$

By extension, the open circuit voltage of the PV module under partial shading condition can be estimated from I-V curve in Figure 5.9 as;

$$V_{oc,M} = V_{oc\_STC} + \mu V_t In\left(\frac{I_{sc} - I_{pv}}{I_{SC\_STC}}\right) \quad (5.20)$$

where, I_{SC} is the short circuit current of the PV string. The number of PV module in the string under partial shading condition can be calculated as;

$$N_s \approx \frac{V_{strng}}{V_M} \quad (5.21)$$

where V_{string} is the PV string voltage exposed to irradiance, V_M is the voltage of one PV module. Therefore, the peak voltage is estimated by modifying equation (5.18) using equation (5.21), which is given in equation (5.22) as;

$$V_{peak} = \left[V_{oc\_STC} + \mu V_t In\left(\frac{I_{SC} - I_{pv}}{I_{SC\_STC}}\right)\right] \times 0.8 \times N_s \quad (5.22)$$

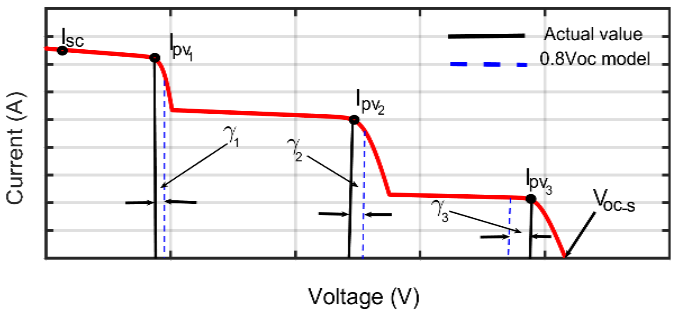

Fig. 5.9. Peak deviation under partial shading condition.

5.5.2 Peak voltage deviation correction

For long PV string with several levels of shading, the peak voltage deviates from the original value. To compensate for the deviation, peak deviation factor correction ε, is deduced from I-V curve in Figure 5.9 given by;

$$\varepsilon = \left(\frac{I_{SC} - I_{pv}}{I_{SC\_STC}}\right)\left(\frac{V_{oc\_S}}{V_{oc\_S\_STC}} - 0.8\right) \quad (5.23)$$

where, V_{oc_S} is the open circuit voltage of PV string deduced from I-V curve under partial shading condition in Figure 5.9 and $V_{oc\_S\_STC}$ is the open circuit voltage of the PV string at standard test condition. The 0.8 in (5.23) is the ratio between voltage at MPP (V_{mpp})and open circuit voltage (V_{oc}) at STC. Table 5.1 gives the STC values. Therefore, the peak voltage deviation correction is obtained using equation (5.21) and (5.23) given as;

$$\gamma = \left(\frac{I_{SC} - I_{pv}}{I_{SC\_STC}}\right)\left(\frac{V_{oc\_S}}{V_{oc\_S\_STC}} - 0.8\right) \times N_s \times V_{oc\_STC} \tag{5.24}$$

Therefore, the voltage at global MPP taking into consideration the peak voltage deviation correction factor is given by;

$$V_{GP} = V_{peak} + \gamma \tag{5.25}$$

A study of eight different cases of partial shading conditions including various irradiance patterns shown in Table 5.2 are conducted. The actual value of V_{oc_s} due to different cases of partial shading conditions is used to estimate the peak voltage deviation correction. On the other hand, a selected value of V_{oc_s} based on trial and error to provide significant correction to voltage deviation is used to estimate the peak voltage deviation correction for the same cases of partial shading conditions. The peak voltage deviation correction

Table 5.2. PV module number and its irradiance value (W/m^2).

PV modules No. / **Case**	**1**	**2**	**3**	**4**	**5**	**6**	**7**	**8**	**9**	**10**
1	1000	1000	1000	700	700	700	700	300	300	300
2	1000	800	800	800	600	600	500	500	200	200
3	900	900	800	800	600	600	600	500	500	200
4	900	900	700	700	700	500	500	300	300	100
5	1000	1000	700	700	700	500	500	500	100	100
6	1000	1000	800	700	700	500	300	300	100	100
7	1000	1000	900	700	700	700	400	400	200	200
8	1000	1000	900	800	800	600	600	200	200	200

Table 5.3. Estimation of peak voltage deviation correction and global peak voltage.

Irradiance patterns	**Actual value of (V_{oc_s})**	**Peak voltage (V_{peak})**	**Peak voltage deviation correction (γ_v)**	**Global peak voltage ($V_{peak} + \gamma_{v)}$**	**Selected value of (V_{oc_s})**	**Peak voltage deviation correction (γ_f)**	**Global peak voltage ($V_{peak} + \gamma_{f)}$**
Case 1	208.10	44.63	0.87	45.50	207.90	0.86	45.49
		112.31	9.25	121.56		9.20	121.51
		166.16	27.81	193.97		27.66	193.82
Case 2	207.50	14.73	0.23	14.96	207.90	0.24	14.97
		63.26	3.86	67.12		3.90	67.16
		97.35	9.87	107.22		9.98	107.33
		131.01	16.03	147.04		16.21	147.22
		167.16	31.18	198.34		31.31	198.68
Case 3	208.00	30.80	1.10	31.90	207.90	1.10	31.90
		63.20	3.85	67.05		3.82	67.02
		113.58	11.73	125.31		11.68	125.26
		147.37	18.28	165.65		18.18	165.55
		167.10	31.46	198.56		31.29	198.39
Case 4	206.80	31.00	1.30	32.30	207.90	1.33	32.33
		80.26	6.47	86.70		6.55	86.81
		114.63	13.79	128.42		14.10	128.63
		149.53	24.18	173.71		24.45	173.98
		167.97	34.00	201.97		34.28	202.25
Case 5	206.60	29.80	0.57	30.37	207.90	0.59	30.39
		80.24	6.40	86.64		6.60	86.84
		131.02	15.71	146.73		16.12	147.14
		167.97	33.88	201.85		34.61	202.58
Case 6	206.20	29.93	0.61	30.54	207.90	0.64	30.57
		47.32	1.50	48.82		1.70	49.02
		80.18	6.22	86.40		6.40	86.58
		98.23	11.56	109.79		11.98	110.21
		132.92	21.15	154.07		21.60	154.52
		167.97	33.52	201.49		33.87	201.84
Case 7	207.50	29.46	0.47	29.93	207.90	0.48	29.94
		46.29	1.76	48.05		1.78	48.07
		96.26	7.79	104.05		7.87	104.13
		132.03	18.92	150.95		19.13	151.16
Case 8	207.50	29.36	0.44	29.80	207.90	0.44	29.80
		46.12	1.70	47.92		1.72	47.94
		81.90	4.66	86.56		4.72	86.62
		113.55	11.46	125.01		11.59	125.14
		167.17	31.21	198.38		31.56	198.73

Table 5.4. Performance comparison between the proposed model, conventional and an improved $0.8V_{oc}$ model

Irradiance patterns	Reference peak voltage (V)	Peak voltage using conventional 0.8Voc [5.17] (V)	Peak voltage using [5.33] (V)	Peak voltage using proposed model (V)	Deviation between 0.8Voc [5.17] and actual voltage (V)	Deviation between [5.33] and actual voltage (V)	Deviation between proposed and actual voltage(V)
Case 1	45.78	50.64	50.64	45.49	4.86	4.86	0.29
	123.10	118.16	121.69	121.51	4.94	1.41	1.59
	192.20	168.80	190.07	193.82	23.40	2.13	1.60
Case 2	10.08	16.88	16.88	14.97	6.80	6.80	4.89
	65.52	67.52	68.36	67.16	2.00	2.84	1.64
	106.90	101.28	109.72	107.33	5.62	2.82	0.43
	147.20	135.04	150.87	147.22	12.16	3.67	0.02
	197.80	168.80	194.12	198.68	29.00	3.68	0.88
Case 3	28.14	33.76	33.76	31.90	5.62	5.62	3.76
	65.73	67.52	69.21	67.02	1.79	3.48	1.29
	124.90	118.16	126.60	125.26	6.74	1.7	0.36
	166.70	151.92	170.38	165.55	14.78	3.68	1.15
	198.20	168.80	197.29	198.39	29.40	0.91	0.19
Case 4	28.35	33.76	33.76	32.33	5.41	5.41	3.98
	85.47	84.40	86.93	86.81	1.07	1.46	1.34
	127.90	118.16	131.35	128.63	9.74	3.45	0.73
	172.20	151.92	173.34	173.98	20.28	1.14	1.78
	200.80	168.80	201.03	202.25	32.00	0.23	1.45
Case 5	28.14	33.76	33.76	30.39	5.62	5.62	2.25
	85.68	84.40	86.93	86.84	1.28	1.25	1.16
	146.40	135.04	148.23	147.14	11.36	1.83	0.74
	199.30	168.80	197.50	202.58	30.50	1.8	3.28
Case 6	28.14	33.76	33.76	30.57	5.62	5.62	2.43
	47.67	50.64	52.33	49.02	2.97	4.66	1.35
	86.10	84.40	88.20	86.58	1.70	2.10	0.48
	110.20	101.28	114.47	110.21	8.92	4.27	0.01
	152.00	135.04	152.76	154.52	16.96	0.76	2.52
	199.20	168.80	197.50	201.84	30.40	1.70	2.64
Case 7	27.30	33.76	33.76	29.94	6.46	6.46	2.64
	47.25	50.64	51.70	48.07	3.39	4.45	0.82
	104.80	101.28	105.08	104.13	3.52	0.28	0.67
	150.60	135.04	152.76	151.16	15.56	2.16	0.56
	196.10	168.80	194.12	198.47	27.3	1.98	2.37
Case 8	27.30	33.76	33.76	29.80	6.46	6.46	2.50
	47.04	50.64	51.70	47.94	3.60	4.66	0.90
	85.05	84.40	86.93	86.62	0.65	1.88	1.57
	126.80	118.16	124.49	125.14	8.64	2.31	1.66
	194.20	168.80	192.43	198.73	25.40	1.77	4.53

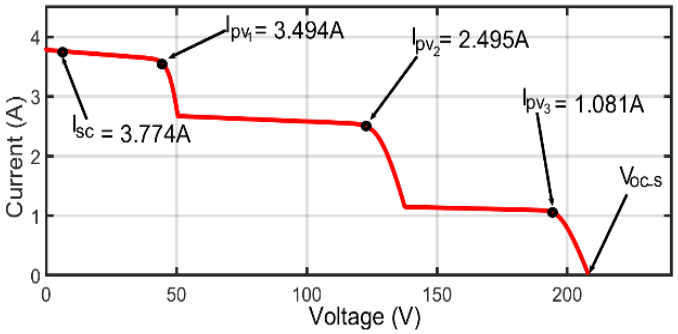

Figure 5.10. I-V characteristic curve under partial shading condition.

expression is a function of V_{oc_s} and a suitable value of V_{oc_s}, gives almost the same results as the actual V_{oc_s} for different cases of irradiance patterns. Table 5.3 compares the peak voltage deviation correction and global peak voltage for selected and actual open circuit voltage. It is evident that both values of V_{oc_s} give almost the same results. Thus, for simple implementation, the value of 207.90V is used throughout for different cases of different irradiance patterns. To demonstrate the effectiveness of the proposed model, a PV string, which consists of ten modules with the following irradiance patterns [1000 1000 1000 700 700 700 700 300 300 300] W/m2 is considered. The first subassembly consists of 3 PV modules (N_s =3), $I_{pv1} = 3.494A$, $I_{SC} = 3.774A$, $I_{SC\_STC} = 3.8A$, $V_{oc_S} = 207.9$A (refer to Figure 5.10) $V_{oc\_S\_STC} = 211V$, $\mu = 0.8$, $V_t = 1.2V$, $V_{oc\_STC} = 21.1V$. Using equations (8), (10) and (11), the V_{PK} and γ are respectively 44.63V and 0.86V. Hence, voltage at global MPP, V_{GPP} is 45.49V which coincides with actual voltage of 45.78V. Similarly, the global peak voltage at I_{pv2} and I_{pv3} are respectively 121.51V and 193.81V. The actual peak values are 123.1V and 192.2V respectively.

5.6 Validation of the proposed $0.8V_{OC}$ model technique

The proposed $0.8V_{oc}$ model technique is validated by using a string of ten modules. These modules are exposed to partial shading conditions given in Table 5.2. Case 2 is taken only as an example. The proposed algorithm is compared with conventional $0.8V_{oc}$ model [5.17] and improved $0.8V_{oc}$ model [5.33] at the same conditions of irradiance and temperature. Due to the five different level of irradiance, five local peaks were generated.

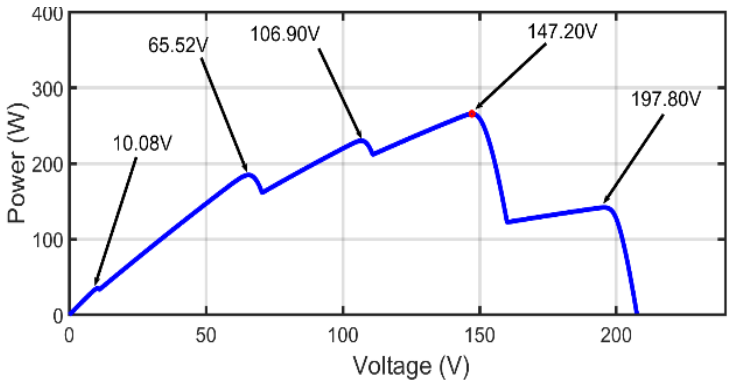

Figure 5.11. Peak location verification.

Using the proposed 0.8V_{oc} model technique, the estimated voltage for the first peak is 14.49V while the actual voltage is 10.08V. This has lower deviation as compared with the conventional0.8V_{oc} model and the improved 0.8V_{oc} [5.33] which have the peak voltage equal to 16.88V. Similarly, the estimated voltage for the second peak voltage is 67.16V while the actual voltage is 65.52V. However, the conventional 0.8V_{oc} and an improved 0.8V_{oc} have the peak voltages equal to 67.52V and 68.36V respectively. The third peak voltage is 107.33V while the actual peak voltage is 106.90V. The third peak voltages for conventional and the improved 0.8V_{oc} model are 101.28V and 109.72V respectively. The proposed technique has fourth peak voltage location at 147.22V while the actual peak voltage is 147.20. Conventional 0.8V_{oc} and the improved model have fourth peak voltages at 135.04V and 150.87V respectively. Finally, the fifth peak voltage for the proposed model is 198.68V while the actual peak voltage is 197.80V. The conventional 0.8V_{oc} model has fifth peak voltage equal to 168.80V while the improved 0.8V_{oc} model equals194.12V. Figure 5.11 illustrates the locations of the actual peaks. It is worth as well to validate the accuracy of the proposed model by calculating the peak voltages deviation. Using different irradiance patterns as in Table 5.2, the performance of the proposed technique, conventional 0.8V_{oc} model and the improved 0.8V_{oc} model in [5.17] are depicted in Table 5.4. For all cases, the peak voltage deviation of the proposed model technique is lower than other methods. On the other hand, the peak voltage deviation for the conventional 0.8V_{oc} is very high for all cases except for third peak of case 8.

5.6.1 Impact of the proposed model on MPPT performance

To demonstrate the effectiveness of the proposed model technique, a MATLAB/SIMULINK simulation is carried out during both normal and partial shading conditions. For simplicity but it can be scaled up for larger PV systems (more strings), ten PV modules in one string were connected in series with the following irradiance patterns [1000, 1000 800, 800, 600, 450, 450, 450, 300, 300] W/m2. The first and second subassemblies comprise 2 PV modules while the third subassembly has only 1 PV module. The fourth subassembly consists of 3 PV modules and the fifth subassembly comprises of

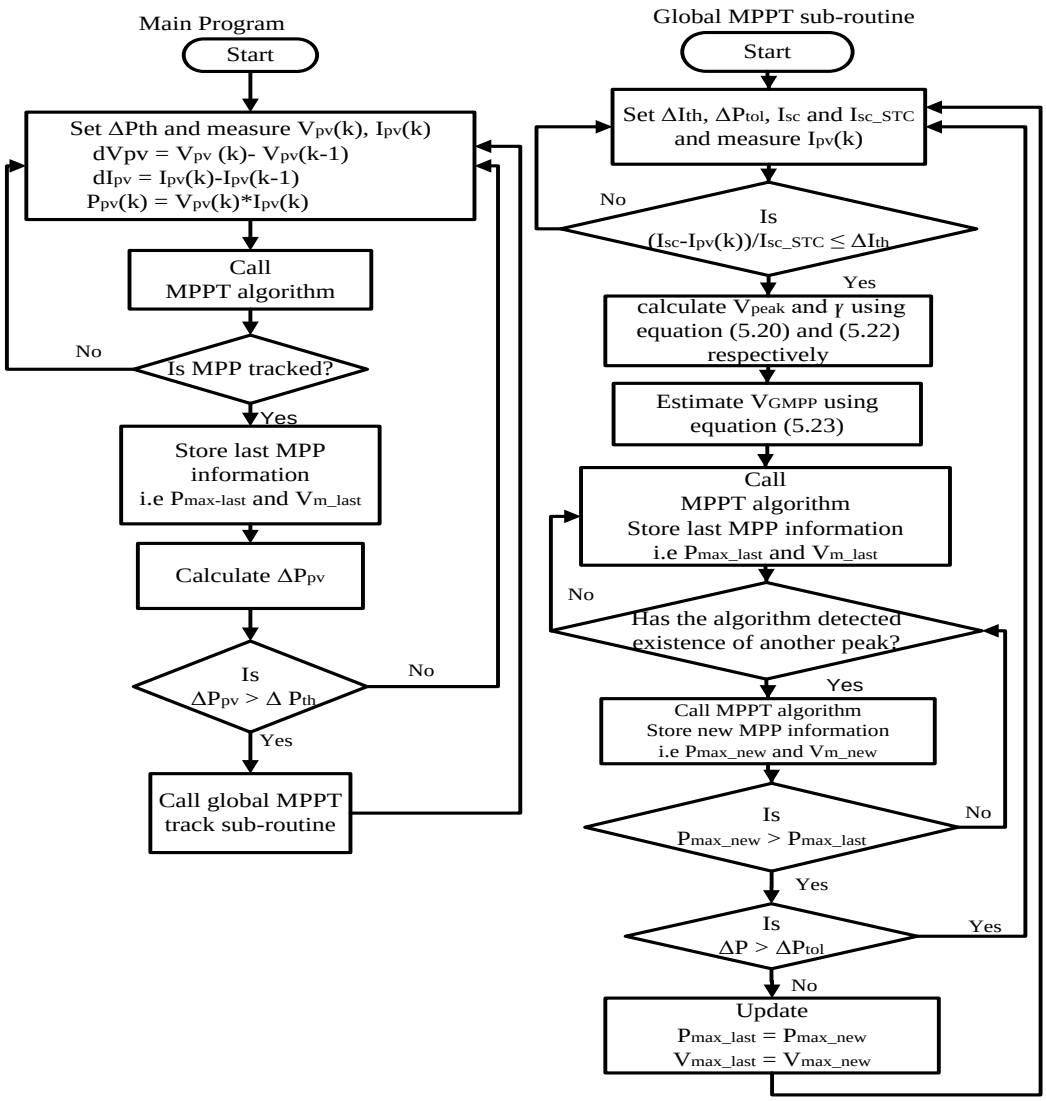

Figure 5.12. Flowchart for the proposed model technique.

2 PV modules. Table 5.1 gives the specifications of the PV modules. Figure 5.12 shows the flowchart of the proposed 0.8Voc model algorithm that tracks GP under partial shading conditions. The execution of the algorithm starts by measuring the PV string voltage and current as shown in the "Main program" in Figure 5.12. Until any disturbance occurs, the algorithm maintains its operation at the GP by continuously implementing conventional MPPT technique. Any conventional MPPT can be used to implement this proposed 0.8Voc model technique. In this work, incremental conductance (INC) algorithm is used due it accurate performance under fast varying weather conditions [5.35-5.36]. When any sudden disturbance like partial shading occur, the "Main Program" detects the condition for tracking the GP and calls the global MPPT sub-routine. The global MPPT sub-routine tracks the new GP and, then, again hand over the control to the "Main Program", which maintains the operation at the new GP. To understand the algorithm, assume that MPP has just been reached during normal weather conditions. The algorithm then stores the information about PV string's output power and output voltage as P_{max_last} and V_{m_last} respectively. Until any disturbance occurs, the algorithm maintains its operation at these stored power and voltage. The sudden occurrence of shading on the PV module due to changes in irradiance level leads to variation of power. If the power difference between the stored operated power and identified maximum power is greater than the pre-set value, means that partial shading has occurred. Subsequently, global peak voltage is estimated, which serves as the reference voltage. MPPT algorithm is then used to track the global MPP based on the reference voltage and the information about PV string's output power and output voltage is stored. If the power tracked is less than the global maximum power, the algorithm further scans other MPPs and compare the new power with the previous one until global maximum power is tracked. In order to minimise the oscillations due to power variation, a tolerable power variation threshold (ΔP_{tol}) is allowed to enable the algorithm tracks global maximum power. Figure 5.13 shows the reference peaks locations of PV modules under partial shading conditions. In Figure 5.14a, during the partial shading conditions, the proposed technique tracks the estimated voltage which is around the actual reference voltage compared to the conventional $0.8V_{oc}$ model and improved 0.8Voc model. The estimated peak voltage of the proposed $0.8V_{oc}$ model is 149.28V while the actual

global peak voltage is 148V. This leads to a peak deviation of 1.28V (less than 2V). However, the peak voltage for the conventional $0.8V_{oc}$ model is 135.04V, therefore the deviation is 12.96V. Also, the peak voltage for the improved 0.8Voc model in [5.33] is. 145.59V and this leads to a deviation of 2.41 (more than 2V). Table 5.5 further gives the details performance of the three 0.8Voc model technique. Figure 5.14b shows the global peak power of the proposed and other two $0.8V_{oc}$ model techniques. The power difference between the proposed and the conventional 0.8Voc model technique is 20W. Also, the power difference between the proposed and improved 0.8Voc model technique in [5.33] is 2W. The efficiency of the conventional $0.8V_{oc}$ model is about 93% while that of the proposed is 99.6%. The efficiency of the improved 0.8Voc model technique in [5.33] is 98.74%. The proposed technique can be used for large scale PV farms, which leads to save high amount of extracting power.

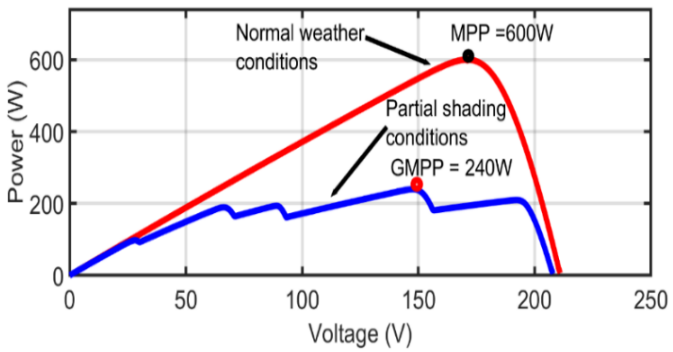

Figure 5.13. P-V characteristic curve under normal weather and partial shading conditions.

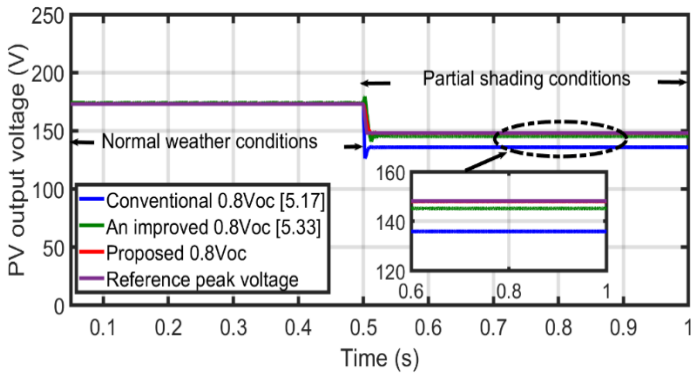

(a)

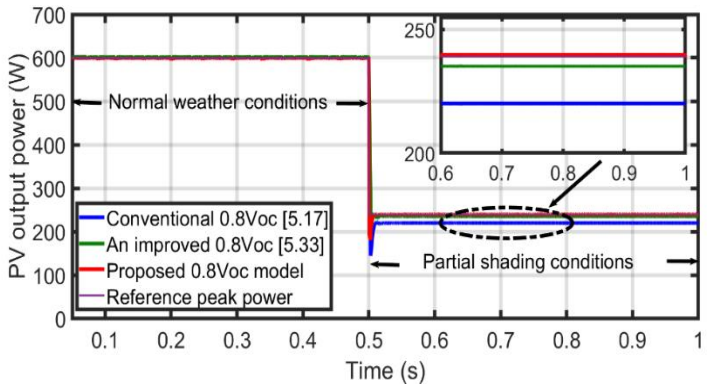

(b)

Figure 5.14. Scanning of peaks by MPPT: (a) PV voltage, and (b) PV power.

Table 5.5. Performance of the three 0.8Voc model techniques on ten PV module under partial shading conditions.

0.8Voc model techniques	Calculated global peak voltage (V)	Global peak voltage deviation (%)	Calculated global peak power (W)	Global peak power deviation (%)	Efficiency (%)
Conventional 0.8Voc model [5.17]	135.04	8.76	223.40	35.31	93.00
Improved 0.8Voc model [5.33]	145.59	1.63	236.00	1.26	98.74
Proposed 0.8Voc model	149.28	1.28	238.00	0.42	99.60

5.7 Summary

In this chapter, a new $0.8V_{oc}$ model technique has been proposed for medium voltage large scale photovoltaic (PV) system integration. As demonstrated mathematically and graphically that, the local peaks near the multiples of $0.8V_{oc}$ are incorrect with long PV string. For a long string of PV modules with low irradiance under partial shading, the deviation of local peaks becomes more obvious. Therefore, the new $0.8V_{oc}$ model technique addresses the drawbacks in the conventional $0.8V_{oc}$ to minimise the power loss and subsequently improves the efficiency. Through the simulation results, the proposed

technique has improved the tracking time and efficiency with minimum peak voltage deviation from actual values. The proposed technique is very beneficial for megawatt large scale PV farms due to the saving of high amount of power.

References

[5.1] IEEE Standard for Interconnecting Distributed Resources with Electric Power Systems, IEEE Standard 1547, 2003.

[5.2] G. Lijun, R. A. Dougal, L. Shengyi, and A. P. Iotova, "Parallel-connected solar PV system to address partial and rapidly fluctuating shadow conditions," IEEE Trans. Ind. Electron., vol. 56, no. 5, pp. 1548–1556, May 2009.

[5.3] A. Bidram, A. Davoudi, and R. S. Balog, "Control and circuit techniques to mitigate partial shading effects in photovoltaic arrays," IEEE J. Photovoltaics, vol. 2, no. 4, pp. 532–546, Oct. 2012.

[5.4] Alajmi, B.N.; Ahmed, K.H.; Finney, S.J.; Williams, B.W. A Maximum Power Point Tracking Technique for Partially Shaded Photovoltaic Systems in Microgrids. *IEEE Trans. Indust. Electron., 2013*, 60,1596-1606.

[5.5] A. Ingegnoli and A. Iannopollo, "A maximum power point tracking algorithm for stand-alone photovoltaic systems controlled by low computational power devices," in IEEE Mediterranean Electrotechnical Conference (MELECON), 2010, pp. 1522–1527.

[5.6] E. Koutroulis and F. Blaabjerg, "A new technique for tracking the global maximum power point of PV arrays operating under partial-shading conditions," IEEE Journal of Photovoltaics, vol. 2, no. 2, pp. 184–190, 2012.

[5.7] B. Bekker and H. J. Beukes, "Finding an optimal PV panel maximum power point tracking method," in AFRICON Conference in Africa (AFRICON), 2004, vol. 2, pp. 1125–1129 Vol.2.

[5.8] E. Koutroulis and F. Blaabjerg, "A New Technique for Tracking the Global Maximum Power Point of PV Arrays Operating Under Partial-Shading Conditions,Q IEEE Journal of Photovoltaics, vol. 2, no. 2, pp. 184-190, April 2012.

[5.9] B. Alajmi, K. Ahmed, S. Finney, and B. Williams, “Fuzzy logic controlled approach of a modified hill climbing method for maximum power point in microgrid stand-alone photovoltaic system,” IEEE Transactions on Power Electronics, vol. 26, no. 4, pp. 1022–1030, 2011.

[5.10] P. Lei, Y. Li, Q. Chen, and J. E. Seem, “Extremum seeking control based integration of MPPT and degradation detection for photovoltaic arrays,” in American Control Conference (ACC), 2010, pp. 3536–3541.

[5.11] Y. H. Ji, D. Y. Jung, J. G. Kim, J. H. Kim, T. Lee, and C. Y. Won, “A real maximum power point tracking method for mismatching compensation in PV array under partially shaded conditions,” IEEE Transactions on Power Electronics, vol. 26, no. 4, pp. 1001–1009, 2011.

[5.12] S. Bifaretti, V. Iacovone, L. Cina, and E. Buffone, “Global MPPT method for partially shaded photovoltaic modules,” in IEEE Energy Conversion Congress and Exposition (ECCE), 2012, pp. 4768–4775.

[5.13] Y. H. Ji, D. Y. Jung, J. G. Kim, J. H. Kim, T. Lee, and C. Y. Won, “A real maximum power point tracking method for mismatching compensation in PV array under partially shaded conditions,” IEEE Transactions on Power Electronics, vol. 26, no. 4, pp. 1001–1009, 2011.

[5.14] S. Bifaretti, V. Iacovone, L. Cina, and E. Buffone, “Global MPPT method for partially shaded photovoltaic modules,” in IEEE Energy Conversion Congress and Exposition (ECCE), 2012, pp. 4768–4775.

[5.15] S. Kazmi, H. Goto, O. Ichinokura, and G. Hai-Jiao, “An improved and very efficient MPPT controller for PV systems subjected to rapidly varying atmospheric conditions and partial shading,” in Australasian Universities Power Engineering Conference (AUPEC) , 2009, pp. 1–6.

[5.16] G. Escobar, C. N. M. Ho, and S. Pettersson, “Maximum power point searching method for partial shaded PV strings,” in IEEE Industrial Electronics Society Conference (IECON), 2012, pp. 5726–5731.

[5.17] H. Patel and V. Agarwal, “Maximum power point tracking scheme for PV systems operating under partially shaded conditions,” IEEE Transactions on Industrial Electronics, vol. 55, no. 4, pp. 1689–1698, 2008.

[5.18] T. L. Nguyen and K. S. Low, “A global maximum power point tracking scheme employing direct search algorithm for photovoltaic systems,” IEEE Trans. Ind. Electron, vol. 57, no. 10, pp. 3456–3467, Oct. 2010.

[5.19] N. A. Ahmed and M. Miyatake, “A novel maximum power point tracking for photovoltaic applications under partially shaded insolation conditions,” Electr. Pow. Syst. Res., vol. 78, no. 5, pp. 777–784, 2008.

[5.20] R. Ramaprabha, M. Balaji, and B. Mathur, “Maximum power point tracking of partially shaded solar pv system using modified fibonacci search method with fuzzy controller,” Int. J. Elec. Power Energ. Sys., vol. 43, no. 1, pp. 754 – 765, 2012.

[21] M. Miyatake, T. Inada, I. Hiratsuka, Z. Hongyan, H. Otsuka, and M. Nakano, “Control characteristics of a fibonacci-search-based maximum power point tracker when a photovoltaic array is partially shaded,” in International Power Electronics and Motion Control Conference (IPEMC), 2004, vol. 2, pp. 816–821 Vol.2.

[5.22] K. Sundareswaran, V. Vigneshkumar, P. Sankar, S. P. Simon, P. S. R. Nayak, and S. Palani, “Development of an improved p&o algorithm assisted through a colony of foraging ants for mppt in pv system,” IEEE Trans. Ind. Informat., vol. 12, no. 1, pp. 187–200, Feb. 2016

[5.23] S. Mohanty, B. Subudhi, and P. K. Ray, "A new mppt design using grey wolf optimization technique for photovoltaic system under partial shading conditions," IEEE Trans. Sustain. Energy, vol. 7, no. 1, pp. 181–188, Jan. 2016.

[5.24] S. Lyden and M. E. Haque, "A simulated annealing global maximum power point tracking approach for pv modules under partial shading conditions," IEEE Trans. Power Electron., vol. 31, no. 6, pp. 4171–4181, Jun. 2016.

[5.25] M. Miyatake, M. Veerachary, F. Toriumi, N. Fujii, and H. Ko, "Maximum power point tracking of multiple photovoltaic arrays: A pso approach," IEEE Trans. Aero. Elec. Sys., vol. 47, no. 1, pp. 367–380, Jan. 2011.

[5.26] Y. H. Liu, S. C. Huang, J. W. Huang, and W. C. Liang, "A particle swarm optimization-based maximum power point tracking algorithm for pv systems operating under partially shaded conditions," IEEE Trans. Energy Convers., vol. 27, no. 4, pp. 1027–1035, Dec. 2012.

[5.27] K. Ishaque, Z. Salam, M. Amjad, and S. Mekhilef, "An improved particle swarm optimization (pso) based mppt for pv with reduced steady-state oscillation," IEEE Trans. Power Electron., vol. 27, no. 8, pp. 3627–3638, Aug. 2012.

[5.28] K. Ishaque and Z. Salam, "A deterministic particle swarm optimization maximum power point tracker for photovoltaic system under partial shading condition," IEEE Trans. Ind. Electron, vol. 60, no. 8, pp. 3195–3206, Aug. 2013.

[5.29] Y. H. Liu, S. C. Huang, J. W. Huang, and W. C. Liang, "A particle swarm optimization-based maximum power point tracking algorithm for pv systems operating under partially shaded conditions," IEEE Trans. Energy Convers., vol. 27, no. 4, pp. 1027–1035, Dec. 2012.

[5.30] Y.-H. Liu, J.-H. Chen, and J.-W. Huang, "A review of maximum power point tracking techniques for use in partially shaded conditions," Renew. Sust. Energ. Rev., vol. 41, pp. 436–453, 2015.

[5.31] W. Herrmann, W. Wiesner, and W. Vaassen, “Hot spot investigations on PV modules-new concepts for a test standard and consequences for module design with respect to bypass diodes,” in Proc. Conf. Record 26th IEEE Photovolt. Spec. Conf , 1997, pp. 1129–1132.

[5.32] N. Mutoh, M. Ohno, and T. Inoue, “A method for MPPT control while searching for parameters corresponding to weather conditions for PV generation systems,” IEEE Trans. Ind. Electron., vol. 53, no. 4, pp. 1055–1065, Aug. 2006

[5.33] J. Ahmed and Z. Salam, “An Improved Method to Predict the Position of Maximum Power Point During Partial Shading for PV Arrays,” IEEE Transactions on Industrial Informatics, vol. 11, no. 6, pp. 1378-1387, Dec. 2015.

[5.34] W. Bingbing, Y. Zhongdong, and X. Xiangning, “Design of simulation model of PV cells based on VSR PWM rectifier circuit,” in Proc. Int. Conf. Energy Environ. Technol., 2009, vol. 2, pp.127–130.

[5.35] M. A. Elgendy, B. Zahawi, and D. J. Atkinson, “Assessment of the incremental conductance maximum power point tracking algorithm,” IEEE Trans. Sustain. Energy, vol. 4, no. 1, pp. 108–117, Jan. 2013.

[5.36] A. Safari and S. Mekhilef, “Simulation and hardware implementation of incremen tal conductance mppt with direct control method using cuk converter,” IEEE Trans. Ind. Electron, vol. 58, no. 4, pp. 1154–1161, Apr. 2011.

Chapter 6

Grid Interfacing of Multi-Megawatt Photovoltaic System under Normal and Partial Shading Conditions

This chapter investigates control issues and implementation for grid interfacing of multimegawatt photovoltaic system. The investigation is focused on current control, DC-link voltage control, MPPT technique and active and reactive power control. Control techniques under investigation are maximum power point tracking (MPPT), grid current and dc link voltage control. A modified 0.8Voc model suggested in chapter five is utilized to optimizes the active power level in the grid interfacing of multi-megawatt photovoltaic system. The new 0.8Voc model is capable of saving high amount of power even under partial shading condition. The feasibility of the grid interfacing system is validated by simulation in multi-megawatt photovoltaic system.

6.1 Background

The main aim of grid interfacing system is to control the active and reactive power generated from the interfacing inverter. The voltage and frequency level are being controlled by the grid system. In grid connected system, the power quality is dependent on the quality of current. A suitable way of controlling the power interfacing inverter is essential as this controls the harmonic injected into the grid. Interfacing large scale PV farms to the grid involves the use of power electronics. Pulse-width modulated voltage source inverter (VSI) or current source inverter (CSI) are the main power electronic devices for grid interfacing system [6.1]. The use of VSI increasingly becoming popular for high power medium voltage. This application involves multilevel and two level VSIs [6.2-6.4]. Because Multilevel VSI require high dc voltage, it is not viable option for implementing grid interfacing PV systems. This is because huge number of PV modules must be used to achieve high voltage for medium voltage applications [6.5-6.8]. Thus, the approach complicates partial shading problems. Even though, the cascaded multilevel inverter is given much attention in the PV system applications [6.9], the approach reduces

the life span of the PV cell as the PV cell is always exposes to ac current component of low frequency [6.1], [6.10]. The most commonly applied inverter for grid interfacing PV system is the two level VSI. This inverter has high switching losses [6.11], but with appropriate pulse width modulation, the inverter can generate high quality output voltage where significant harmonic can be suppressed from penetrating power frequency range, around and beyond the carrier frequency. Thus, small ac filter size is required. Additionally, the generated output active and reactive power can be controlled independently. To achieve robust control in grid interfacing PV system, certain conditions need to be met [6.12-6.13]. First, there should be MPPT that will force the PV module to operate at maximum power point (MPP) to improve system efficiency. Second, grid current control and voltage regulation using the dc link are important requirement for smooth injection of active power. The aforementioned requirements can be implemented using one of the existing topologies namely, single stage and two stage topologies [6.1]. The single stage topology involves only one conversion stage and uses one inverter. Thus, the number of components is reduced which increases system efficiency [6.14]. Figure 6.1a shows the configuration of the topology. The main limitation for this topology is the voltage ripple on the dc bus which is caused by double line frequency grid power oscillation [6.15]. To limit the ripple propagation, the single stage topology inverter must be designed with large electrolytic capacitor. However, the bigger size of the capacitor affects the converter dynamic response [6.16]. Additionally, the topology requires PV array of high dc voltage and such configuration requires huge number of PV modules which increases control complexity. This PV configuration suffers from hotspot during partial shading [6.17] leading to a severe power loss. Also, it could lead to a possible increased in leakage current between the PV modules and the ground through the parasitic capacitor of PV modules. For PV modules of low dc voltage, the use of step-up transformer to match the inverter output in this topology increases the inverter losses. Thus, this topology is limited to small scale PV application. A two-stage topology involves two conversion stage which has inverter and decoupling dc-dc converter as an additional component. The additional dc-dc converter increases the cost of implementation and also adds additional losses to the entire grid connected PV system.

However, the decoupling dc-dc converter step-up the PV voltage level, which leads to an increase in operating range and flexibility to increase number of PV modules [6.1]. Additionally, the energy changes between the dc link capacitor of the output inverter stage and PV string can be decoupled [6.18]. Figure 6.1b shows a typical configuration of two-stage grid connected system. Effective optimization and utilization of active power in the grid connected PV system can be achieved by the use of suitable MPPT, and effective external and internal control loops [6.18].

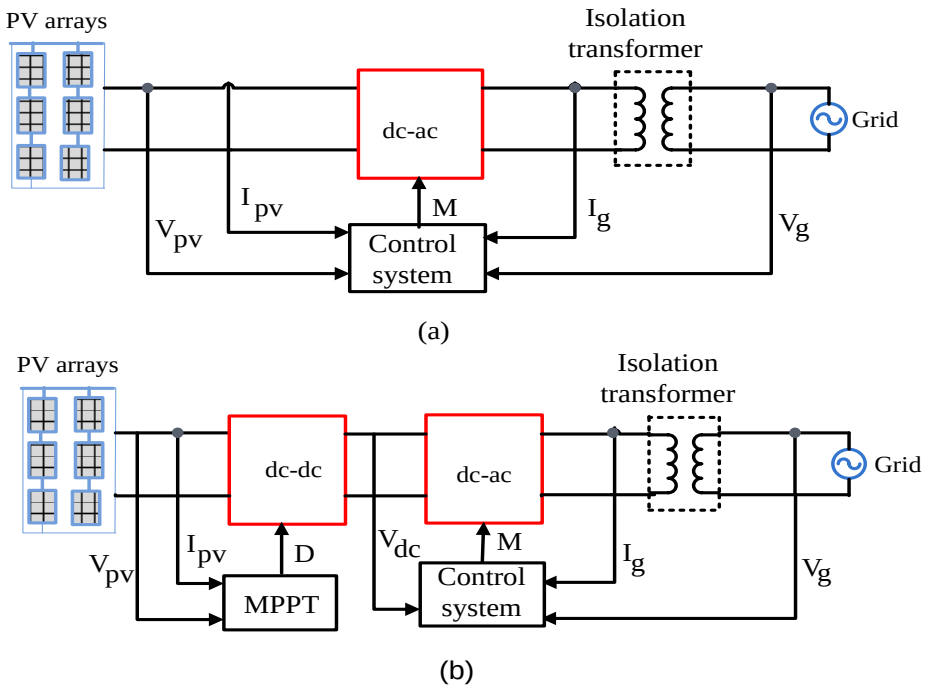

Figure 6.1. Topology of grid connected system (a) Single-stage system, (b) Two-stage system.

6.2 Issues in Various Control schemes of Grid Interfacing PV System

The following subsections discuss issues related to control schemes in grid connected PV system. The control parts under investigation in grid interfacing PV system are MPPT, DC-link control, current control and active and reactive power control.

6.2.1 MPPT Technique

The grid interfacing PV system requires a suitable MPPT device to be able to control the power generated from the PV module. However, such device also has control issues emanating from implementation and operation under environmental weather conditions. These control issues have the tendency to compromises the grid power quality as explained below:

- Trade-off issue in most conventional MPPTs. This has the tendency of reducing the grid power level due to oscillation around MPP and also slow down the tracking process of the algorithm.
- Drift is also another issue in most MPPT hardware devices. An increase in irradiance courses most MPPT drift away from MPP and this after the amplitude of grid current and system instability particularly under rapid increased in irradiance condition.
- The occurrence of partial shading on the PV modules produces multiple peaks on P-V characteristic curve. This is a critical issue that need to be address in grid connected system. Significant power loss occurred which in turn decreases the injection of grid power level when local peak is tracked instead of global peak. It is believed that there is no standards or procedures to test MPPT unlike, BSEN50530 which was published in 2010 [6.19]. This provides procedure to measure the efficiency of MPPT.

6.2.2 Grid Current control

In grid connected PV system, the inverter is responsible for producing the sinusoidal current and this inverter must satisfy strict standard and grid codes specified by international organizations such as IEC 16727 and IEEE 1547 standards [6.20]. These standards allow at most 5% injection of current harmonic into the grid, with restrictions enforced on the individual harmonic as a percentage of the fundamental component for low voltage applications. These standards are applied to prevent the use of current controller that shows high rejection capability to the grid background distortion. In the grid interfacing PV system, the reference grid current amplitude is the output of dc voltage controller. The current controller in the loop then forces the grid current to line up with sinusoidal reference. Proportional–integral (PI) with feed forward and proportional-

resonant (PR) are common in grid interfacing PV systems [6.21]. PR controller performs better than that of PI controller because it can withstand grid harmonic disturbance, ensuring unity power factor and provides pure sinusoidal current. However, with severe variation of grid frequency in the utility network, an improved PR controller is recommended to absorb the impact [6.21]. Figure 6.2 shows the inner current control loop for grid connected system. The PR controller has a transfer function given by:

$$G_{PR}(s) = k_p + k_i \frac{S}{S^2 + \omega^2} \tag{6.1}$$

where, k_i and k_p are integra and proportional gains respectively. ω represents the resonance frequency. $G_P(S)$ is the LCL filter. $G_D(s)$ is the microcontroller processing delay and is given by:

$$G_D(s) = \frac{1}{1 + sT_S} \tag{6.2}$$

where, T_S represents the sampling time.

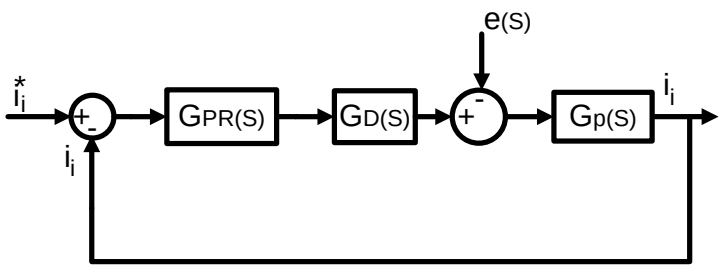

Figure 6.2. Resonance controller diagram.

6.2.3 DC-link voltage control

This controller is specifically designed to regulate the amplitude of the sinusoidal reference grid current, align with the voltage of the grid. This sinusoidal reference grid current is responsible for instantaneous power available at the input of the inverter [6.22].

By using the current controller where the amplitude of the grid current is properly controlled, the power at the inverter dc side is smoothly transferred into the grid. This results in power balance at the dc-link where dc-link voltage becomes constant. There are two main components that causes possible linear increment and decrement of dc-link voltage in grid connected PV system. The first is the dc component, which is the average power difference between the power extracted by the dc-dc converter and the dc-ac inverter. The second is the ac power, which constitutes ripples with frequency twice of the main frequency. The power balance in grid connected system shown in Figure 6.3 is given by:

$$P_{in} = P_{out} + P_{dc} \tag{6.3}$$

where, P_{in} is the power extracted by dc-dc converter, P_{out} is the power extracted by the dc-ac inverter, P_{dc} is the power to dc-link capacitor.

$$P_{dc} = V_{dc} C_{dc} \frac{dV_{dc}}{dt} \tag{6.4}$$

where, V_{dc} is the dc-link voltage and i_g is assumed to be sinusoidal and is align with the grid voltage, then:

$$P_{out} = P_g = 3\,\widehat{V_g}\ \widehat{I_g}\ sin^2 \tag{6.5}$$

$$= 3\widehat{V_g}\ \widehat{I_g}\left(\frac{1-\cos(2\omega t)}{2}\right) \tag{6.6}$$

$$P_{out} = \frac{3}{2} P_g (1-\cos(2\omega t)) \tag{6.7}$$

where, $\widehat{V_g}$ and $\widehat{I_g}$ are grid voltage injected current respectively, P_g is the injected instantaneous active power at unity power factor. Substituting (6.4) and (6.7) into (6.3),

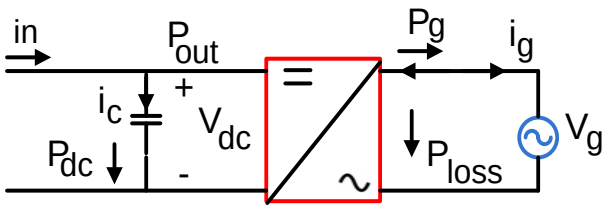

Figure 6.3. Power balance in grid connected system.

$$P_{in} = \frac{3}{2}P_g(1 - \cos(2\omega t)) + V_{dc}C_{dc}\frac{dV_{dc}}{dt} \tag{6.8}$$

Considering the power loss (P_{loss}) in the converter due to switching and conduction losses as well as the losses in the capacitor, the general power balance equation is written as:

$$P_{in} = \frac{3}{2}P_g(1 - \cos(2\omega t)) + V_{dc}C_{dc}\frac{dV_{dc}}{dt} + P_{loss} \tag{6.9}$$

In order to meet the condition for power balance, it is important that the dc-link voltage is maintained constant at all time under any given irradiance conditions. A simple conventional PI controller is suitable and is given by;

$$G_{PI}(S) = k_P + \frac{k_i}{S} \tag{6.10}$$

where, k_P and k_i are proportional and integral gain of PI controller respectively. This will ensure effective power transfer from the PV module(s) into the grid. Thus, effective control strategy is required in grid connected PV systems.

6.2.4 Control of Voltage source inverter (VSI) in photovoltaic system

The main objective of inverter in grid connected mode is to achieve good tracking of controlled variable with minimum phase error. The tracking accuracy is dependent on the inverter switching frequency, the dc link voltage and the output inductor of the inverter. By properly controlled the grid current, controls the harmonic content and stable power is

injected into the grid. Voltage source inverter can be operated in standalone ac system or grid connected mode as shown in figure 6.4. In standalone ac system, the overall ac power is transmitted to the system through inverter. In standalone mode, the system voltage and frequency do not require any reference generated from synchronous alternator. The inverter is responsible for providing a stable voltage and frequency in an event of arbitrarily load variation. The main challenge in this mode of operation is the quality of output voltage which determines the power quality. The control system should be able to supply enough reactive and active power to match the load demand by maintaining the frequency and voltage within the standard specification limit. On contrarily, the inverter in the grid connected mode controls and handle any distorted grid voltage that may draw from the network. Figure 6.5 shows a typical inverter equivalent circuit connected to the grid through an inductance.

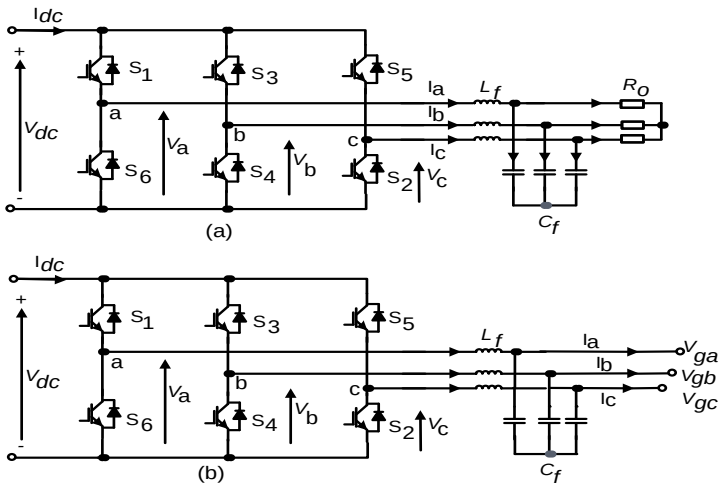

Figure 6.4. The operation of voltage source inverter.

The expression for active and reactive power is respectively obtained as follows;

$$P = \frac{3V_1V_G \sin\delta}{X} \tag{6.11}$$

$$Q = \frac{3V_G}{X}\,(V_1 \cos\delta - V_G) \tag{6.12}$$

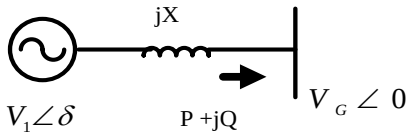

Figure 6.5. Grid connected system.

where, X is the coupling inductance or the reactance of the line between the grid and inverter, δ is the phase angle between voltage of the bus V_G and the output voltage of the inverter V_1. It is evident from the expression (6.11) and (6.12) that the active power depends on the angle δ while reactive power is a dependent on the amplitude of the output voltage of the inverter.

6.3 Modeling of Grid Interfacing Systems

The following section discusses the modeling of various control schemes in grid connected system. This includes the inverter control in d-q synchronous reference frame and MPPT control scheme.

6.3.1 The proposed GMPPT controller

A new GMPPT control scheme developed from conventional 0.8Voc model in chapter five is used to implement multimegawatt PV grid connected system. A new global peak voltage developed consists of two components: the voltage at peak and peak deviation factor correction. The voltage at peak is expressed as:

$$V_{peak} = \left[V_{oc\_STC} + \mu V_t In\left(\frac{I_{SC} - I_{PV}}{I_{SC\_STC}}\right)\right] \times 0.8 \times N_S \qquad (6.13)$$

Where, V_{oc_STC} is open circuit voltage, I_{SC_STC} is short circuit current all at standard test condition (STC), μ and V_t are ideality factor and thermal voltage respectively, I_{SC} is the short circuit current for PV string, and I_{SC_STC} is the shirt circuit current of PV string at STC. Also, the deviation factor correction is given by:

$$\beta = \left(\frac{I_{SC} - I_{PV}}{I_{SC\_STC}}\right)\left(\frac{V_{oc\_s}}{V_{oc\_s\_STC}} - 0.8\right) \times N_S \times V_{oc\_STC} \quad (6.14)$$

where, V_{oc_s} is open circuit voltage of PV string under partial shading conditions and $V_{oc\_s\_STC}$ represents open circuit voltage of the PV string at STC.

Thus, the calculated global peak voltage under partial shading condition is given by:

$$V_{GMPP} = V_{peak} + \beta \quad (6.15)$$

6.3.2 Inverter control in dq reference frame

The active power injected into the grid by the inverter can be controlled in the synchronous reference frame, where the voltage magnitude is lined up with d-axis. Since the control design requires only fundamental frequency dynamic, the equations that describes the inverter ac dynamic can be presented given below:

$$L_t \frac{dI_d}{dt} = V_{cdr} - V_d - R_t I_d + \omega L_t I_q \quad (6.16)$$

$$L_t \frac{dI_q}{dt} = V_{cqr} - V_q - R_t I_q - \omega L_t I_d \quad (6.17)$$

Equations (6.16) and (6.17) can be written as

$$\frac{dI_d}{dt} = -\frac{R_t I_d}{L_t} + \frac{V_{cdr} - V_d + \omega L_t I_q}{L_t} \quad (6.18)$$

$$\frac{dI_q}{dt} = -\frac{R_t I_q}{L_t} + \frac{V_{cqr} - V_q - \omega L_t I_d}{L_t} \quad (6.19)$$

Assume $U_d = V_{cdr} - V_d + \omega L_t I_q$ and$U_q = V_{cqr} - V_q + \omega L_t I_d$.

Equations (6.18) and (6.19) can be re-written as:

$$\frac{dI_d}{dt} = -\frac{R_t I_d}{L_t} + \frac{U_d}{L_t} \tag{6.20}$$

$$\frac{dI_q}{dt} = -\frac{R_t I_q}{L_t} + \frac{U_q}{L_t} \tag{6.21}$$

Where, U_d and U_q are obtained from PI controller given as

$$U_d = K_P(I_d^* - I_d) + K_I \int (I_d^* - I_d)dt \tag{6.22}$$

$$U_q = K_P\left(I_q^* - I_q\right) + K_I \int \left(I_q^* - I_q\right)dt \tag{6.23}$$

By using the following change of variables:

$$\gamma_d = K_I \int (I_d^* - I_d)dt \text{ and } \gamma_q = K_I \int \left(I_q^* - I_q\right)dt,$$

Equations (6.22) and (6.23) can be written as:

$$U_d = K_P(I_d^* - I_d) + \gamma_d \tag{6.24}$$

$$U_q = K_P\left(I_q^* - I_q\right) + \gamma_q \tag{6.25}$$

$$\frac{dI_d}{dt} = -\frac{(R_t + K_P)I_d}{L_t} + \frac{\gamma_d}{L_t} + \frac{K_P I_d^*}{L_t} \tag{6.26}$$

$$\frac{dI_q}{dt} = -\frac{(R_t + K_P)I_q}{L_t} + \frac{\gamma_q}{L_t} + \frac{K_P I_q^*}{L_t} \tag{6.27}$$

$$\frac{d\gamma_d}{dt} = K_I(I_d^* - I_d) \tag{6.28}$$

$$\frac{d\gamma_q}{dt} = K_I(I_q^* - I_q) \tag{6.29}$$

By differentiating equation (6.26) - (6.29), the inverter ac dynamic can be represented in state space equation as:

$$\begin{bmatrix} \frac{dI_d}{dt} \\ \frac{dI_q}{dt} \\ \frac{d\gamma_d}{dt} \\ \frac{d\gamma_q}{dt} \end{bmatrix} = \begin{bmatrix} -\frac{(R_t + K_P)}{L_t} & 0 & \frac{1}{L_t} & 0 \\ 0 & -\frac{(R_t + K_P)}{L_T} & 0 & \frac{1}{L_t} \\ -K_I & 0 & 0 & 0 \\ 0 & -K_I & 0 & 0 \end{bmatrix} \begin{bmatrix} I_d \\ I_q \\ \gamma_d \\ \gamma_q \end{bmatrix} + \begin{bmatrix} \frac{K_P}{L_t} & 0 \\ 0 & \frac{K_P}{L_t} \\ K_I & 0 \\ 0 & K_I \end{bmatrix} \begin{bmatrix} I_d^* \\ I_q^* \end{bmatrix} \tag{6.30}$$

The control system for 3-phase inverter in d-q synchronous reference frame can be summarised as shown in Figure 6.6. The feed-forward terms are calculated as $V_{cdr} = Q_d + V_d - \omega L_t I_d$ and $V_{cqr} = Q_q + V_q + \omega L_t I_d$. The active power is expressed as:

$$P = \frac{3}{2} V_d I_d \tag{6.31}$$

Similarly, the reactive power is expressed as:

$$Q = -\frac{3}{2} V_q I_q$$

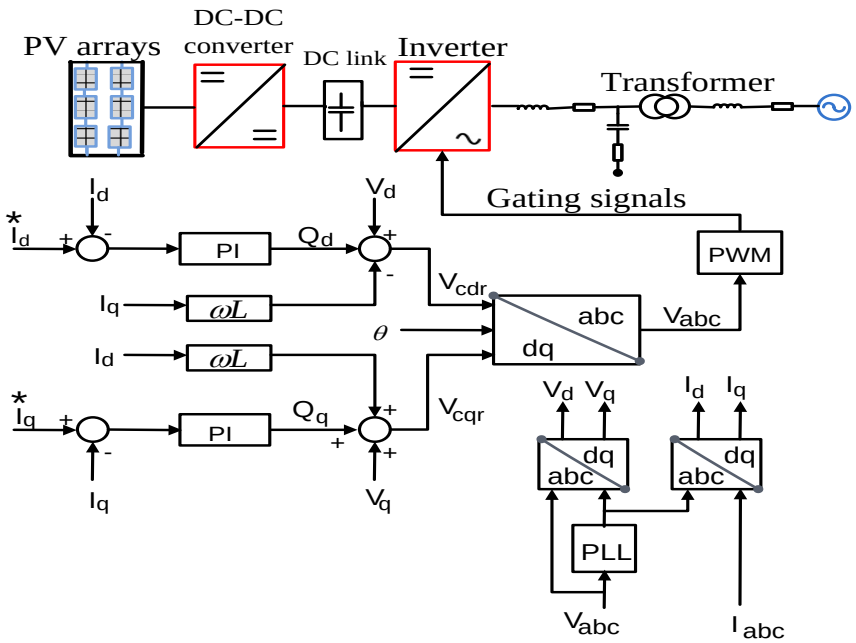

Fig. 6.6. Schematic control diagram of grid interfacing PV system.

6.4 Simulation results and discussion

In this section, simulation results of 5 MW grid interfacing PV system subjected to both normal and partial shading conditions are presented. The tested PV array consists of a combination of a string of 190 series connected PV modules and 50 parallel connected string with overall rated power of 5MW. Each PV module is rated at 530W. The system parameters are shown in Table II. The system delivers 5 MW on normal weather condition string with overall rated power of 5MW. Each PV module is rated at 530W. The system parameters are shown in Table II. The system delivers 5 MW on normal weather condition and 2 MW on partial shading condition. The proposed 0.8Voc model is implemented with conventional incremental conductance to adjust the PV array voltage to voltage at maximum power point and subsequently generates maximum power from the PV modules. The effectiveness of both conventional and proposed 0.8Voc model techniques for grid interfacing multi-megawatt is demonstrated using MATLAB/SIMULINK. Fig. 7 parts (a) and (b) show the global voltages and peak powers of both conventional and the proposed 0.8Voc model. It is evident that the proposed 0.8Voc model improves both PV array voltage and power. This in turn improves the grid injected active power as shown in

Figure 6.7 (c). Figure 6.8 (a) demonstrates the effectiveness of the external control loop, where the dc link voltage controller regulated dc bus voltage at 14.25 kV and 13 kV at normal and partial shading conditions respectively. The external control loop regulates both active (I_d) and reactive (I_q) current components. The I_q current is set to zero in order to achieve unity power factor and zero injected reactive power. Figure 6.8 parts (b) and (c) demonstrate the effectiveness of the internal control loop. The active power from the PV arrays is 5 MW, while the injected power into the ac is 4.73 MW, which represents 95% of the PV arrays power at normal condition. Similarly, during partial shading conditions, the active power of PV module is 2 MW and the injected power at that condition is 1.89 MW. The 5% loss is due to switching loss of the converters which is normal for a typical grid interfacing PV system. It is evident based on these results that the proposed 0.8Voc model with INC technique is capable of delivering optimum power of PV arrays, which improves the active power injected into the grid.

Table 6.1: System parameters.

Transformer	Rated power, frequency	5 MW, 50 Hz
	Turns ratio	1:1
	Leakage reactance(pu)	0.1
	Resistance (pu)	0.002
Control parameters	Current controller [Kp Ki]	[21 106]
	Voltage controller [Kp Ki]	[0.8 60]
Boost converter	Inductor	2 mH
	Input capacitor	150 μF
	DC link capacitor	400 μF
	Switching frequency	10 kHz
Two level inverter	DC link voltage	14.3 kV-13.1 kV
	Rated power	5 MW
	AC voltage line to line	11 kV
	Grid frequency	50Hz
PV module	V_{MPP}, I_{MPP}, P_{max}	40.74 V 13.01 A 530 W
	V_{OC} , I_{SC}	49.26V, 13.69A
PV array	V_{MPP}, I_{MPP}, P_{max}	7.74kV,160.5A, 5MW

Harmonic filter	L_t , R_t C_t	1 mH 0.03 Ω, 40 μF

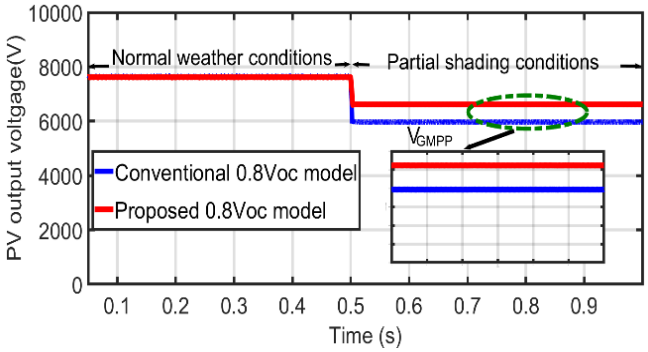

(a)

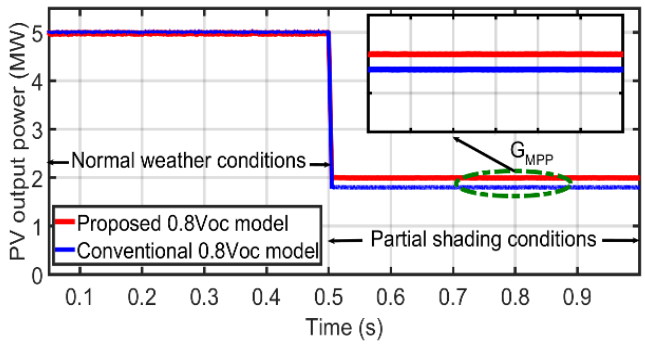

(b)

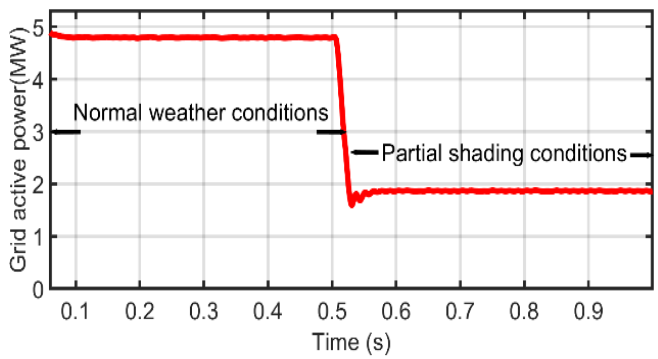

(c)

Fig. 6.7. (a) Voltage of proposed and conventional 0.8Voc, (b) Output power of proposed and conventional 0.8Voc, (c) Injected grid active power.

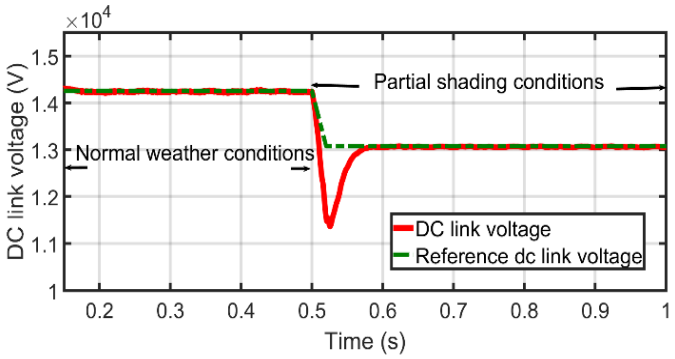

(a)

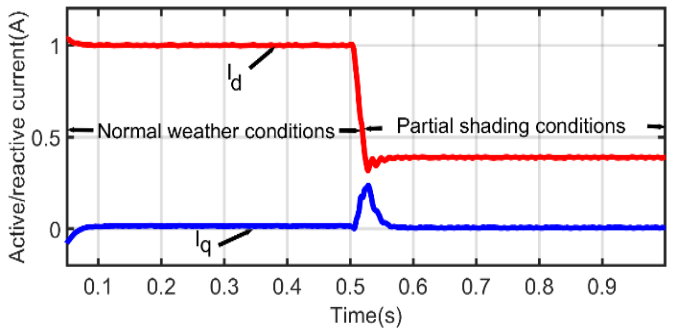

(b)

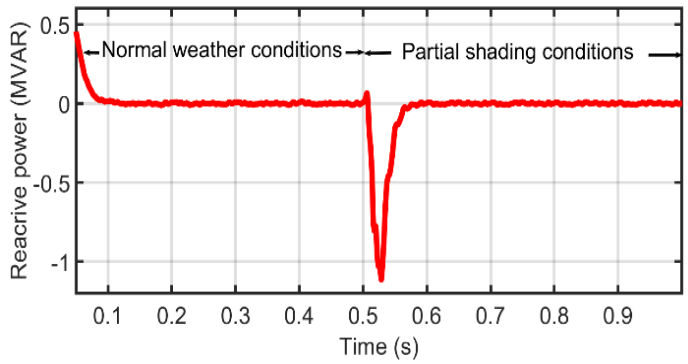

(c)

Fig. 6.8. (a) DC link voltage, (b) Active and reactive current, (c) Reactive power.

6.5 Summary

In this chapter, issues associated with controls in grid interfacing of multi-megawatt PV system have been investigated. This investigation focused on MPPT, grid current and dc link voltage control to highlight the main challenges and limitations. A new 0.8Voc model

technique suitable for multi-megawatt grid interfacing PV system has been developed and implemented with INC technique. It was demonstrated that the interval between two successive peak of PV modules under partial shading in conventional 0.8Voc model is not correct. The simulation results attest that the proposed technique is capable of improving PV arrays voltage and power significantly. The injected power is about 95% of the PV array power. This means that the proposed method is suitable for large scale multi-megawatt PV system since it is capable of saving high amount of power even in partial shading conditions.

References

[6.1] S. B. Kjaer, J. K. Pedersen, and F. Blaabjerg, "A review of single-phase grid-connected inverters for photovoltaic modules," IEEE Trans. Ind. Appl., vol. 41, no. 5, pp. 1292–1306, Sep.–Oct. 2005.

[6.2] S. Alepuz, S. Busquets-Monge, J. Bordonau, J. Gago, D. Gonzalez, and J. Balcells, "Interfacing renewable energy sources to the utility grid using a three-level inverter," IEEE Trans. Ind. Electron., vol. 53, no. 5, pp. 1504– 1511, Oct. 2006.

[6.3] S. Daher, J. Schmid, and F. L. M. Antunes, "Multilevel inverter topologies for stand-alone PV systems," IEEE Trans. Ind. Electron., vol. 55, no. 7, pp. 2703–2712, Jul. 2008.

[6.4] L. Asiminoaei, R. Teodorescu, F. Blaabjerg, and U. Borup, "A digital controlled PV-inverter with grid impedance estimation for ENS detection," IEEE Trans. Power Electron., vol. 20, no. 6, pp. 1480–1490, Nov. 2005.

[6.4] X. Chavarria, D. Biel, F. Guinjoan, C. Meza, and J. Negroni, "Energybalance control of PV cascaded multilevel grid-connected inverters under level-shifted and phase-shifted PWMs," IEEE Trans. Ind. Electron., vol. 60, no. 1, pp. 98–113, Jan. 2013.

[6.6] W. Fei, B. Wu, and Y. Huang, "Half-wave symmetry selective harmonic elimination method for multilevel voltage source inverters," IET Power Electron., vol. 4, pp. 342–351, 2011.

[6.7] D. Floricau and F. Richardeau, "New multilevel converters based on stacked commutation cells with shared power devices," IEEE Trans. Ind. Electron., vol. 58, no. 10, pp. 4675–4682, Oct. 2011.

[6.8] J. Chiasson, B. Ozpineci, D. Zhong, and L. M. Tolbert, "Conditions for capacitor voltage regulation in a five-level cascade multilevel inverter: Application to voltage-boost in a PM drive," in Proc. IEEE Int. Electric Mach. Drives Conf., May 2007, pp. 731–735.

[6.9] N. A. Rahim and J. Selvaraj, “Multistring five-level inverter with novel PWM control scheme for PV application,” IEEE Trans. Ind. Electron., vol. 57, no. 6, pp. 2111–2123, Jun. 2010.

[6.10] E. Villanueva, P. Correa, J. Rodriguez, and M. Pacas, “Control of a singlephase cascaded H-bridge multilevel inverter for grid-connected photovoltaic systems,” IEEE Trans. Ind. Electron., vol. 56, no. 11, pp. 4399– 4406, Nov. 2009.

[6.11] Y. Bo, L. Wuhua, Z. Yi, and H. Xiangning, “Design and analysis of a gridconnected photovoltaic power system,” IEEE Trans. Power Electron., vol. 25, no. 4, pp. 992–1000, Apr. 2010.

[6.12] F. Blaabjerg, R. Teodorescu, M. Liserre, and A. V. Timbus, “Overview of control and grid synchronization for distributed power generation systems,” IEEE Trans. Ind. Electron., vol. 53, no. 5, pp. 1398–1409, Oct. 2006.

[6.13] M. A. Eltawil and Z. Zhao, “Grid-connected photovoltaic power systems: Technical and potential problems—A review,” Renew. Sustain. Energy Rev., vol. 14, no. 1, pp. 112–129, Jan. 2010.

[6.14] S. Jain and V. Agarwal, “A single-stage grid connected inverter topology for solar PV systems with maximum power point tracking,” IEEE Trans. Power Electron., vol. 22, no. 5, pp. 1928–1940, Sep. 2007.

[6.15] S. Jain and V. Agarwal, “Comparison of the performance of maximum power point tracking schemes applied to single-stage gridconnected photovoltaic systems,” IET Electric Power Appl., vol. 1, no. 5, pp. 753–762, Sep. 2007.

[6.16] Y.-M. Chen, C.-H. Chang, and H.-C. Wu, “DC-Link capacitor selections for the single-phase grid-connected PV system,” in Proc. Int. Conf. Power Electron. Drive Syst. (PEDS), Nov. 2009, pp. 72–77.

[6.17] N. E. Zakzouk, A. K. Abdelsalam, A. A. Helal and B. W. Williams, "PV Single-Phase Grid-Connected Converter: DC-Link Voltage Sensorless Prospective," in IEEE Journal of Emerging and Selected Topics in Power Electronics, vol. 5, no. 1, pp. 526-546, March 2017.

[18] N. E. Zakzouk, A. K. Abdelsalam, A. A. Helal and B. W. Williams, "PV Single-Phase Grid-Connected Converter: DC-Link Voltage Sensorless Prospective," in IEEE Journal of Emerging and Selected Topics in Power Electronics, vol. 5, no. 1, pp. 526-546, March 2017.

[19] Overall Efficiency of Photovoltaic Inverters, BS EN 50530, May 201

[6.20] C. Yaow-Ming, W. Hsu-Chin, C. Yung-Chu, L. Kung-Yen, and S. ShianShing, "The ac line current regulation strategy for the grid-connected PV system," IEEE Trans. Power Electron., vol. 25, no. 1, pp. 209–218, Jan. 2010.

[6.21] N. E. Zakzouk, A. K. Abdelsalam, A. A. Helal and B. W. Williams, "PV Single-Phase Grid-Connected Converter: DC-Link Voltage Sensorless Prospective," in IEEE Journal of Emerging and Selected Topics in Power Electronics, vol. 5, no. 1, pp. 526-546, March 2017.

[6.23] A. Kotsopoulos, J. L. Duarte, and M. A. M. Hendrix, "Predictive DC voltage control of single-phase PV inverters with small DC link capacitance," in Proc. IEEE Int. Symp. Ind. Electron. (ISIE), vol. 2. Jun. 2003, pp. 793–797

Chapter 7

Conclusions and Future Works

7.1 General conclusion

The ever-increasing rate of greenhouse gas emission due to high global demand of electricity has generated enormous interest in development of renewable energy. Integration of renewable energy such as tidal, wind and solar has increased significantly. Globally, PV systems are one of the most accepted and efficient renewable energy sources for generation of electricity in small and utility scales. This is due to their applications in satellite systems, transportation systems, distributed generation and mobile applications. However, due to voltage and current characteristic curve of PV module(s), which is described as non-linear, the generated power is always affected by the variation of irradiance and temperature. Additionally, in an event of non-equally distributed irradiance around the PV module, multiple peaks comprising of local and global maxima are generated in the power (P)-voltage (V) characteristic curve. For PV system applications, the PV module plays crucial role and its operations must be controlled effectively. Chapter one and two deliberated the technologies and applications of PV system in order to establish the research gap. In chapter three, the impacts of temperature and irradiance on the performance of proportionality constants in both FOCV MPPT and FSCC MPPT techniques were investigated. Based on the combined temperature and irradiance effects, an optimum proportionality constants values were developed and new FOCV MPPT and FSCC MPPT techniques were suggested. The advantages of the proposed techniques were validated by Matlab/Simulink. By comparing the proposed techniques to the conventional counterparts shows that the proposed techniques have high tracking efficiency and their optimum proportionality constants values were re-tuned during variable temperature and irradiance conditions.

In chapter four, a modified variable step-size incremental conductance MPPT technique for PV system was developed. In the new MPPT technique, a new autonomous scaling

factor based on the PV module voltage in a restricted search range to replace the fixed scaling factor in the conventional variable step-size algorithm was proposed. Additionally, a slope angle variation algorithm was also developed. The merits of the proposed MPPT technique were verified using simulation and practical experimentation. The performance of the proposed MPPT technique was compared to the conventional variable step-size INC MPPT and the results show fast tracking, less oscillations under steady-state and dynamic conditions and good tracking efficiency. The performance of the proposed algorithm was further evaluated with simulation and compared to the two different existing variable step-size INC MPPT.

A new 0.8Voc model technique to estimate the peak global voltage under partial shading condition for medium voltage megawatt photovoltaic system integration has been proposed in chapter five. The proposed technique consists of two main components; namely, peak voltage and peak voltage deviation correction factor. The proposed 0.8Voc model was implemented by using simulation and its performance is compared to the conventional 0.8Voc. The performance of the proposed technique was further compared to the existing modified 0.8Voc model. The results show that performance of the proposed 0.8Voc model has high tracking efficiency and can be used for large scale PV farm, thus, it can be used to save high amount of PV power.

In chapter six, control issues confronting grid interfacing PV system has been investigated. A modified 0.8Voc model suggested in chapter five was utilized to optimize the active power level in the grid interfacing of multi-megawatt photovoltaic system under normal and partial shading conditions. The proposed system was successfully verified using simulation and is suitable for high power under normal and partial shading conditions.

7.2 Author's contributions

The contributions in this thesis can be summarised as follows:

- New FOCV MPPT and FSCC MPPT techniques have been proposed. The techniques utilize new developed optimum proportionality constants due to the

combine temperature and irradiance effects on the performance of the proportionality constants.

- Modified variable step-size incremental conductance MPPT technique for photovoltaic systems. The system uses autonomous scaling factor instead of fixed scaling factor to minimize oscillations around the MPP.
- New 0.8Voc model technique to estimate the peak global voltage for medium voltage megawatt photovoltaic system integration.
- Proposing as grid interfacing of Multi-Megawatt photovoltaic system under normal and partial shading conditions by utilizing a new 0.8Voc technique to improve the active power in the grid.

7.3 Suggestions for future work

The research commenced in this thesis addresses some key limitations of PV system, which is related to maximum power point tracking techniques under normal and variable weather condition, control issues in grid interfacing PV systems and effect of partial shading on the PV modules. It is important to consider the following for future research work:

- The concept of the combined temperature and irradiance effect on the performance of FOCV MPPT and FSCC MPPT have led to the development of new optimum proportionality constants values. Adoption of this idea in proposing a hybrid MPPT from the combination of FOCV MPPT and FSCC MPPT techniques could be a promising work for the future.
- The new variable step-size INC MPPT can further be modified and applied in standalone photovoltaic storage pumping system for better performance for water irrigation applications.
- The use of 0.8Voc model has been demonstrated to be one of the best techniques to be apply in high power PV system, however, this technique involves computation deviations. The use of the machine learning tools can be used in this

technique to minimize the deviations in order to enhance its performance in a large-scale PV system.

Appendix A

List of Tables and Figures

List of Figures

List of Tables

Appendix B

Summary of Relevant Published Research by the Author

[1] Owusu-Nyarko, I.; Elgenedy, M.A.; Abdelsalam, I.; Ahmed, K.H. Modified Variable Step-Size Incremental Conductance MPPT Technique for Photovoltaic Systems. MDPI Electronics 2021, 10, 2331. https://doi.org/10.3390/electronics 1019233.

Abstract

A highly efficient photovoltaic (PV) system requires a maximum power point tracker to extract peak power from PV modules. The conventional variable step-size incremental conductance (INC) maximum power point tracking (MPPT) technique has two main drawbacks. First, it uses a pre-set scaling factor, which requires manual tuning under different irradiance levels. Second, it adapts the slope of the PV characteristics curve to vary the step-size, which means any small changes in PV module voltage will significantly increase the overall step-size. Subsequently, it deviates the operating point away from the actual reference. In this paper, a new modified variable step-size INC algorithm is proposed to address the aforementioned problems. The proposed algorithm consists of two parts, namely autonomous scaling factor and slope angle variation algorithm. The autonomous scaling factor continuously adjusts the step-size without using a pre-set constant to control the trade-off between convergence speed and tracking precision. The slope angle variation algorithm mitigates the impact of PV voltage change, especially during variable irradiance conditions to improve the MPPT efficiency. The theoretical investigations of the new technique are carried out while its practicability is confirmed by simulation and experimental results.

[2] I. Owusu-Nyarko, K. H. Ahmed, F. Alsokhiry and Y. Al-Turki, "A New 0.8Voc Model Technique to Estimate the Peak Global Voltage for Medium Voltage

Megawatt Photovoltaic System Integration," *2020 9th IEEE International Conference on Renewable Energy Research and Application (ICRERA)*, 2020, pp. 439-444

Abstract

The paper proposes a new 0.8Voc model technique for medium voltage megawatt photovoltaic (PV) system integration. The power-voltage characteristic of photovoltaic (PV) modules shows multiple of local maximum power point when the modules are exposed to different irradiance levels. It is predicted that the local peaks are located near the multiples of 0.8, where is the open circuit voltage of the PV module. However, this prediction is not necessarily correct especially with long string of PV modules exposed to lower irradiance level. It is most likely that the algorithm will deviate from the original peak locations and unnecessary scanning will be essential. Therefore, a new 0.8Voc model is proposed, which estimates the voltage at global maximum power point. By scanning the PV current on I-V characteristic curve to map out solar irradiance pattern, peak voltage and related deviation correction expressions are calculated. Afterwards, the position of the global peak voltage is estimated. The proposed algorithm is capable of exploiting the advantages of conventional 0.8Voc model, while improving its performance. The principles of design and theoretical analysis of the proposed algorithm are presented and its feasibility also validated by simulation for medium voltage megawatt photovoltaic (PV) system integration.

[3] I. Owusu-Nyarko, M. A. Elgenedy and K. Ahmed, "Combined Temperature and Irradiation Effects on the Open Circuit Voltage and Short Circuit Current Constants for Enhancing their Related PV-MPPT Algorithms," *2019 IEEE Conference on Power Electronics and Renewable Energy (CPERE)*, 2019, pp. 343-348

Abstract

The increasing demand for energy and the environmental impact from the excessive use of fossil fuels has increased the interest in the renewable research. Solar energy is increasingly becoming an area of interest to researchers due to its abundance source and

accessibility. This can be achieved by utilizing photovoltaic (PV) panels. Nevertheless, due to PV nonlinear characteristics, maximum power point tracking (MPPT) algorithm are applied. Many MPPT techniques and improvement have been reported in the literature. In this paper, the impact of temperature and irradiation on the performance of proportionality constants in both fractional open circuit voltage (FOCV) MPPT and fractional short circuit current (FSCC) MPPT techniques are explored. Normally in these algorithms the irradiation effect is solely considered. However, the obtained results show that the value of these constants can be re-tuned for better energy harvesting when both the temperature and the irradiation change.

[4] I. Owusu-Nyarko, K. H. Ahmed, F. Alsokhiry and Y. Al-Turki, "Grid Interfacing of Multi-megawatt Photovoltaic System under Normal and Partial Shading Conditions," *2021 9th IEEE International Conference on Smart Grid (icSmartGrid)*, 2021, pp. 118-123

Abstract

Weather conditions have several impacts on the photovoltaic (PV) system power generation. Interfacing PV system to the grid is done by using power electronic devices and frequent switching results in various disturbances and power losses. With PV grid integration, many grid requirements have been provided to guide the interconnection procedures. These regulations only address issues associated with the performance of power electronic devices, however, do not address control issues in grid interfacing system. Control in grid connected PV system such as maximum power point tracking (MPPT), grid current and dc link voltage control have been given significant attention. In this paper, MPPT, grid current and dc link voltage control are reviewed. A new 0.8Voc model MPPT technique for active power optimization is proposed for grid interfacing of multi-megawatt PV system. The results show that an optimum active power can be injected into the grid. The design principles and theoretical analysis are presented while the feasibility is validated by simulation in grid interfacing multi-megawatt PV system.